COMPLEX IMPEDANCE SPECTROSCOPIC STUDIES ON BISMUTH SILICON OXIDE (BSO)

by

S. Balasubramanian

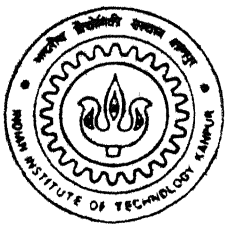

MATERIALS SCIENCE PROGRAMME

INDIAN INSTITUTE OF TECHNOLOGY KANPUR

April, 1999

COMPLEX IMPEDANCE SPECTROSCOPIC STUDIES ON BISMUTH SILICON OXIDE (BSO)

A Thesis submitted
in partial fulfillment of the requirement
for the Degree of

Master of Technology

by

S. Balasubramanian

to the

MATERIALS SCIENCE PROGRAMME

INDIAN INSTITUTE OF TECHNOLOGY, KANPUR

April 1999

CERTIFICATE

It is certified that the work contained in this thesis entitled " **Complex impedance spectroscopic studies on Bimuth Silicon Oxide (BSO)** ", by S Balasubramanian has been carried out under my supervision and that this work has not been submitted elsewhere for a degree

April , 1999

(K . Shahi)

Thesis supervisor

Materials Science Programme

Indian Institute of Technology , Kanpur

ABSTRACT

Bismuth Silicon Oxide popularly known as BSO , is a potential candidate for Optical image processing and Holographic applications This thesis deals with the synthesis, electrical and dielectric characterization of this very important material using Complex impedance spectroscopy as a tool . This is called spectroscopy because from the immittance plots of the dispersion data good visual information is obtained about the characteristics of the electrochemical system, so that individual processes can be separated out in accordance with the various circuit elements present in the system In other words , the various circuit elements are related to the respective processes in the system. e g. Resistance element gives rise to ionic conductivity of the system and the Capacitor gives rise to double layer capacitance and dielectric loss etc.

BSO is a very complicated system Various phases like γ and δ are associated with this material at different temperatures. This thesis deals with only γ - BSO . Three single crystals of BSO pure , BSO doped with 2 mole % of γ - Al_2O_3 and BSO doped with 2 mole % of MgO are synthesized using Czochralski growth technique . Three corresponding polycrystals have been prepared by mixing the appropriate powders and subsequent solid state reactions followed by pelletization Powder XRD was used to confirm the formation of the compounds. The lattice parameters of the doped single crystals have been obtained through single crystal XRD studies. The SEM analysis and density measurements have been made on all the polycrystals. DTA was done on all the six samples to check the purity of the compounds from the observed melting point .

Impedance and dielectric measurements on all the six samples, (3 single crystals and 3 polycrystals) were carried out over a wide frequency (500 Hz to 10 MHz) and temperature range (room temperature to 700^0 C). From these measurements, various parameters like dc, ac conductivity, dielectric constant and dielectric loss have been obtained . They are discussed in detail in the last chapter.

Acknowledgements

I am deeply indebted to Prof. K Shahi and Dr. K. V Rao for their inspiring guidance. I am very fortunate as I had been under their tutelege. Both constantly encouraged me and the freedom that I got was absolutely remarkable I should also appreciate the help rendered by Mr. Dinesh Deva, who was largely responsible for the single crystals used in this thesis as well as his suggestions at various stages of this work. I am very thankful to Prof Jitendra Kumar who encouraged me a lot .

I also express my sincere acknowledgement and special thanks to Prof. Bharadwaj of Chemistry department, who collected XRD data on all the three single crystals. I am very thankful to Mr Umasankar singh for collecting the powder XRD data Thanks are also to Dr Bhatnagar for DTA, Mr. P.K. Paul for SEM , Mishraji and Balaji for useful suggestions. I also express my sincere thanks to Mr Viswanath singh, Mr. Joshi and other office staff for their nice cooperation and help .

I should appreciate the help offered by my labmates Gopal and Anshuman in setting up the Solid state ionics lab

I am extremely pleased to have friends like Kalyan, Rajesh, JP, Sridevi, Mahesh,Prabakar,Murali,Johnson and Raja. Their affection towards me cannot be described by mere words They helped me a lot during my stay here at IIT, Kanpur I always cherish the moments that I have spent with them I also thank my classmates Manmohan, Amit, Rashmi and other friends of IIT, Kanpur for their cooperation and help.

Last but not the least , I thank my Parents and my brother whose constant source of encouragement throughout this work should really be lauded.

Contents

PAGE

LIST OF FIGURES

CHAPTER -1 Introduction

1 1 Importance of BSO 1

1 2 Literature survey on BSO 2

1 2.1 BSO structure 2

1 2 2 Photorefractive effect in pure and doped single crystals 2

1 2 3 Solidification characteristics of BSO phases 5

1 2 4 BSO in optical image processing and Holography 5

1.2.5 Growth of BSO thin films 6

1 3 Complex impedance spectroscopy 6

1 4 Complex impedance studies on various systems 7

1 5 Modelling with circuit elements 8

1.6 Depressed semicircles 10

1.7 Aim of the present work 11

CHAPTER - 2 Experimental details 13

2.1 Preparation of BSO pure and doped polycrystals 13

2.1.1 Preparation of pellets (polycrystals) 15

2.2 Preparation of BSO pure and doped single crystals 17

2 2 1 Seed preparation 17

2.2.2 Pulling and Rotation systems 17

2.2.3 Furnace 17

2.2 4 Crystal growth 18

2.2.5 Crystal cutting, grinding and polishing 18

2.3 Phase diagram of Bi_2O_3 - SiO_2 system 19

2.4 Complex impedance analysis measurement 21

2.4.1 Furnace 21

2.4.2 Sample holder 21

2 4 3 The experimental set-up 23
2.4.4 Theory of Complex impedance analysis 25
2.4.5 Measurement details 26
2.4.6 Complex impedance plots 29
2 5 Density measurement 29
2.5.1 Xylene test 29
2 5.2 Geometrical method 30
2.6 Powder x-ray diffraction studies 30
2 7 Single crystal XRD studies 31
2.8 Differential Thermal Analysis (DTA) 31
2.9 Scanning electron microscopy (SEM) 31

CHAPTER -3 Results and Discussions 33

3.1 Powder XRD studies on BSO 34
3.2 Phase change of BSO at various temperatures 35
3.3 Comparison of powder XRD with single crystal XRD studies 35
3.4 Density measurements 41
3.5 Differential Thermal Analysis (DTA) results 42
3.6 SEM studies 46
3.7 Complex impedance spectroscopy studies 46
(a) RC combination studies 46
(b) Conductivity studies 51
(i) Low temperature behaviour 52
(ii) High temperature behaviour 52
DC conductivity 59
AC conductivity 63
(c) Dielectric studies 63
3.8 Conclusions and future directions 68

References 78

LIST OF FIGURES

		PAGE
1 1	Admittance plots for simple R-C circuits	8
1 2	Debye circuit	9
1 3	Equivalent circuit for a typical polycrystalline material	10
1 4	Cole - Cole equivalent circuit	11
2 1	Stainless steel die for making pellets	15
2 2	Part of the phase diagram for the system Bi_2O_3 - SiO_2	19
2.3	Complete phase diagram of Bi_2O_3 - SiO_2 system	20
2 4	Sample holder for electrical conductivity measurements from room temperature to 1000^0 C	22
2.5	Block diagram connections for electrical conductivity measurements	24
2.6	Four terminal pair measurement principle	27
2.7	Impedance vector representation	28
3.1	XRD pattern of BSO pure powder	36
3.2	XRD pattern of BSO sintered pellet	37
3.3	XRD pattern of Bi_2O_3-SiO_2 mixture at 690^0 C	38
3.4	XRD pattern of BSO mixture at 750^0 C	39
3.5	XRD pattern of BSO at 835^0 C	40
3.6	DTA of BSO polycrystal	43
3 7	DTA of BSO single crystal	43
3.8	DTA of BSO:Al polycrystal	44
3.9	DTA of BSO:Al single crystal	44
3.10	DTA of BSO:Mg polycrystal	45
3.11	DTA of BSO:Mg single crystal	46
3.12 (a)	SEM micrograph of BSO pressed pellet	47
3.12 (b)	SEM micrograph of BSO pressed pellet	47
3.13	SEM micrograph of BSO:Al pressed pellet	48
3.14	SEM micrograph of BSO:Mg pressed pellet	48
3.15	Elemental analysis profile of BSO.Al polycrystal	49

3 16 Elemental analysis profile of BSO:Mg polycrystal 50

3 17 (a) Complex impedance and admittance plots for Resistor (R) 53

3 17 (b) Complex impedance and admittance plots for Capacitor (C) 53

3 17 (c) Complex impedance and admittance plots for R and C in series 54

3 17 (d) Complex impedance and admittance plots for R and C parallel 54

3 18 (a) Complex impedance plot for R = 4.4 k, C = 3nf in series 55

3 18 (b) Complex impedance plot for R = 4.4 k, C = 3nf in parallel 55

3 19 (a) Complex impedance plots for BSO polycrystal at room temperature and 300^0 C 56

3.19 (b) Complex impedance plots for BSO polycrystal at 400^0 C and 427^0 C 56

3 20 Complex impedance plots for BSO single crystal at three different temperatures 600^0 C , 650^0 C and 700^0 C 57

3.21 (a) Complex impedance plots for BSO:Al polycrystal at three different temperatures 430^0 C, 460^0 C and 500^0 C 57

3 21 (b) Complex impedance plots for BSO.Al single crystal at three different temperatures 600^0 C , 650^0 C and 700^0 C 58

3.22 Complex impedance plots for BSO:Mg polycrystal at three different temperatures 430^0 C, 460^0 C and 500^0 C 58

3.23 (a) DC conductivity plots for pure BSO, BSO.Al and BSO Mg single crystals and polycrystals 61

3.23 (b) DC conductivity fit for BSO pure and doped single crystals and polycrystals 62

3.24 (a) Variation of ac conductivity as a function of inversion of temperature for pure BSO single crystal 64

3.24 (b) Variation of ac conductivity as a function of inversion of temperature for pure BSO polycrystal 64

3.25 (a) Variation of ac conductivity as a function of inversion of temperature for BSO:Al single crystal 65

3.25 (b) Variation of ac conductivity as a function of inversion of temperature for BSO:Al polycrystal 65

3.26 (a) Variation of ac conductivity as a function of inversion of temperature for BSO:Mg single crystal 66

3.26 (b) Variation of ac conductivity as a function of inversion of temperature for BSO: Mg polycrystal 66

3.27 Variation of dielectric constant ε' as a function of log frequency for pure and doped single crystals and polycrystals 69

3.28 Variation of dielectric constant ε'' as a function of log frequency for pure and doped single crystals and polycrystals 70

3.29 (a) Variation of log dielectric constant ε' as a function of temperature for pure BSO single crystal 71

3.29 (b) Variation of log dielectric constant ε' as a function of temperature for pure BSO polycrystal 71

3.30 (a) Variation of log dielectric constant ε' as a function of temperature for BSO.Al single crystal 72

3.30 (b) Variation of log dielectric constant ε' as a function of temperature for BSO·Al polycrystal 72

3.31 (a) Variation of log dielectric constant ε' as a function of temperature for BSO:Mg single crystal 73

3.31 (b) Variation of log dielectric constant ε' as a function of temperature for BSO:Mg polycrystal 73

3.32 (a) Variation of log ε'' as a function of inversion of temperature for BSO single crystal 74

3.32 (b) Variation of log ε'' as a function of inversion of temperature for BSO polycrystal 74

3.33 (a) Variation of log ε'' as a function of inversion of temperature for BSO:Al single crystal 75

3.33 (b) Variation of log ε'' as a function of inversion of temperature for BSO:Al polycrystal 75

3.34 (a) Variation of log ε'' as a function of inversion of temperature for BSO:Mg single crystal 76

3.34 (b) Variation of log ε'' as a function of inversion of temperature for BSO:Mg polycrystal 76

Chapter 1

INTRODUCTION

1.1 Importance of BSO

Bismuth Silicon Oxide is popularly known as BSO in scientific parlance As the information technology(IT) is leapfrogging into the third millennium with tremendous success, materials technology which is the backbone of IT is also booming. Nowadays lots of innovative materials have been synthesized from the applications point of view. These materials have been characterized using various techniques and if the properties are interesting then more and more research will be going on with the ultimate aim of commercializing the materials BSO comes into the above mentioned category as it is a potential candidate for optical image processing and holographic applications. Also Bismuth Silicon Oxide $Bi_{12}SiO_{20}$ is a technologically interesting material, because it can function as a Pockels readout optical modulation (PROM) device. It is an intermediate band-gap material with $E_g = 3.25eV$ and an electrical resistivity in excess of 10^{14} Ω cm at room temperature. That means it is essentially a wide bandgap semiconductor at room temperature. Above all, it is photorefractive. Photorefractive effect is nothing but light induced changes in the optical properties of a material when the incident light has a non uniform intensity. This is a nonlinear optical effect which is a hotfield nowadays for Physicists and Materials scientists. Also one of the most important features of photorefractive effect is the operation at very low light intensities. Most non linear optical processes require large light intensities, to drive the material into it's range of nonlinear response. This thesis basically deals with the synthesis and characterization of BSO using complex impedance analysis as a tool.

1.2 Literature survey on BSO

1.2.1 BSO structure

Bismuth silicate $Bi_{12}SiO_{20}$ belongs to a group of compounds described by the general formula 6 Bi_2O_3 .MeO where Me =Ge, Si, Ti, Al, Fe, Ce,Tl,Pb, B, P and a number of other elements These are usually called sillenites, named after the Swedish chemist Sillen who first studied these substances[1] . Large single crystals of these compounds are usually grown by the Czochralski method[2, 3] . The sillenite crystals are isomorphous, have a symmetry group T23, and belong to the space group T^3 (123)[4] . Their unit bcc cell contains two formula units[5] BSO crystallizes in body centered cubic and the structure has been solved using single crystal X-ray diffraction studies[6, 7] . The effect of non-steady state photovoltage is a powerful technique for the measurement of different parameters of photoconductors, such as the Maxwell relaxation time, the diffusion length and type of photocarriers, the Debye screening length etc The photovoltage is observed as an alternating electric current J^{ω} through a short-circuited sample of photoconductor illuminated by a vibrating pattern of interference between two coherent waves, one of which is phase-modulated with frequency ω. The theoretical analysis based on the widely accepted model of a photoconductor with one partially compensated donor level and a finite photoelectron lifetime is in reasonable agreement with the experiments on cubic BSO crystals[8]

1.2.2 Photorefractive effect in Pure and doped BSO single crystals

The phenomenon of photorefraction arises on the uniform illumination of materials like BSO and with the diffusion of the ensuing photogenerated carriers toward lesser illuminated regions where they are subsequently retrapped. The resulting redistribution of charge gives rise to space charge regions with associated electric fields that, through the Pockels effect, cause localized changes in the refractive index. It is such photoinduced variations in the refractive index that are utilized in what is commonly referred to as the photorefrative effect Basically the photorefractive effect[9-11] begins with the photogeneration of charge carriers which are free to move. This followed by trapping of charge carriers, thereby forming the space charge density inside the material. The last stage is the conversion of internal space charge electric field into refractive index of the material. This conversion is done through

electro optic effect Due to this effect the refractive index of the material can be varied by varying the externally applied electric field.

Photorefractive materials must be insulators or semi -insulating semiconductors otherwise excess free carriers screen the trapped space charge On the other hand, the photorefractive materials must have appreciable photoconductivity to allow the charge to separate and to form space charge fields Oxides like $BaTiO_3$,$KNbO_3$, and BSO have large electro -optic effect that makes them attractive for photorefractive applications As already mentioned, BSO is a wide band gap semiconductor which often contains donors(or acceptors) When the electrons (or holes) are photoexcited into the conduction (or valence) band they migrate until they recombine or are captured by an empty shallower trap[12]

BSO single crystals possess fast responsive and highly sensitive photorefractivity, even to laser beams of only several mW/cm^2 They are, therefore, widely applied in phase conjugation optics, optical information processing and pattern recognition Although the BSO crystals perform marvelously in the blue-green regime of laser beams, their response, speed and photorefractive sensitivity is a cause of concern in the long wavelength regime

According to the band transport model proposed by Kukhtarev etal.[13] the photorefractivity of the crystals arises from the charge transport between traps via a three step process of photoexcitation, drift or diffusion and recombination. The absorption coefficient of the crystals to the incident beam thus plays an important role in determining the photorefractivity of the materials.

The modification of the absorption coefficient of BSO crystals, due to a small amount of dopants has been studied extensively[14-16]. The Fe^{3+} ions have been observed in undoped BSO crystals and have a significant effect on the photorefractivity. The doping of BSO with Cr_2O_3 has a desirable effect on the optical properties and essentially the goal is to increase the photorefractive response of these materials to 633 nm laser beams[17] .

BSO crystals doped with Co,Ni,Cr,Mn,V and Fe have been studied[18]. Classical transmission and reflection measurements and the constant photocurrent method have been employed to obtain the absorption coefficient in the 1.3-3 25 eV range. Temperature dependencies of the photocurrent and thermostimulated currents have also been measured.

From the changes induced in the absorption spectrum, the doping metals can be divided into three groups. The first group (Mn,Cr) causes a large increase in the total absorption coefficient. The second group (Co,Ni) leads to relatively weak changes in the whole spectral

region studied. The third group (V,Fe) induces a strong "bleaching" effect in the "shoulder" region ($hc/\lambda \cong 2\,5$ -2.8 eV) at high doping concentrations (> 1 mol % in the melt) accompanied by an absorption increase at the lower energies ($hc/\lambda < 2$ eV)

Undoped Cz grown BSO crystals normally have a yellow coloration This coloration is due to a native deep donor which has an absorption band extending from $\cong 2\,5$ eV to the band edge near 3 4 eV Phosporous is one of the several dopants that electronically compensate the native deep donor responsible for the yellow coloration observed in BSO[12]. The coloration can also be removed by doping with gallium or aluminium[14,16] Low temperature optical absorption measurements of a series of Czochralski-grown P -doped BSO crystals show that $\cong 0.1$ - 0.15 at % P is needed in the sample to fully remove the yellow coloration. The absorption cutoff in the fully compensated P -doped sample was at 3.2 eV while for compensated Al- and Ga- doped samples the cutoff was at 3 35 eV Excitation at 10 - 15 K with near band - edge light produces photochromic absorption bands.In the lightly -doped (partially bleached) samples these bands were identical to those observed in undoped BSO. In the fully bleached sample a new spectrum was observed Also the impurities of transition metals, especially Cr and Cu , reduce photoconductivity and increase the light absorption of the crystals in the visible and near IR region[19] . The low chromium contents ($\cong 10^{-4}$ wt .%)in BSO crystal displace the maximum of the gain factor to higher spatial frequencies that could be useful for some applications.

Harris,Larkin and Martin have reported the growth of colorless, near intrinsic BSO using a hydrothermal technique[20]. The deep donor absorption shoulder is missing in these hydrothermal crystals At 10 K, their absortion edge is at 3.45 eV, while it is at 3.1 and 3 35 eV,respectively in yellow undoped and Al-doped Cz crystals.Interestingly,undoped crystals pulled from melts of hydrothermal material show the normal yellow color and low - temperature photochromic response of conventional Cz material[12]. These results strongly suggest that the deep donor is a growth defect rather than an impurity

The traps which take part in the photorefractive response are most likely impurities and point defects A number of point defect studies on undoped and doped BSO have been carried out. Thermally stimulated conductivity[21,22] and thermoluminescence techniques[23,24] have been used to study the electron and hole traps.

1.2.3 Solidification characteristics of BSO phases

BSO is a very complicated system. It exists in γ-$Bi_{12}SiO_{20}$ and δ-$Bi_{12}SiO_{20}$ phases and the solidification characteristics of metastable δ-$Bi_{12}SiO_{20}$ and stable γ-$Bi_{12}SiO_{20}$ from $Bi_{12}SiO_{20}$ melts were systematically investigated by x-ray diffraction, differential thermal analysis and thermogravimetry[25]. The experimental results show that the solidification of both the phases depends on the melt temperature and on the cooling rate To produce stable single - crystal γ-$Bi_{12}SiO_{20}$, the melt temperature should be controlled to be less than 935° C and the cooling rate near the solidifying temperature should be less than 30° C s^{-1} The interesting aspect is the stable γ-$Bi_{12}SiO_{20}$ has a body centered cubic structure (BCC) and the metastable δ-$Bi_{12}SiO_{20}$ has a face -centered cubic structure (FCC)[26,27].

1.2.4 BSO in Optical image processing and Holography

In optical image processing it is very important to have a means of converting a spatially incoherent input to a coherent replica in order to perform further operations, for instance, to implement the optical Fourier transform of incoherently illuminated images. Such an operation can be performed with some crystals like BSO which exhibit photorefractive effect[28]. The diffraction efficiency of holograms formed in BSO crystals by pulsed excitation has been studied as a function of the recording pulse energy, readout light polarization and crystal's temperature[29]. Using the results of this study the contributions of the photochromic and photorefractive gratings into the volume hologram can be estimated and the origin of the process that underlies the short -pulse holographic recording can be elucidated.

To enhance the holographic recording a broadband antireflection coating is used[30]. This coating comprises two-electron -beam -deposited quarter -wave dielectric layers of MgF_2 and ZrO_2, and increases the beam throughput by as much as 20% per interface at normal incidence. For holographic recording applications the antireflection coating eliminates multiple internal reflections that produce extraneous gratings. The combination of these two factors significantly increases the diffraction efficiency and the two-beam coupling gain

Lots of theoretical papers related to the standard model of the photorefractive nonlinearity in BSO crystals are available. Also the papers deal with a detailed theoretical analysis of mechanism of photorefractive enhancement of BSO gratings.

1.2.5 Growth of BSO thin films

$Bi_{12}SiO_{20}$ thin films were grown by the Metal organic chemical vapor deposition(MOCVD) technique[31]. The growth was carried out in an atmospheric and low pressure reactor using Bi (CH_3)$_3$ and Si (OCH_3)$_4$ (or Si (OC_2H_5)$_4$) as metal sources and O_2 or N_2O gas as an oxidizing gas.The single crystal films have been grown over a wide composition range of $5.5 < Bi_2O_3 / SiO_2 < 8$. The lattice constants of the films increase in proportion with Si deficiencies Films with good compositional uniformity were obtained using the N_2O gas as an oxidizing gas. For these epitaxial films, it was found that the photoconductivity was ten to fifteen times as large as that of bulk crystals and there was a strong relationship between the film composition and the photoconductivity spectral response. This is highly useful in spatial light modulators and reversible holographic media One possible explanation for the large photoconductivity in the epitaxial films is due to the extremely reduced content of impurities which otherwise may obstruct the transport of the photoexcited carriers.

1.3 Complex impedance spectroscopy

Impedance spectroscopy is a popular tool nowadays to study the electrochemical systems[32-34] This is called spectroscopy because from the immittance plots of the dispersion data good visual information is obtained about the characteristics of the electrochemical system, so that the individual processes can be separated out in accordance with the various circuit elements present in the system. In other words, the various circuit elements are related to the respective processes in the system, e g , resistance element gives rise to ionic conductivity of the system and the capacitor gives rise to double layer capacitance and dielectric loss etc.

The term **"complex"** in real sense means intricate i.e. not too simple. In Mathematics complex means imaginary. For example, if we write $Z = x + iy$ where x is a real part and y is the imaginary part. This can be graphically represented in a diagram popularly known as Argand diagram. Mathematics is the language for Physics, wherever we see imaginary number in Physics that refers to phase. e.g. in the case of sound waves the equation is $e^{i(kx-wt)}$. Here 'i' refers to phase Impedance means ac resistance which depends on frequency Here phase is taken into account. So Complex impedance analysis(CIA) is nothing but measurement of impedance as a function of frequency. After measuring impedance for various frequencies, plot the real part Vs imaginary part i.e. $Z\cos\theta$ vs $Z\sin\theta$. Here Z is impedance and θ is the

phase angle.If the plot gives rise to semicircle then the diameter is nothing but dc resistance which is independent of frequency So CIA is highly useful in retrieving the dc conductivity of the sample

The conventional method of electrical characterization of solid electrolytes is to measure the ac conductivity at 1 khz frequency It has been used for years and continues to be so even today It is now well recognized that this method is applicable only when the system under test is purely resistive. Strictly speaking,only metallic systems would fall in this category For all other materials,the cell assembly, i.e the sample + electrodes + leads, represents a complex impedance involving resistance and capacitance. The latter arises due to the capacitance between the electrodes and the sample and the capacitance due to grain boundaries etc Thus the unknown sample is like a blackbox consisting of resistance and capacitance in an unknown configuration Hence to determine the resistivity/conductivity of the sample a complex impedance analysis has to be used

1.4 Complex impedance studies on various systems

The method of Complex impedance analysis (CIA) was first introduced by Bauerle[35] for the solid electrolyte system in a stabilized zirconia. Since this pioneering work, a lot of experimental results which include among others polymers, oxides, glasses, halides etc. have been presented by many researchers. The separation of complex polarization components in a frequency dispersion makes impedance spectroscopy a potentially powerful technique for the study of high temperature conduction process in solids. Jonscher[36] has been instrumental in acquiring the huge amount of impedance information pertaining to dielectric loss. This in turn is useful to determine the conductivities of solid electrolytes[37]. Macdonald and coworkers have developed methods for analyzing the experimental impedance results of semiconductors[38]. Matsui[39] has discussed the application of impedance spectroscopy to the study of Fe_2O_3 doped zirconia which is a high temperature electrolyte.

With the availability of modern tools such as impedance analyzers with which one can sweep from 50 Hz to 40 MHz and computers, this technique is highly useful not only in Materials science but also in many other fundamental and applied sciences such as Solid state Physics, Chemistry, Biology and medicine. By building an equivalent electrical circuit from the observed frequency response, one gets a valuable information about the microlevel processes in the material.

1.5 Modelling with circuit elements

As the need for the impedance spectroscopy methodology increased, several researchers started working on suitable hardware and software tools One major task in the impedance spectroscopy technique is the estimation of equivalent circuit parameters from the impedance data Various models have been proposed to support the observed data The different equivalent circuits and their admittance plots (Y_I vs Y_R) are shown in fig 1 1

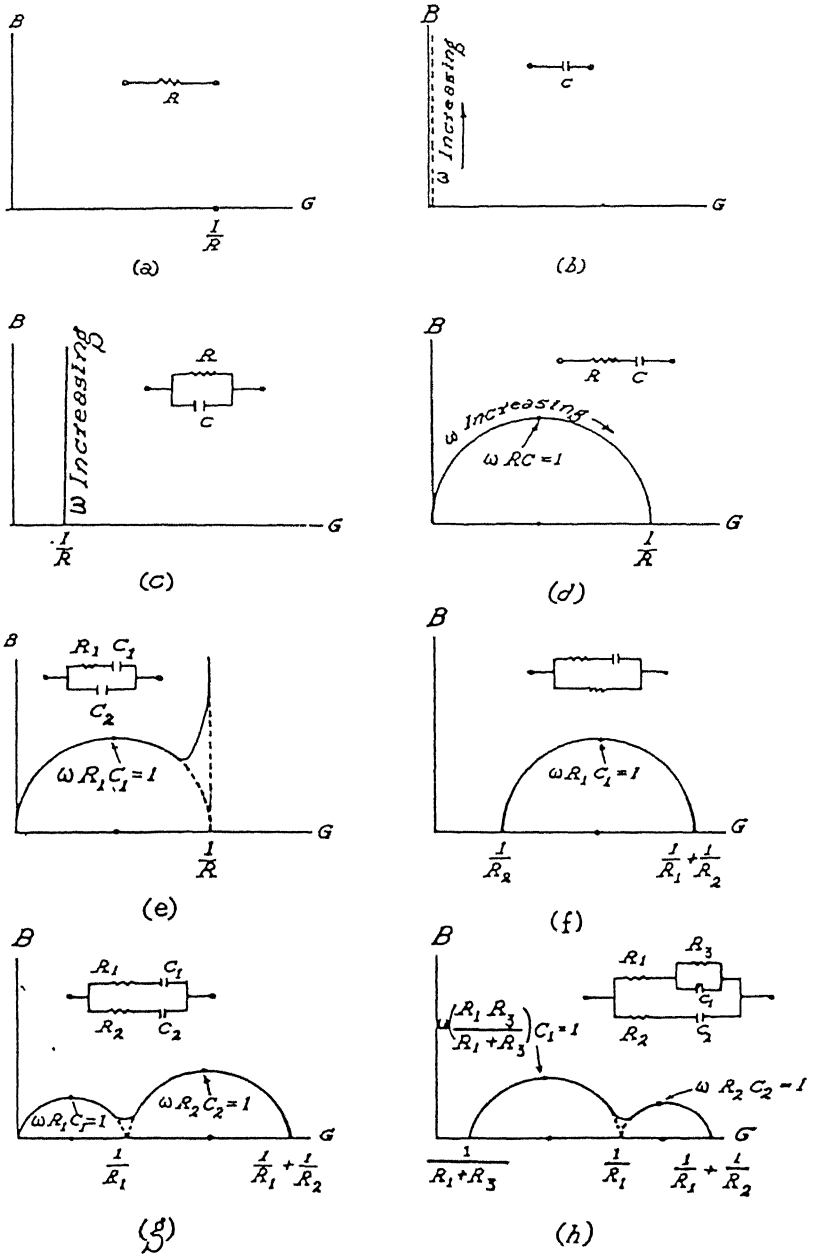

Fig 1.1. Admittance plots for some simple R-C circuits.

Macdonald and Garber[40] have discussed general theory of complex nonlinear least square fitting (CNLS) as applied to impedance data Boukamp[41] developed a package for impedance/admittance analysis An excellent review of all relevant literature on impedance spectroscopy has been presented by Macdonald[42] and now it is available in the form of a book

When a dielectric material is placed between the two electrodes of a sample holder, the sample is modelled as a parallel combination of resistance and capacitance The idealized equivalent circuit for this is the Debye circuit as shown in fig 1 2

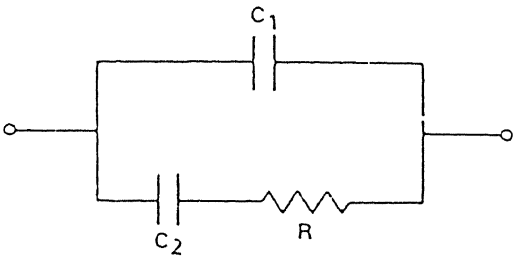

Fig. 1.2. Debye circuit

This circuit predicts a perfect high frequency semicircle in the complex impedance plane This type of behaviour is often seen for the single crystal samples and the bulk conductivity is determined unambiguously from the real axis intercept However, some times more complicated configurations have to be employed to explain the observed complex impedance/admittance plots For example, the behaviour of polycrystalline solid electrolytes is not as simple and obvious. Ravaine and Souquet[43] proposed a circuit, where a circuit element called constant phase element (CPE), is connected in parallel with the bulk resistance. Refer Fig 1 3.

This CPE accounts for the distribution of relaxation time and it describes nicely the observed depressed semicircle in the complex impedance plane In light of this, several theoretical models have been proposed. These models have satisfactorily explained the various factors

e g block electrodes, adsorption of ions etc More importantly one has to be very cautious before comparing the data of various authors, because the actual experimental arrangements

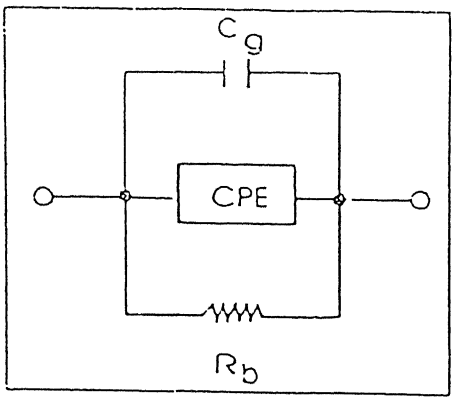

Fig. 1.3. Equivalent circuit for a typical polycrystalline material

used in solid electrolyte studies in different laboratories are different not only in the types of equipment but in the methods of analysis, so it is advisable to know the limitations of experimental arrangement before comparing the data of various authors[44]

1.6 Depressed semicircles

One important feature that has attracted attention in the complex impedance analysis is the depression of semicircles in the impedance plane. In most cases, instead of an ideal Debye type of semicircle, where the centre lies on the real axis; the circular arc with centre lying below the real axis has been noticed. This gives angle of depression, θ. Matsui mentioned in his classical paper[39] the depressed semicircle with its centre lying below the x-axis for Fe_2O_3 -doped Yttria stabilized zirconia (YSZ). To express the arc, a large number of empirical distribution functions have been developed over the years, one of the most important being that due to Cole and Cole[45]. The Cole-Cole equivalent circuit satisfactorily explains the depressed semicircle Fig 1 4.

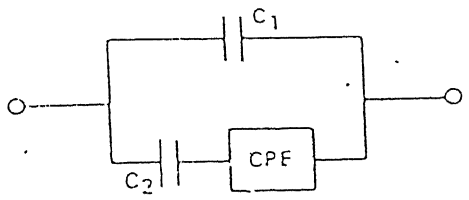

Fig 1 4 Cole-Cole equivalent circuit

Polycrystalline materials are not quite so simple to understand. Two things happen when the density of a ceramic solid electrolyte is lowered[46]. First, at high densities, the conductivity begins to show appreciable frequency dependence. This manifests itself in a lowering of the centre of the high frequency impedance semicircle below the real axis The most useful description seems to be in terms of the constant phase element mentioned earlier

1.7 Aim of the present work

The present studies are aimed at examining the effect of doping on the conductivity enhancement, dielectric properties, phase behaviour of BSO, sintering and single crystal X-ray studies on BSO doped single crystals.

i) Three samples of single crystals namely BSO pure , BSO doped with 2 mole % of Al_2O_3 and BSO doped with 2 mole % of MgO were grown by using the Czochralski technique

ii) Three polycrystals of BSO pure, BSO doped with 2 mole % of Al_2O_3 and BSO doped with 2 mole % of MgO were synthesized through the powder route.

iii) Powder XRD on powders and pressed pellets have been taken to confirm the formation of compounds as well as in the determination of lattice parameters and the crystal system.

iv) Differential thermal analysis (DTA) was carried out on all the six samples (single crystals and powders) which pinpoints the temperature at which the phase change occurs as well the purity of the sample.

v) Density of sintered polycrystals were measured using Xylene test and compared with the geometric method .

vi) Single crystal XRD data on BSO,BSO :Al and BSO:Mg crystals were taken and the lattice parameters were compared with that of the powder XRD .

vii) An attempt was made to solve the single crystal structures of doped BSO crystals

viii) Using HP 4192A impedance analyzer, complex impedance and dielectric measurements over a wide frequency range (500 Hz to 10 MHz) and at various temperatures starting from room temperature to 700° C were carried out. From the experiments the various bulk properties such as dc conductivity, ac conductivity, dielectric constant and dielectric loss have been extracted

Chapter 2

Experimental Details

In this chapter the preparation of polycrystals and single crystals of BSO in pure and doped forms is discussed in detail as well as the characterization techniques. Various experimental techniques used for synthesis and characterization of these materials have been elucidated.

2.1 Preparation of BSO pure and doped polycrystals

The two starting materials required for the synthesis of BSO powder are Bi_2O_3 and SiO_2.

Physical properties of Bi_2O_3

Molecular weight - 465.96

Crystal system - Monoclinic

Lattice parameters - a= 5 8499(3) A°

b= 8 1698(4) A°

c= 7 5123(3) A°

Space group - $P2_1/c$

Density - 9.364 gm/cc

colour - Light yellow

Melting point - $825 \pm 3^{\circ}$ C

Boiling point - 1890° C

Refractive index - 1.91

Physical properties of SiO_2

Molecular weight - 60.08

Crystal system - Hexagonal

Lattice parameters - a = 4.91344(4) A°

b = 4.91344(4) A°

c = 5.40524(8) A°

Space Group - $P3_221$

Density	-	2.649 gm/cc
color	-	White
Melting point	-	1610^{O} C
Boiling point	-	2230^{O} C (2590)
Refractive index	-	1.544

Bismuth Oxide (Bi_2O_3) of 99 99 % purity (powder of < 10 μ size) made by Aldrich Chemical Co USA and SiO_2 (powder of 0.8 μ size) made by Johnson Matthey were thoroughly mixed together in an agate mortar and pestle in a stoichiometric ratio of 6·1[25]. Acetone is added to enhance the homogeneity of the mixture The mixture is then calcinated in a furnace at a temperature of 640° C for 23 hours and quenched. Solid state reaction of oxides involves the inter diffusion of the ions concerned to form a compound or solid solution which may or may not be homogeneous in composition. The time taken to reach a given level of homogeneity depends on the size and physical state of the interacting particles. If grinding is combined with mixing,defects are introduced into the particles at the same time as they are reduced in size. The grinding action also breaks up aggregates so that a random mixture of the crystals of the components can be achieved. Homogeneity is greatly improved when powders are ground together, calcined and ground again. A second calcination and grinding can also be beneficial. The purpose of calcination is to promote sufficient interaction between the constituents to form a material. The calcinated powder is subjected to Powder XRD so as to confirm the formation of BSO powder

This is followed by pelletization(as discussed in the next paragraph) at 6 ton/cm^2. Before making the pellets a small amount of Polyvinyl alcohol (PVA) binder is added to the powder mixture. Oxide pellets are generally fragile in nature and to avoid the pellets being broken, the binder is added. Then the pellets are sintered at a temperature of 750° C for 8 hrs. The density of the pellets has been measured with the help of Xylene test as well as by the Geometrical method (as discussed in section 2.5). During sintering the binder flies off . The sintered pellet is also checked through XRD.

Two doped compositions of BSO are synthesized.They are

1.BSO doped with 2 mole % of γ - Al_2O_3 powder

2.BSO doped with 2 mole % of MgO powder

The same procedure as mentioned above for the preparation of BSO pure powder and polycrystals, was followed in the preparation of the doped powder and pellets Table 2 1 gives the preparation details of the samples of pure and doped compositions

2.1.1 Preparation of pellets (Polycrystals)

The fine powder of each composition (with binder) was transferred to a stainless-steel die which is shown in Fig 2 1 After levelling the powder by means of the die-piston, the whole assembly was placed in a hand-operated hydraulic press. The pressure used in all cases was 6 ton/cm^2 The piston diameter fixed the diameter of the pellets at 1.1 cm, while the thickness of the pellets usually ranged between 0 2 and 0 3 cm Thorough cleaning of the die with acetone, before and after use was observed as a usual practice. Pellets were kept in small specimen bottles which in turn were stored in a vacuum desiccator for further use

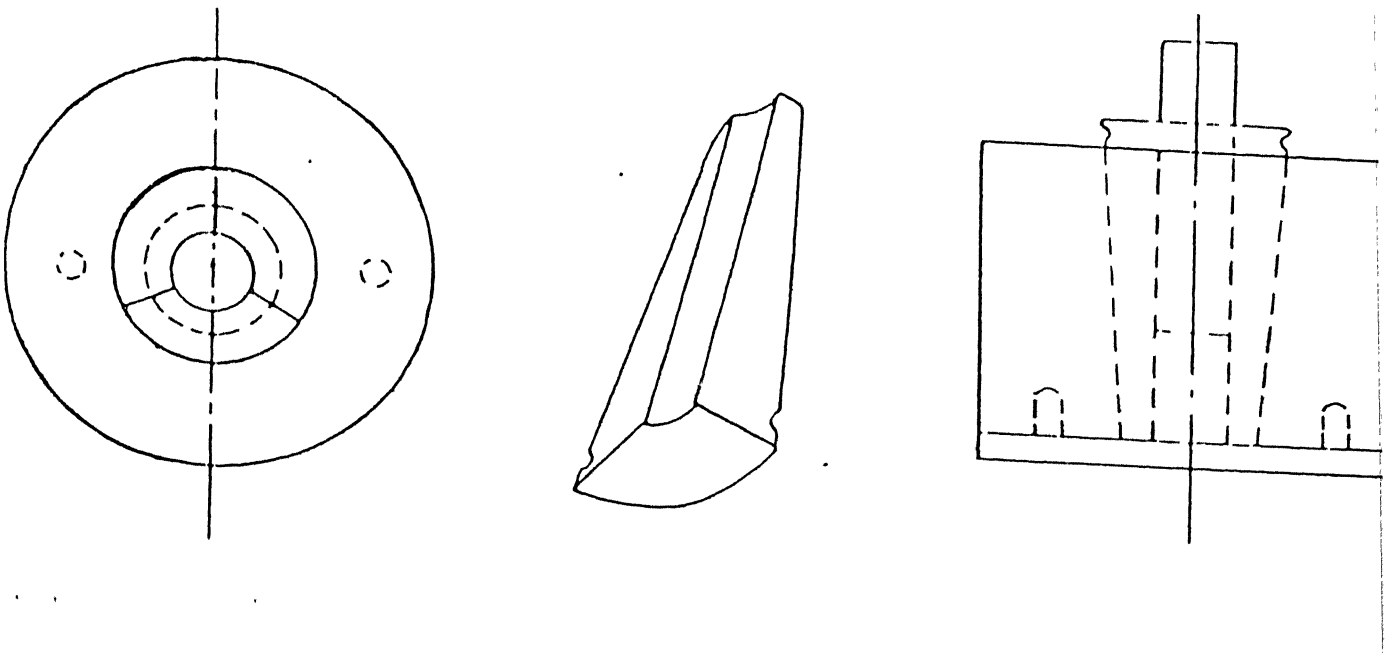

FIG 2.1 STAINLESS STEEL DIE FOR MAKING PELLETS

Table 2.1

Details of preparation of Polycrystal samples

Composition	Wt.of Bi_2O_3 (gms)	Wt of SiO_2 (gms)	Wt of γ- Al_2O_3 (gms)	Wt.of MgO (gms)	Pelliti-zation pressure (ton/cm^2)	Calcination Temp and Time
Pure BSO	9.7900	0 2100	-	-	6	640 ± 10°C 23 hrs
BSO:Al (BSO doped with γ-Al_2O_3)	9.7828	0.2099	0.0073	-	6	640 ± 10°C 23 hrs
BSO:Mg (BSO doped with MgO)	9.7871	0.2100	-	0.0029	6	640±10°C 23 hrs

2.2 Preparation of BSO pure and doped single crystals

Single crystals of Bismuth Silicon Oxide (BSO) are commonly grown by Czochralski technique,the vertical Bridgman method,or the top-seeded technique from an off-stoichiometric melt[47]. The most popular method is the Czochralski technique and the furnaces employed are either resistance heated or radio frequency heated ones. The furnace used in our lab, for growing the crystal is a resistance heated one Suitable rates of pull and rotation had to be maintained to grow crystals of good quality Due to the corrosive nature of the material,and in order to maintain the requisite purity of the crystals, platinum crucible was used for holding the melt .

2.2.1 Seed preparation

The first step in the growth of single crystals is the growth and preparation of seed crystals. This is a very laborious process The initial preparation of the seed is attempted by dipping a platinum wire and pulling it out from the melt Each time a visually acceptable crystal was obtained and suitable portions of the crystals were then cut and subsequently used as seed material. This chain process was repeated a number of times till a good seed crystal was obtained The first few trials were made with platinum wire of about 0.3mm diameter. By adjusting the rate of pull and temperature, so as to make the resulting solid piece as conical as possible or in other words to get a single crystalline grain at the bottom which is then used as a seed.

2.2.2 Pulling and Rotation Systems

For good quality crystal a pulling rate of $\cong$ 2 5 - 6 mm/hr and a rotation rate of 25 $\cong$ 45 rpm is used. Many techniques have been used to control the stepper motors, regarding the above matter. For growing the crystal in our laboratory, the rotation rate and pulling rate were kept at 30 rpm and 4 mm/hr respectively.

2.2.3 Furnace

The resistance wire wound furnaces, utilise a three - zone heating system consisting of(from bottom upwards)a guard zone, a melt zone and an annealing zone This arrangement is desirable since BSO has a high thermal expansion and low thermal conductivity. Thus the

thermal gradients can produce internal stresses which in turn can lead to the formation of cracks etc. A three-zone furnace was designed and fabricated in Dr..K.V.Rao's laboratory to accomplish the task with the pulling and rotation system .

2.2.4 Crystal Growth

Pure BSO boules were pulled from the melt in our laboratory in a specially fabricated Czochralski growth system in air. The crystals were grown using a platinum crucible and Kanthal wire wound furnace.A stoichiometric mixture of Bi_2O_3 and SiO_2 powders in the ratio 6:1 were used for growing pure BSO crystals. During the growth process the pulling and rotation rates were kept at $\equiv$ 4 mm/hr, and $\equiv$ 30 rpm respectively. The crystal boule was oriented by the X-ray method and from it a slice of about 1 mm thick and area of 100 mm^2 was cut along a particularplane. The two flat faces of the sample (crystal) were coated with silver paint and then it was introduced into the sample holder for taking measurements.

It should be noted that a failure in the crystal growth can result not only in the wastage of the material and time but also the loss of the seed crystal itself. Therefore it is necessary to have at least three prepared seed crystals readily at hand all the times. In spite of all these precautions, power supply problem did sometimes cause the loss of all the seed crystals. If the seed crystals are lost, then there is no other way except to start from the beginning. However this problem can be overcome by using the UPS system.

The doped single crystals can also be grown in the same manner as mentioned above for the BSO pure single crystals. The two doped single crystals grown are

1. BSO doped with 2 mole % of γ - Al_2O_3
2. BSO doped with 2 mole % of MgO

These single crystals were grown by Dr. K.V. Rao and Coworkers.

2.2.5 Crystal Cutting,Grinding,and Polishing

The single crystals grown above were cut with a Metals Research Microslice -2 crystal cutter,employing a very thin (50 μm) diamond impregnated blade. The crystals are usually mounted in wax. After cutting the crystal, it is removed carefully, by warming the base. Due to the brittle nature of the material and thermal stress problems, great care has to be exercised during this process. The cut crystal is then ground on a glass plate with various grades of silicon carbide powder and the final polishing was done on a rotating aluminium base fitted with polishing cloth, loaded with γ - alumina.

2.3 Phase diagram of Bi_2O_3 - SiO_2 system

Phase diagrams of the Bi_2O_3 - MO_2 (M=Si,Ge etc) systems were originally determined by Levin and Roth[48] and revised by Takamori and Watson[49] for the Bi_2O_3 - SiO_2 system However all these phase diagrams show only the equilibrium phases after synthesis,and the phase transitions during the reaction process do not seem to have been reported[47]. Here, part of the phase diagram of Bi_2O_3 SiO_2 system and complete phase diagram of Bi_2O_3 - SiO_2 system are shown in figures Fig 2 2 and Fig 2 3

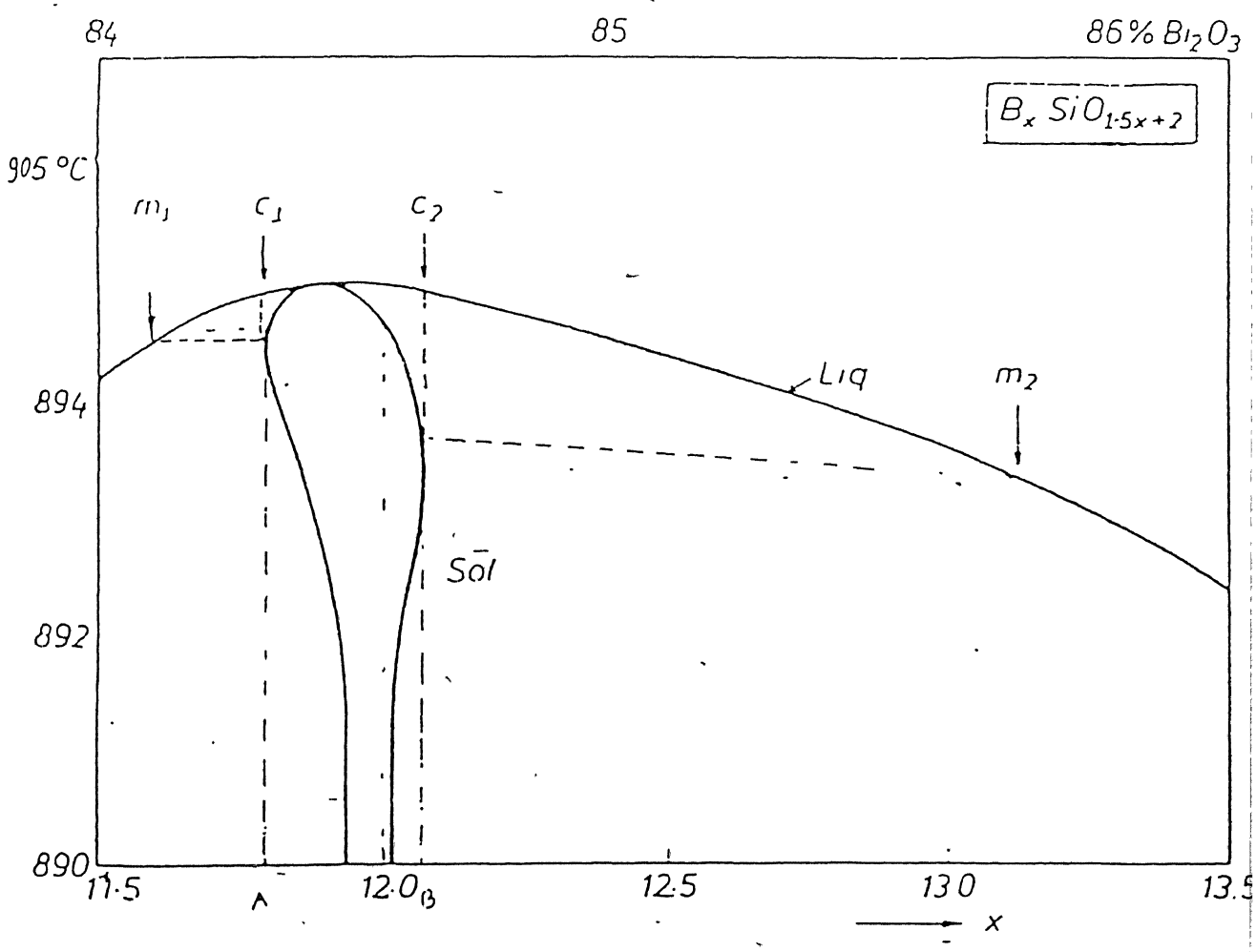

Fig. 2.2 Part of the phase diagram for the system Bi_2O_3 . SiO_2

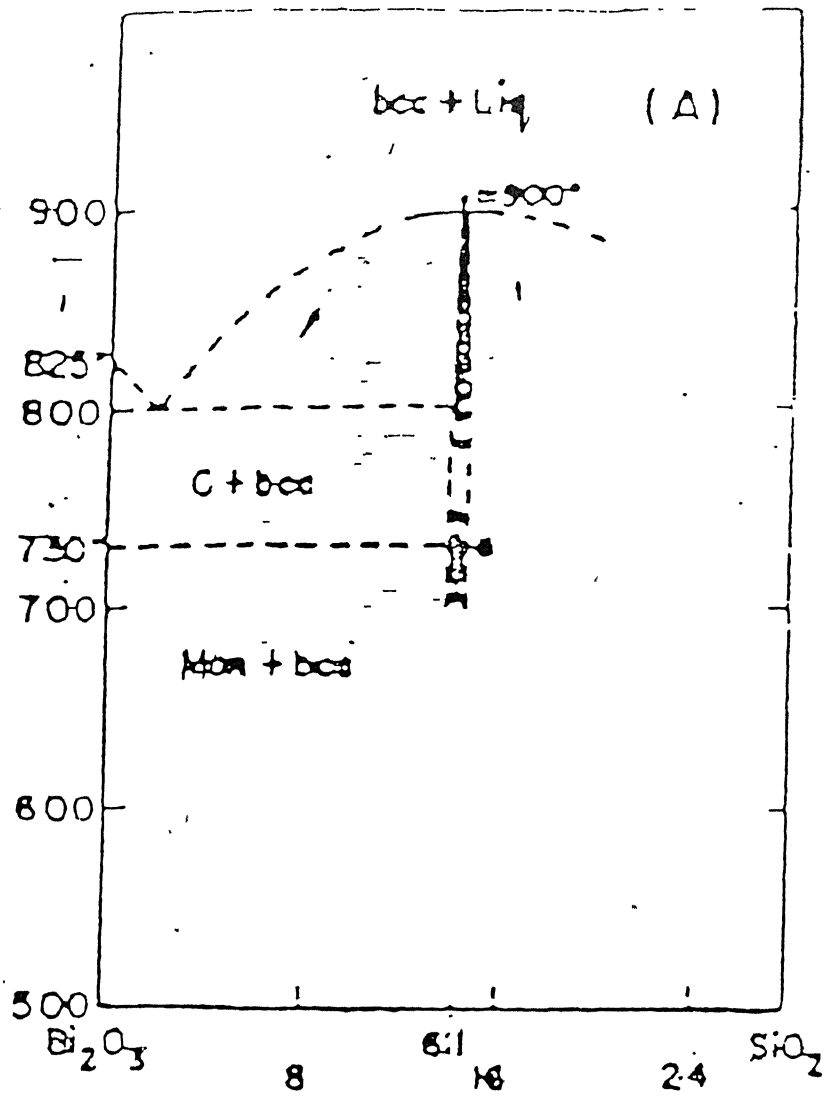

Fig. 2.3 Complete phase diagram of Bi_2O_3 . SiO_2 system

2.4 Complex impedance analysis measurement

The electrical conductivity measurements as a function of temperature requires a furnace,a sample holder,a temperature controller and an impedance bridge.The sample holder and the furnace were designed and fabricated locally in our laboratory as discussed below.

2.4.1 Furnace

Kanthal wire of 2mm diameter was wound inductively and uniformly at the rate of about 10 turns per inch on a mullite tube (18 inches in length and 2 25 inches in diameter) . The total resistance of the heating element was ≈ 34 ohms A layer of pellendum fire cement was applied over the heating element so that no kanthal wire was visible from outside. A high temperature current was applied directly over the windings to a thickness of about 0.5 inch, and then allowed to dry at room temperature for a few days and later a small current was passed to further dry up the cement.

The mullite tube wound with kanthal wire was housed in a cylindrical aluminium shell which was open at both ends. Two asbestos plates and aluminium circular plates were used to cover the two flat ends of the furnace and were fixed in place with screws. The space between the mullite tube and aluminium enclosure was filled with MgO powder to minimize the heat loss.

2.4.2 Sample Holder

Fig.2.4 shows the schematic diagram of the sample holder used for electrical conductivity measurements. Using this sample holder one can do the two probe resistivity and dielectric measurements from room temperature to 1200° C. It consists of an inner body of three identical lava discs. The outstanding qualities of lava material are that it is machinable,can withstand high temperatures (upto 1400° C) and a good electrical insulator. The lava discs which can be moved smoothly along the two parallel stainless steel support rods, in combination with the spring and the quartz tube, applies uniform pressure to ensure a firm contact between the electrodes and the sample. A Chromel - Alumel thermocouple leads pass through one of the holes of the lava discs as well as through a double holed thin alumina rod. Two silver lead wires one of which passes through the quartz tube, are brazed to two platinum electrodes as shown in fig.2.4. The silver lead wire which passes

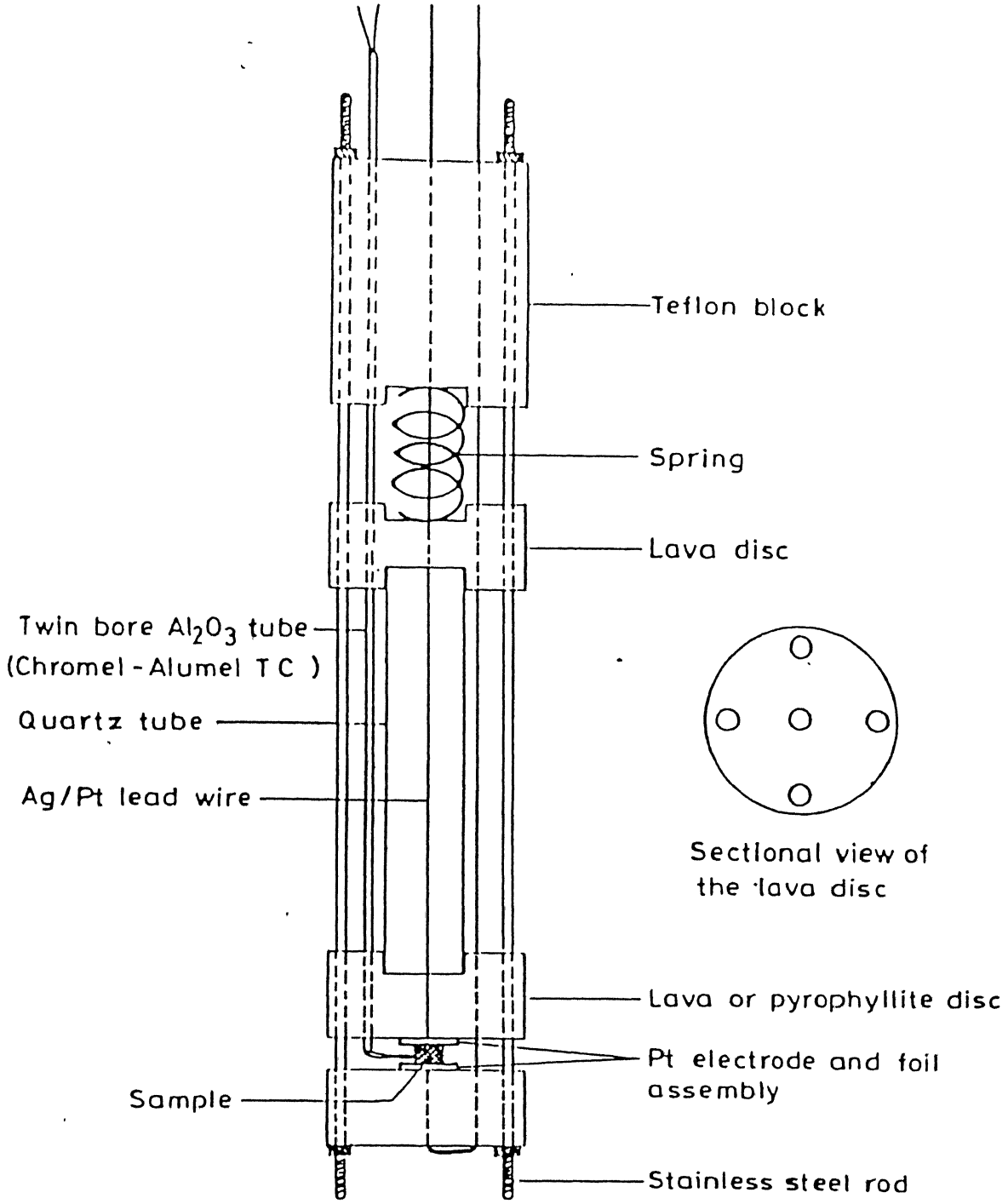

FIG 2.4 SAMPLE HOLDER FOR ELECTRICAL CONDUCTIVITY MEASUREMENTS FROM ROOM TEMP. TO 1000° C

through the quartz tube, eventually comes through the central hole of the teflon block while the other one comes via.the lava disc hole The spring located outside the furnace is used to exert a sufficient and uniform pressure required for point to point contact between the electrodes and the sample.

The lava discs, after machining were heated slowly to 1000° C and kept at that temperature for 2 hours before cooling inside the furnace This kind of heat treatment is necessary to harden the lava disc and also to remove any moisture content The effect of the latter is to increase the resistivity of the disc significantly

2.4.3 The Experimental set-up

This work involved extensive electrical conductivity measurements. A block diagram of the set up used is given in Fig 2.5 The temperature inside the furnace was controlled by using an Indotherm temperature controller (Model 401) A Keithley microvolt DMM (model HIL -2301)was used to measure the thermocouple voltage and hence the temperature. (We use Chromel - Alumel thermocouple and from the calibration tables for the thermocouple the conversion from μV to the corresponding temperature is made) The accuracy of the DMM is ± 1° C A Low frequency Impedance analyzer HP- 4192 was used for impedance measurements at various temperatures. Using this instrument one can sweep the frequency from 50 Hz to 13 MHz.

Before we start measuring the impedance of the samples,the two flat surfaces of the cylindrical pellet was first polished on different grades of fine polishing papers to remove surface contaminations and to obtain parallel and smooth surfaces This was followed by coating the two surfaces of the pellet with silver paint in order to avoid the air gap effect between the electrode and the sample. The sample was then loaded onto the sample holder and kept between two platinum electrodes of same diameter as the pellet. These platinum electrodes ensure proper contact between the sample and the electrodes. Also platinum can withstand very high temperatures. As temperature increases the electrical contact becomes very strong. The sample holder was then put inside the furnace which was closed at one end to ensure a steady state to be reached rapidly. Having loaded the sample in the holder, the tip of the Chromel - Alumel thermocouple wire was placed as close to the sample as possible to measure as well as to control the temperature of the sample For each sample the room temperature measurement was done followed by measurements at high temperatures upto

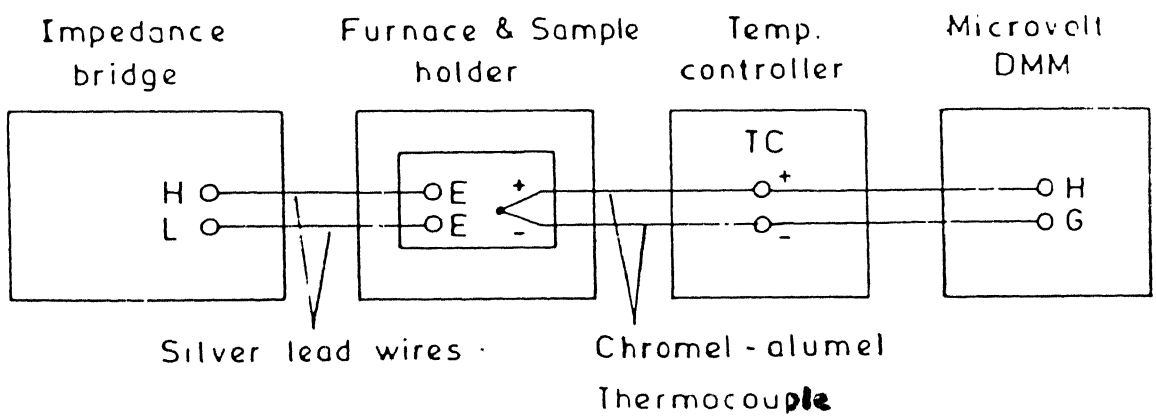

FIG 2.5 Block diagram connections for electrical conductivity measurements

700° C For each temperature the instrument was kept for more than 15 minutes so as to attain the thermal equilibrium. For each temperature the Z, θ values as well as C,D values at different frequencies (500 Hz - 10 MHz) were measured.

2.4.4 Theory of Complex impedance Analysis

When the sample is kept between the electrodes of the sample holder, the arrangement looks like a capacitor with a dielectric between them The electrodes of the sample holder act as parallel plates and the sample acts like a dielectric. The equivalent circuit for such arrangement can be expressed as the parallel combination of Resistor (R) and Capacitor (C) For RC parallel combination we have the net impedance Z(ω) whcih can be written as follows

$$Z(\omega) = R\,(1/j\omega C) / (R + 1/j\omega C)$$
$$= R/ j\omega C(R + 1/j\omega C)$$
$$= R/ (j\omega CR + 1)$$

This can be written as,

$$Z(\omega) = R - j\omega CR^2/ (1 + \omega^2 C^2R^2)$$

If Z' and Z'' denote the real and imaginary parts of the complex impedance Z(ω) then

$$Z' = R / (1 + \omega^2 C^2R^2) = Z\cos\theta$$
$$Z'' = -R^2\omega C/ (1 + \omega^2 C^2R^2) = Z\sin\theta$$

from these 2 equations , $(Z')^2 + (Z'')^2 = Z' * R$

This can be modified as

$$(Z' - R/2)^2 + (Z'')^2 = (R/2)^2$$

this equation describes the equation of a circle of radius R/2 with centre (R/2,0)

So,if we plot a graph,taking Z' along the X axis and Z'' along the Y axis, then the plot will be a semi circle, having a radius of magnitude R/2. Therefore the diameter of the semicircle gives the value of the resistance R. The value of C can be evaluated by putting the value of R in any

one of the above equations. Similarly one can measure admittance values Y(ω) for different frequencies and from that also resistance can be deduced.

Y(ω) is nothing but 1/Z(ω)

$$Y(\omega) = Y' + jY''$$

where $Y' = 1/R = Y\cos\theta$

$$Y'' = \omega C = Y\sin\theta$$

2.4.5 Measurement details

The HP - 4192 A Low frequency Impedance Analyzer can accurately measure the impedance parameters of a component or a circuit at various frequencies,test signal levels and dc bias levels . The ranges available are .

(1). Frequency · 5 Hz to 13 MHz
(2). OSC level . 5mV rms to 1.1 V rms
(3). DC bias voltage : -35 V to +35 V

Frequency of the signal and bias voltage can be automatically swept in full range, and in either direction. OSC level can also be swept (manual only) at 1 mv steps (5 mV steps at levels above 100mV).

For connecting the sample to be tested, the HP - 4192A employs measurement terminals in a four terminal configuration which has a significant measuring advantage for component parameter requiring high accuracy in the high frequency region. Generally any mutual inductance, interference of the measurement signals, and unwanted residual factors in the connection method which are incidental to ordinary terminal methods significantly affect the measurement at a high frequency. The four terminal pair configuration measurement permits easy,stable and accurate measurements and avoids the measurement limitations inherent in such effects. Fig.2.6 shows the four terminal pair configuration which consists of four connnectors:

They are High current (H_{cur}), High potential (H_{pot}), Low current (L_{cur}) and Low potential (L_{pot}) The purpose of the current terminals is to cause a measurement signal current to flow through the device under test or sample. The potential terminals are for detecting the voltage drop across the sample. The main principle is that, the signal current does not develop an inductive magnetic field and thus the test leads do not contribute additional measurement errors due to self or mutual inductance between the individual leads However, the four terminal system must be converted to a two terminal configuration at/near to the sample because the sample/device under test has only two leads

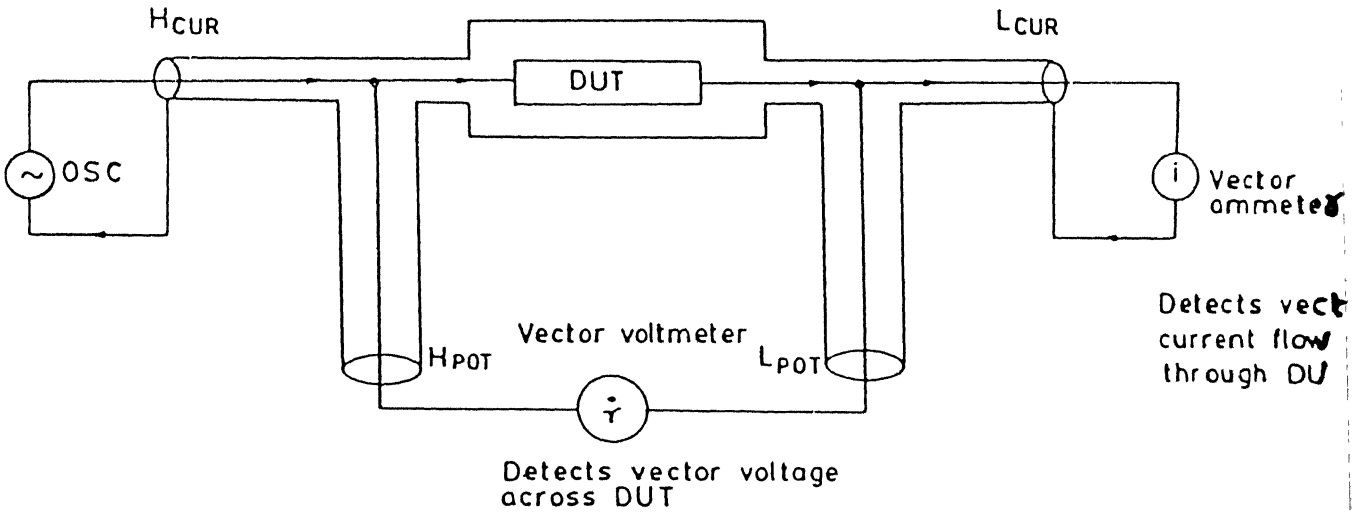

Fig.2.6 Four terminal pair measurement principle

The impedance of a component can be expressed in vector representation by a complex number as shown in Fig 2 7 In such a representation, the effective resistance and effective reactance correspond to the projections of the impedance vector (Z,θ) on the real axis (R) and imaginary axis (jX) ,respectively. When the phase angle θ changes , both Re and x change in accordance with the above definition.The measurements made by this instrument were then analyzed by using the complex impedance plots.

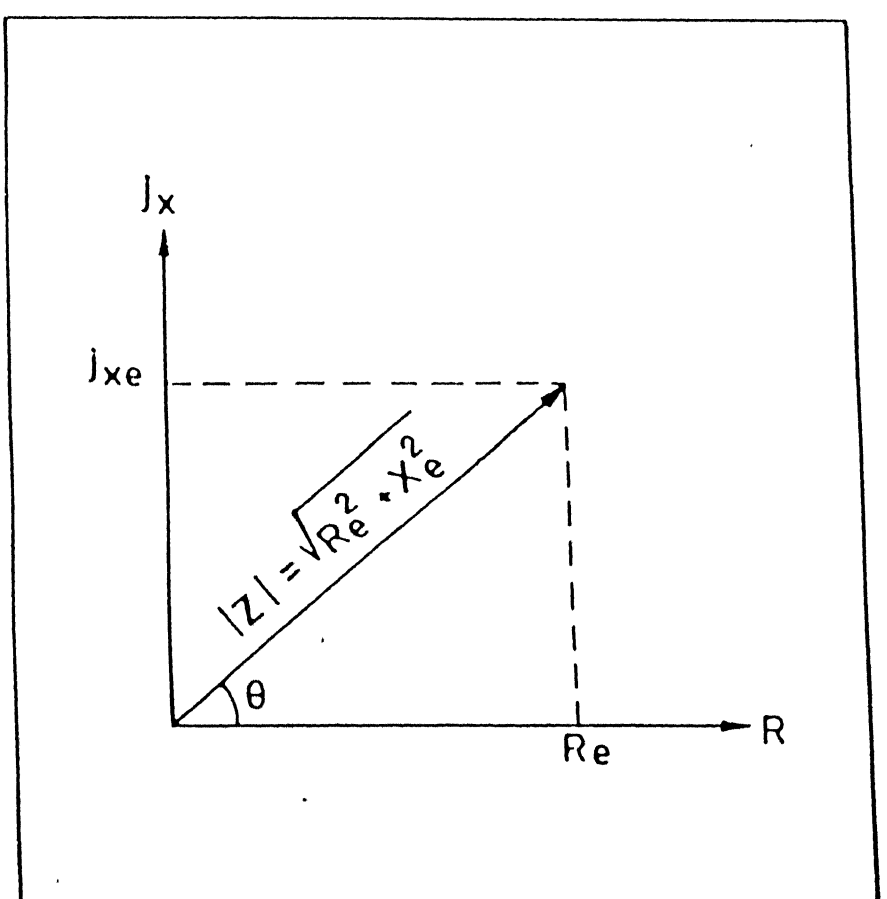

FIG 2.7 IMPEDANCE VECTOR REPRESENTATION

2.4.6 Complex impedance plots

Complex impedance plots are useful for determining an appropriate equivalent circuit for a system and for estimating the values of the circuit parameters. The complex impedance $Z(\omega)$ of a system at an applied angular frequency ω, can be expressed as the sum of a resistance $R(\omega)$ and a reactance Xe

$Z(\omega) = R(\omega) + j\, Xe(\omega)$

This can be written as follows.

$$Z(\omega) = Z' + j\, Z''$$

Where $Z' = |Z|\cos\theta$ and

$Z'' = |Z|\sin\theta$

Phase angle $\theta = \tan^{-1}(Z''/Z')$ and $|Z| = ((Z')^2 + (Z'')^2)^{1/2}$

If one plots the real part of the impedance along x-axis and imaginary part of the impedance along the y -axis i.e. $Z\cos(\theta)$ Vs $Z\sin(\theta)$ the resulting locus shows distinctive features for certain combinations of circuit elements. The method is best illustrated by specific examples of such plots and are shown in section 3.7 for some simple circuits. By seeing the plot one can say that each semi circular arc corresponds to a "lumped R-C combination". The diameter of the semi circular arc is nothing but the resistance of the circuit.

2.5 Density measurement

The density of the polycrystals (pellets) was determined by using

1. Xylene test
2. Geometrical method

2.5.1 Xylene test

The density of the pellets was determined by using the formula

Density $= W_1 / (W_2 - W_3)$

where W_1 = wt.of the pellet in air

W_2 = wt.of the pellet in xylene

W_3 = wt.of the pellet in water (excluding the wt.of the suspension wire)

The sintered pellet has to be taken for the density measurement. Initially the wt of the sample(W_1) whose density is to be determined, was measured with the help of an electrical balance. Then the sample was put in xylene. All polycrystals have open porosity and hence the xylene goes and occupies the pores of the pellet. A stream of bubbles indicate the presence of pores and these being occupied by xylene This should continue until all the bubbles disappear. This has to be done in vacuum at a pressure of $\cong 10^{-2}$ torr Then the wt.of the sample with xylene was measured(W_2). Then the sample was again kept in the same vacuum as applied before for 5 minutes and allowed to dry. The dried sample was tied with a wire and inserted into a beaker filled with distilled water and it's wt.was measured. This weight minus the wt.of the suspension wire gives the wt.of the pellet in water(W_3). This is based on Archimedes principle. Here the difference between W_2 and W_3 gives the volume displaced by xylene and this volume displaced is the volume of the pellet. The density is then determined by the formula weight in air / Volume displaced The readings are tabulated in section 3.4.

2.5.2 Geometrical method

Here the pressed pelllet before sintering was taken and it's weight, diameter and thickness were measured first. The pellet has circular area of cross section and this multiplied with thickness of the pellet gives the volume of the pellet. Now density can be easily evaluated by using the formula

Density = wt.of the pellet/ Volume of the pellet.

where ,

Volume of the pellet= π (diameter / 2)^2 * thickness of the pellet

After this the pellet was sintered in the furnace at a temperature of around 750° C for 8 hrs. Now the sintered pellet's weight, diameter and thickness were measured. The denity for the sintered pellet is evaluated next. From this the degree of sintering can be known. This sintered density can also be compared with the theoritical density of the sample. These results are also tabulated in section 3.4.

2.6 Powder x-ray diffraction studies

From Powder XRD, the information about the formation of the compound as a result of reaction between the constituents and the constituent phases present in the sample can be known. Powder X-ray diffraction patterns of powders and sintered pellets have been recorded

using a Rich seifert (ISO - Debyeflex 2002 D) counter diffractometer employing a filtered Cu K_α radition (λ = 1.542 A°). The X-ray generator was operated at 30 kV and 20 mA. The chart speed was fixed at 12 mm/ minute and the scanning speed was 3° / minute in 2θ. All XRD studies were done at room temperature For powder samples, the sample was fixed on glass slides with a drop of methanol

2.7 Single crystal XRD studies

The single crystals of BSO pure and doped ones (BSO doped with alumina and BSO doped with MgO) were subjected to Single crystal x-ray diffraction studies. Single crystals were observed underneath the optical microscope and the crystal of best quality was chosen and mounted onto the Goniometer. Then the Goniometer was kept inside the Enraf-Nonius CAD4 (4 circle) diffractometer controlled by an IBM PC under Enraf-Nonius software. The radiation used was MoKα radiation. 25 standard reflections were collected and from these 25 reflections the crystal system and unit cell parameters were retrieved. The lattice parameters are compared with those of the Powder XRD and are tabulated in section 3.1

2.8 Differential Thermal Analysis (DTA)

The differential thermal analysis of both single crystals and polycrystals were carried out using a Linsies L - 62 Mini Differential Thermal Analyzer. This equipment employs a SiC furnace which can go upto 1500° C. The heating rate employed was 5° C/min in all cases. DTA involves the heating/cooling of the test sample at a constant rate alongwith a reference sample (Al_2O_3 powder) which does not undergo any phase transformation in the temperature range of investigation. Any phase change or chemical reaction accompanied by absorption or evolution of heat can be readily detected by DTA. The phase tranformation temperature can be determined by this method and hence the presence or absence of the phase can be known. The DTA of all the six samples are shown in section 3.5

2.9 Scanning electron microscopy (SEM)

The SEM studies were carried out using Jeol model JSM-840 A. The equipment has a range of magnification from 10x to 300000x. The Scanning electron microscopy (SEM) is the most powerful tool to study the surface topography and morphology with an unprecedented

advantage of depth of field and a capability of studying any surface in its original unaltered state From the standpoint of actual microscopy, the SEM images give topographical details with maximum contrast and depth of field by the detection, amplification and display of secondary electrons The elemental analysis of the BSO pure and doped polycrystals were also carried out and the results are discussed in section 3.6.

The sintered pellet was first thoroughly polished on very fine emery paper and cleaned with acetone.Then the sample was gold/silver coated by using a sputtering unit (International scientific Instruments PS-2 coating unit) before taking micrographs. The micrographs were taken at 10^{-11} A probe current and 15 kV accelerating voltage. The maginfication was fixed according to our need from 3000x to 10000x

Chapter 3

Results and Discussions

Here the investigations on Bismuth Silicon Oxide $Bi_{12}SiO_{20}$ (BSO) are reported. They are discussed in the following manner.

1. Powder XRD studies on BSO
2 Phase change of BSO at various temperatures
3. Comparison of powder XRD with single crystal XRD studies
4 Density measurements
5. Differential Thermal Analysis (DTA) results
6. SEM studies
7 Complex impedance spectroscopy studies
   (a) . RC combination studies
   (b) Conductivity studies
   (c). Dielectric studies
8. Conclusions and future directions

Table 3.1 summarises the general properties of BSO.

Table 3.1

General properties of BSO[50]

Chemical composition : $Bi_{12}SiO_{20}$

Symmetry : Body centered cubic

Point group : 23

Refractive index : 2.54

Transparency (%) : 70

Density (gm/cm^3) : 9.21

Lattice parameter (A°) : 10.103

Electro optic

coefficient (γ_{41}) : 5×10^{-10} cm/V

Optical activity(for $\lambda = 0.633$ μm) : 22° /mm

Powder XRD measurements on BSO powder was first carried out to confirm the formation of the compound. The mixture of Bi_2O_3 and SiO_2 was subjected to calcination, at a temperature of 640° C for 23 hrs and quenched . The resulting powder was taken for XRD studies. The XRD studies confirm the formation of BSO single phase. The 2θ values as well as the relative intensities agree well with the literature[51] . Refer Table 3.2.

Table 3.2

Indexing of Powder XRD data on BSO

2θ (obs)	I (obs)	hkl (std)	2θ (std)	I (std)	hkl (std)
21.6	3	211	21.522	3	211
25.0	22	220	24.894	22	220
27.9	100	310	27.891	100	310
30.7	40	222	30.615	21	222
33.2	72	321	33.134	72	321
35.5	3	400	35.492	3	400
37.8	11	330	37.720	11	330
39.9	12	420	39.843	12	420
41.9	16	332	41.882	16	332
43.8	9	422	43.840	9	422
45.8	16	510	45.728	16	510
49.3	12	521	49.343	12	521
52.8	40	530	52.763	41	530
54.5	16	600	54.420	18	600
56.1	32	611	56.042	28	611
62.2	28	631	62.245	20	631

The preparation methodology was done at a trial and error basis, because of the nature of the various phases associated with BSO. Even though literature is available regarding the preparation of BSO[25,47], nothing concretely tells at which temperature the γ -BSO phase is formed. The formation of various phases associated with BSO at different temperatures is discussed in the next section. Fig 3.1 shows the XRD pattern of BSO powder formed at 640°C. A small amount of Poly vinyl alcohol (binder) was added to BSO powder to avoid the pellets being broken. The BSO powder was then pelletized and sintered at a temperature of 750° C for 8 hrs. The sintered polycrystal was again subjected to powder XRD so as to confirm the single phase of BSO. Fig 3.2 shows the XRD pattern of BSO polycrystal. The relative intensities of sintered pellet of BSO were lower than that of the BSO powder due to compaction.

3.2 Phase change of BSO at various temperatures

As already mentioned in chapter 1, BSO is a very complicated system . It was prepared in our laboratory after much of experience. The various phases that are associated with BSO are shown in figures 3.3,3.4 and 3.5 . Fig 3.3 shows the presence of a doublet with 310 reflection (max.intensity peak) when the Bi_2O_3 and SiO_2 mixture was heated to 700° C for 8 hrs. Fig 3. 4 shows the presence of the doublet again but a different one from that of fig 3.3, when the mixture was heated to 750° C for 16 hrs. Fig 3.5 shows the 310 and 321 reflections are reversed when the mixture was heated to 835°C for 23 hrs. Also when the pressed pellet of BSO was sintered beyond 750° C there appears a doublet in the 310 reflection and the sintered density was also very poor. Similarly when the doped BSO pellets (doped with γ -Al_2O_3 and MgO) are sintered beyond their calcination temperature (640° C) there appears a doublet again in the 310 reflections (max.intensity peaks) of their powder XRDs. The sintered densities of doped pellets also reduce with the appearance of the doublet . This needs further investigation .

3.3 Comparison of powder XRD with single crystal XRD studies

The lattice parameter of pure BSO obtained through the indexing of the Powder XRD pattern, is compared with the lattice parameter as obtained through the single crystal XRD studies. Also Powder XRDs were taken for BSO doped with 2 mole % of γ - Al_2O_3 and BSO doped with 2 mole % of MgO . But these patterns don't throw any light on the doping and

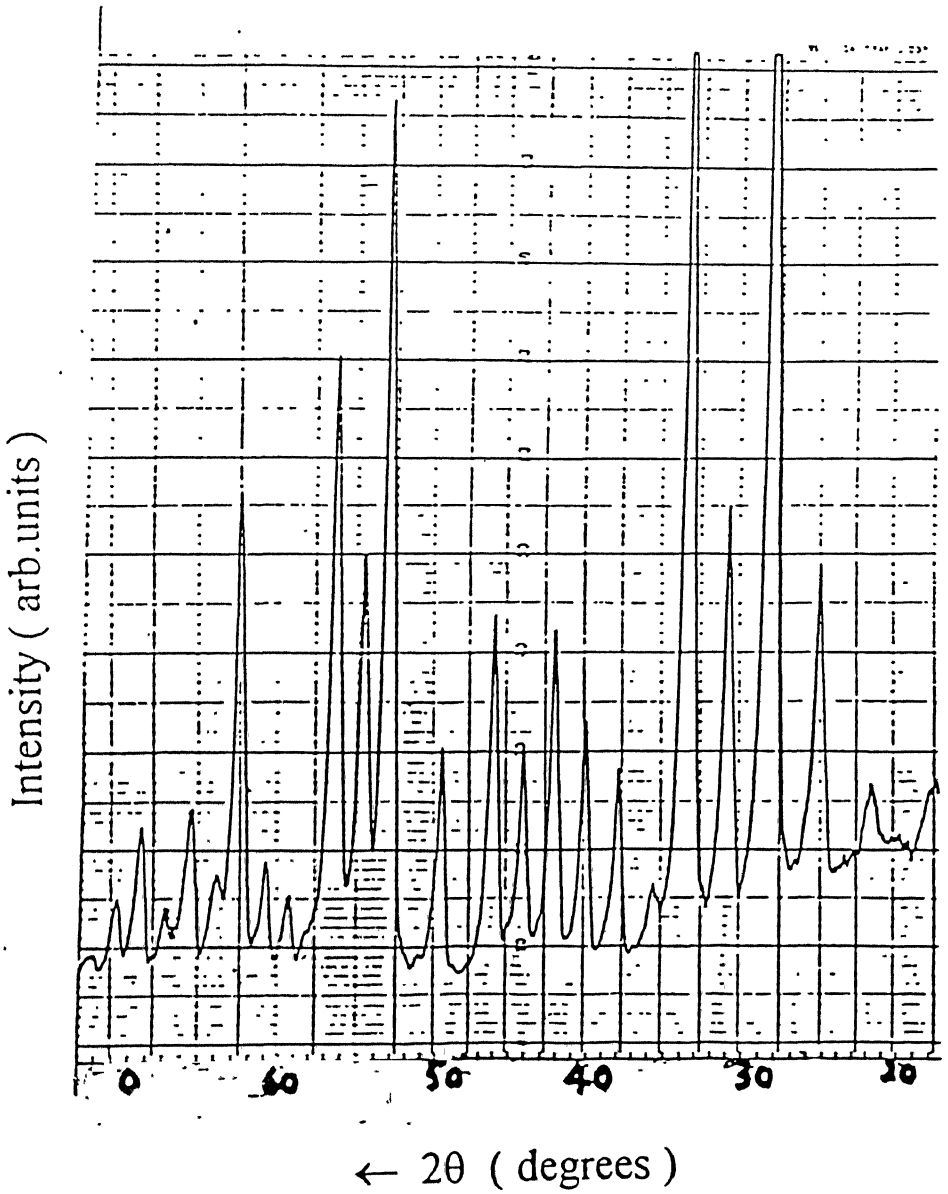

Fig.3.1 XRD pattern of BSO pure powder

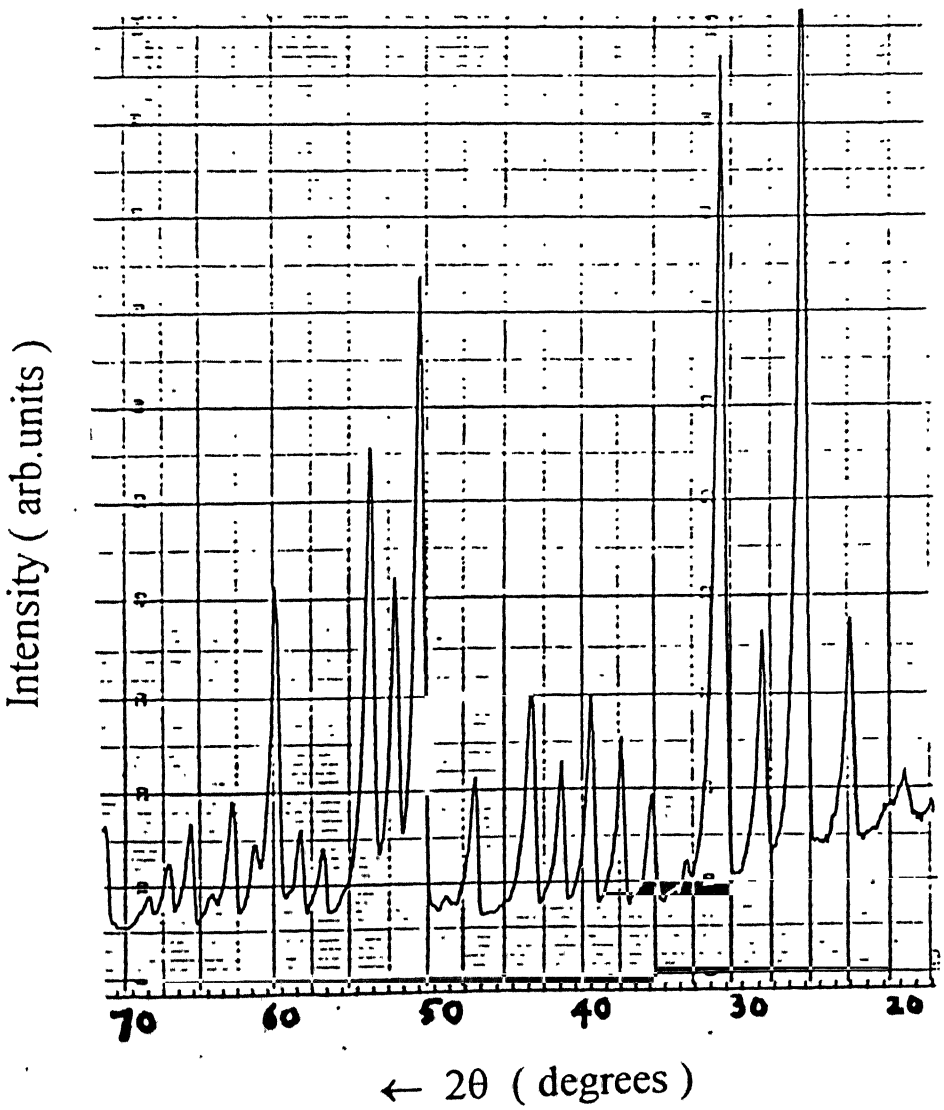

Fig 3.2 XRD pattern of BSO sintered pellet

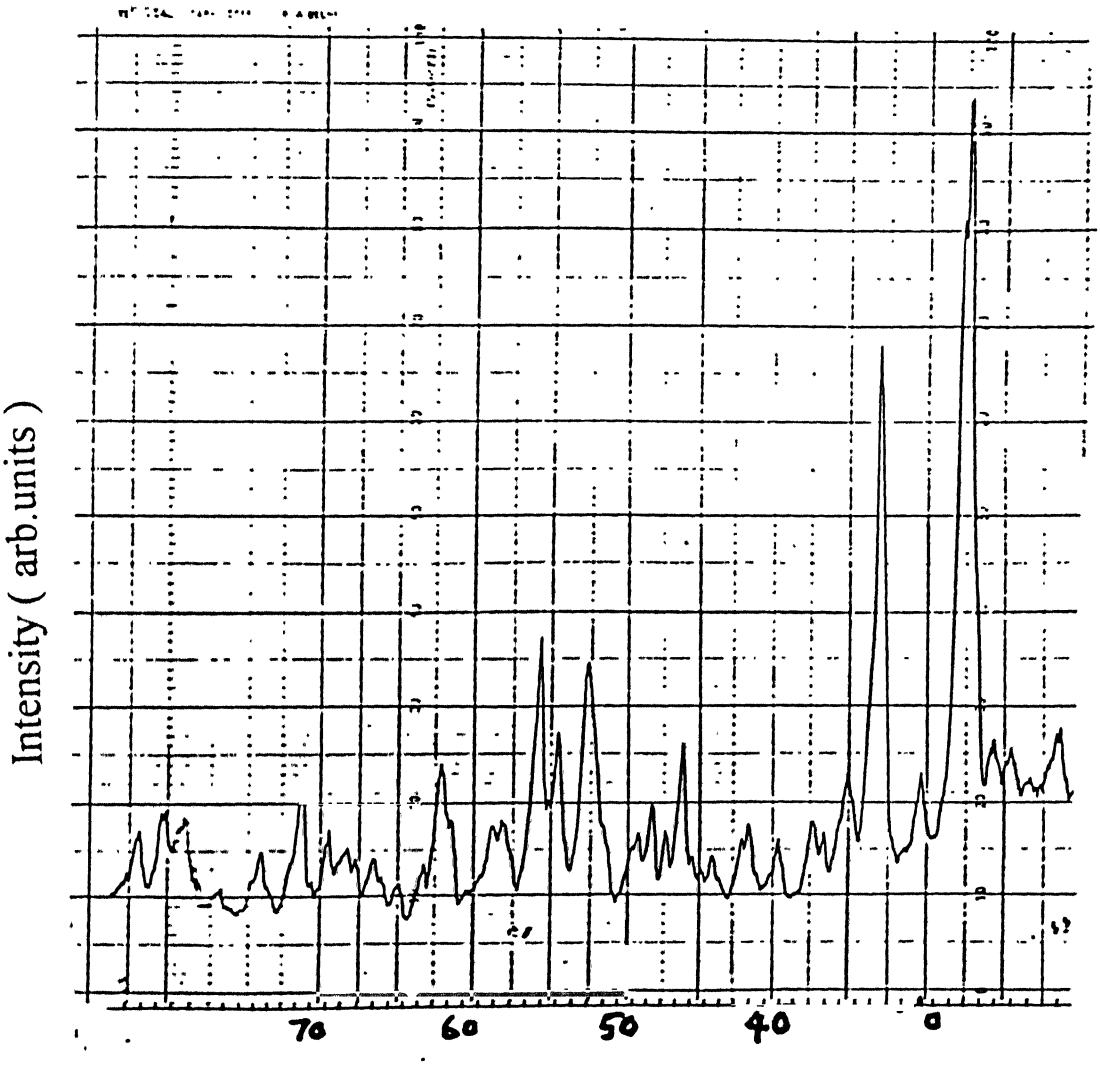

Fig 3.3 XRD pattern of Bi_2O_3 and SiO_2 mixture at 690° C

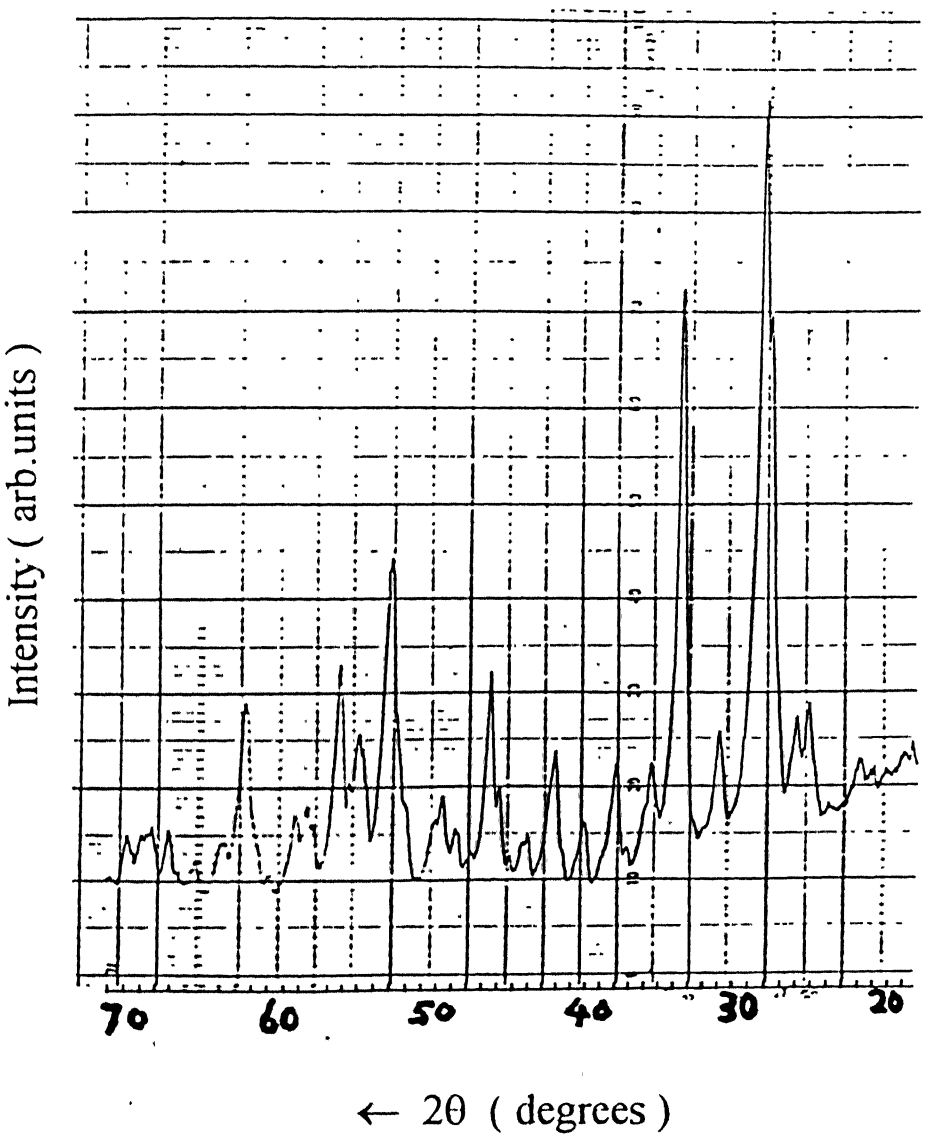

Fig 3.4 XRD pattern of the BSO mixture at 750° C

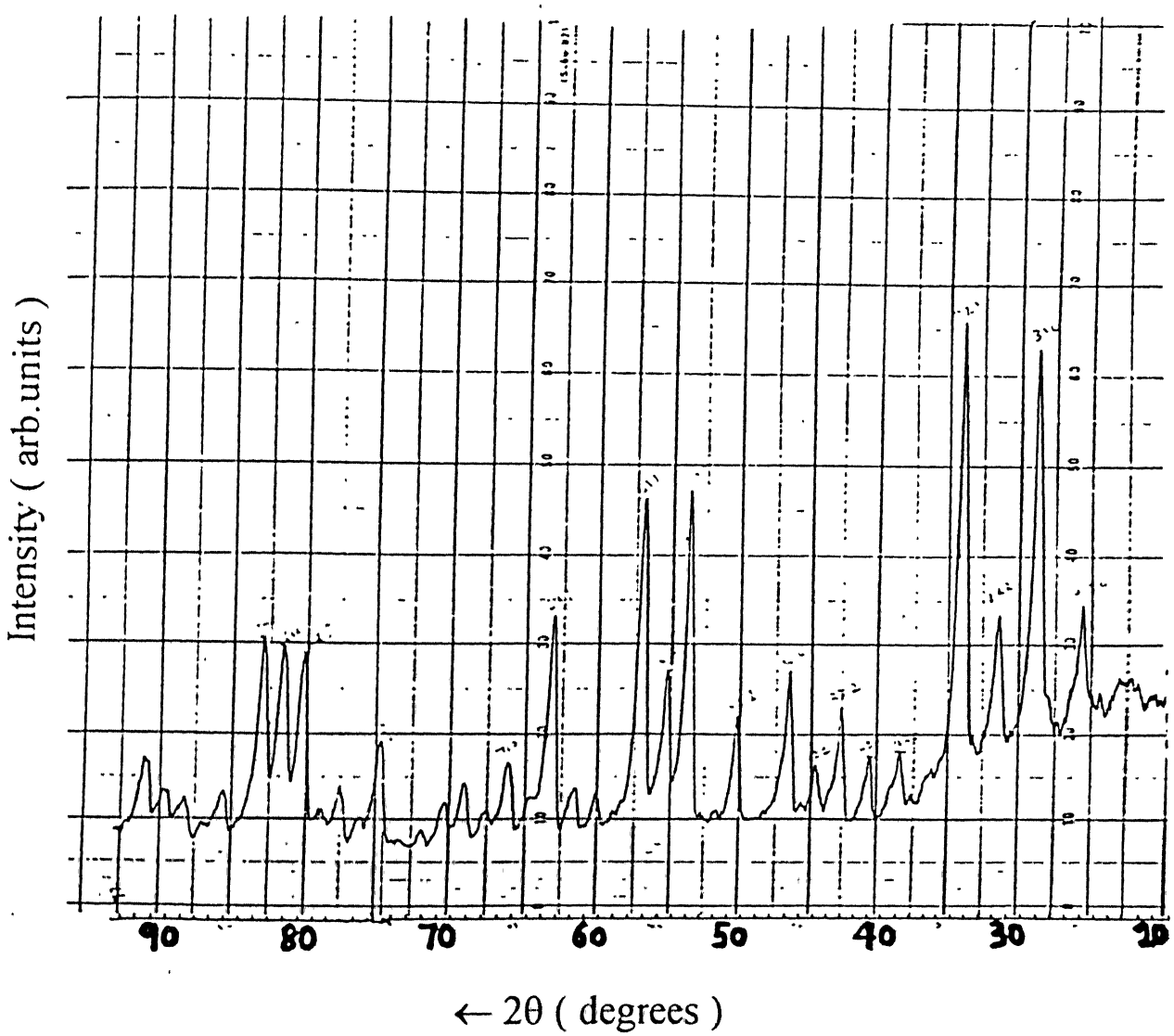

Fig. 3.5 XRD pattern of BSO at 835° C

the XRD patterns of these doped ones are similar to that of the BSO pure XRD pattern. The lattice parameter values, as obtained through the Powder XRD and single crystal XRD studies are tabulated in Table 3.3 as follows:

Table 3.3

Composition	Powder XRD Lattice parameter	Single crystal XRD Lattice parameter
Pure BSO	a = 10.106 A° (Cubic system)	a = 10.081 A° (Cubic system)
BSO (doped with 2 mole % of γ - Al_2O_3)	-	a = 10.063 A° (Cubic system)
BSO (doped with 2 mole % of MgO)	-	a = 10.092 A° (Cubic system)

3.4 Density measurements

The density measurements of BSO pure and doped polycrystals, obtained through the Xylene test as well as by Geometrical method are tabulated in Table 3.4 The densities obtained by both the methods are almost the same. So geometrical method is sufficient for further work. From the density measurements, one can get how much percent the sample has sintered compared to the theoretical density. Sintering will aid the increase in density.

For single crystals the density is calculated as follows:

No.of molecules/volume = Avagadro no. × density/ molecular weight

From this we can get the theoretical density.

BSO was sintered at a temperature of 750° C for 8 hrs

BSO Al and BSO.Mg were sintered at a temperature of 640° C for 8hrs.

Table 3. 4

Composition	Xylene test		Geometrical method	
	Density(gm/cm^3)	Relative density(%)	Density(gm/cm^3)	Relative density(%)
Pure BSO	8.400	91.21	8 415	8.415/9 21=91.368
BSO (doped with 2 mole % of γ - Al_2O_3)	6.375	70.04	6.380	6.380/9 102=70.09
BSO (doped with 2 mole % of MgO)	6.40	70.33	6.39	6 39/9.10 =70.22

3.5 Differential Thermal Analysis (DTA) results

Figures 3.6 to 3.11 show the DTA curves of BSO pure and doped single crystals as well as the DTA curves of pure and doped polycrystals. For all the six samples both the heating and cooling cycles have been taken. The samples were heated from room temperature to 1000° C at a rate of 5° C / minute and cooled from 1000° C to 500° C . The polycrystals and the corresponding single crystals more or less have same thermal events . Interestingly all the samples during the cooling cycle didn't resolidify at the point at which they got melted.

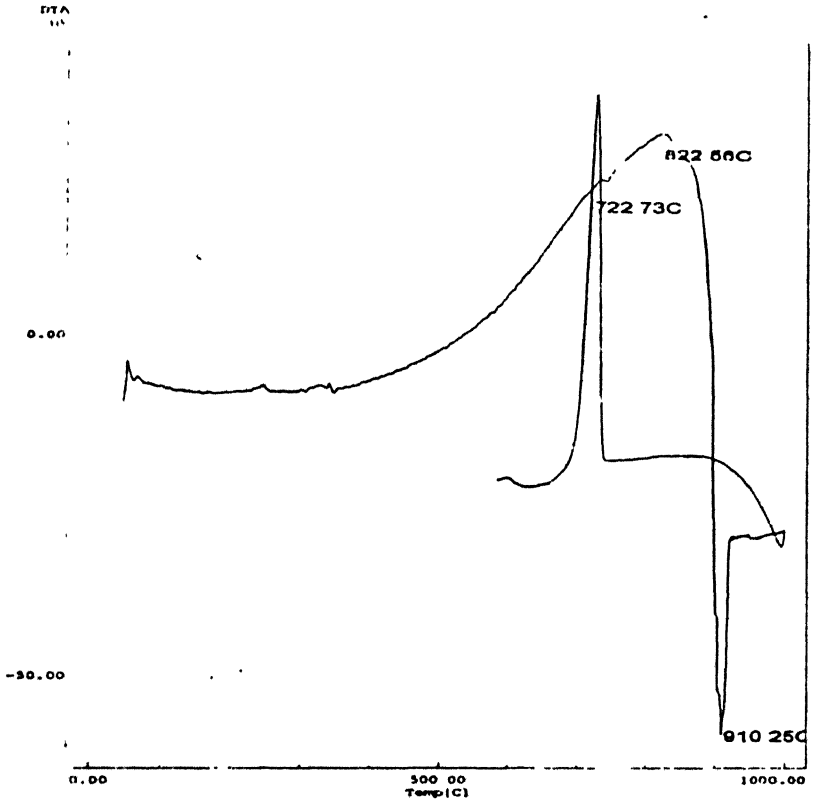

Fig . 3.6 DTA of BSO polycrystal

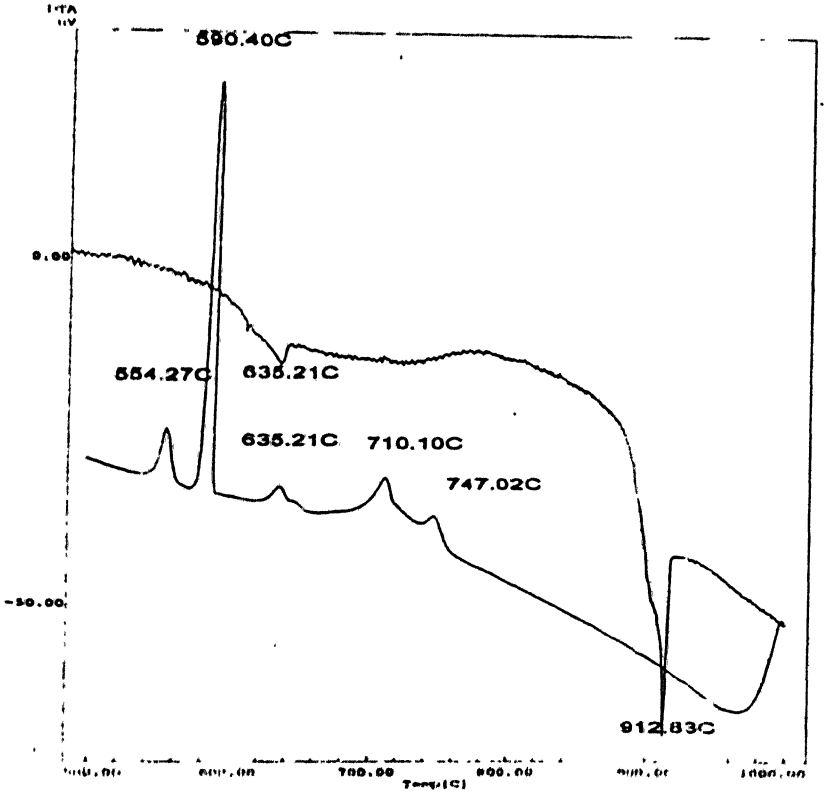

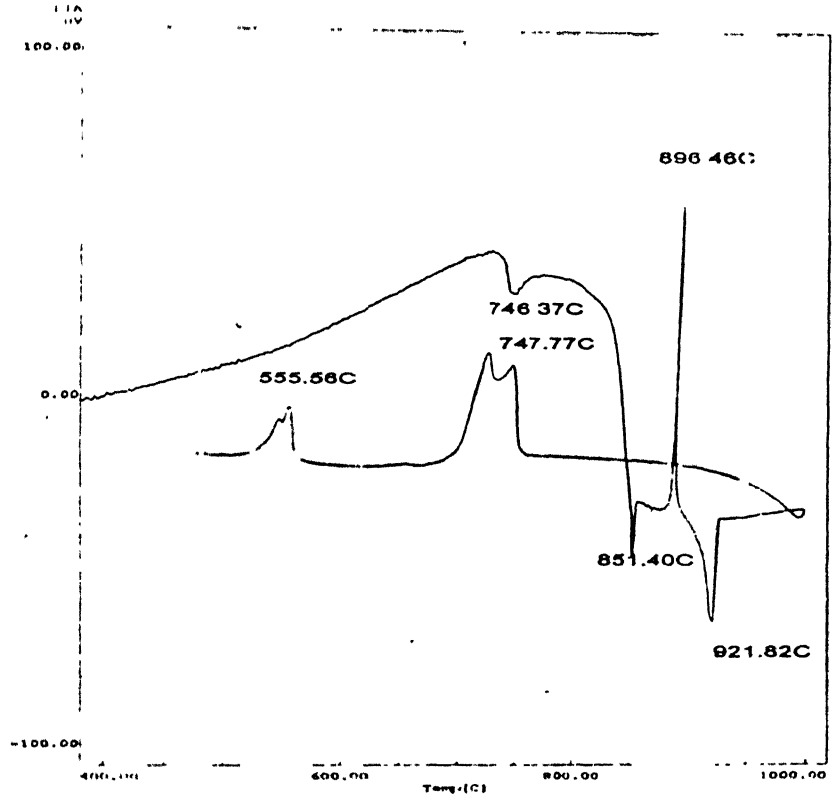

Fig. 3.8 DTA of BSO : Al polycrystal

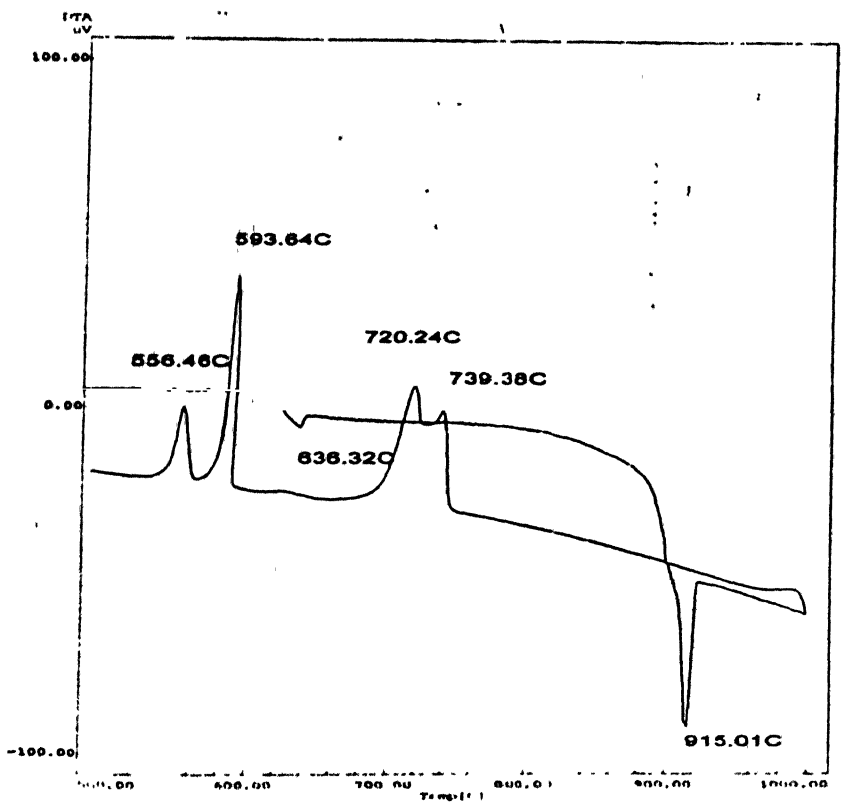

Fig.3.9 DTA of BSO: Al single crystal

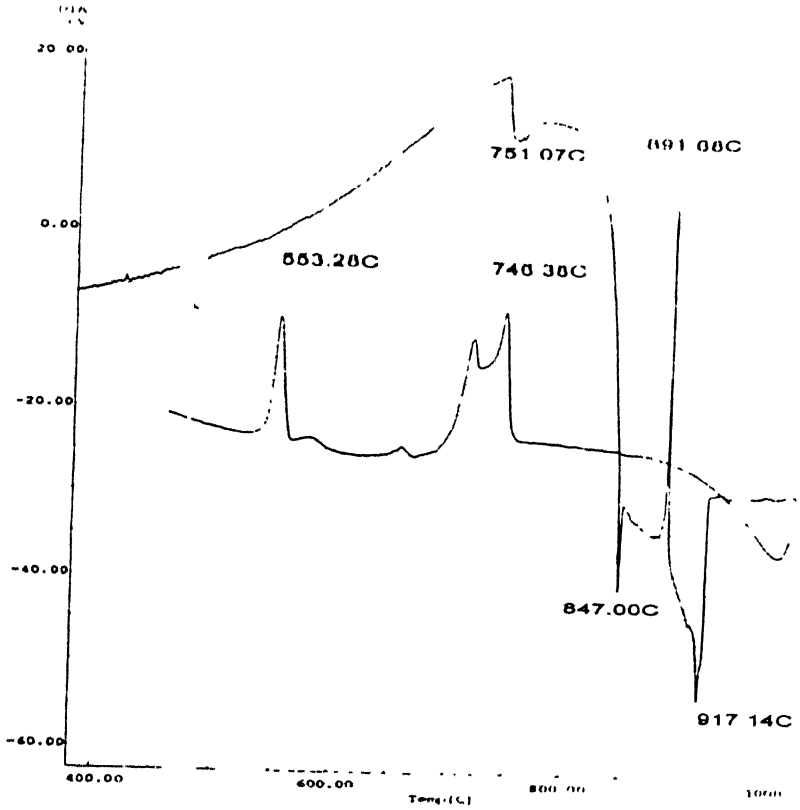

Fig. 3.10 DTA of BSO.Mg polycrystal

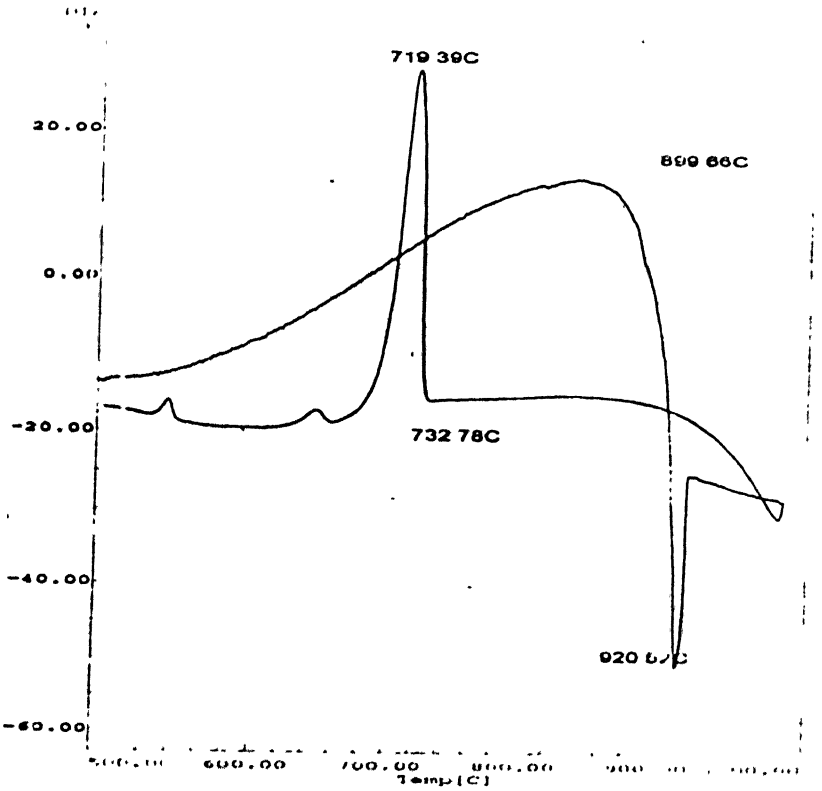

Fig 3.11 DTA of BSO·Mg single crystal

According to the literature, after the melting point there occurs a phase change from γ - BSO to δ - BSO and the transition from δ - BSO to γ - BSO during the cooling cycle was proved to be irreversible[125].

3.6 SEM studies

The SEM micrographs of BSO pure and doped polycrystals are displayed in figures 3.12, 3.13 and 3.14 The elemental analysis was done on all the three samples and it confirms the presence of Aluminium and Magnesium The elemental analysis profiles are shown in figures 3 15 and 3.16.

3.7 Complex impedance spectroscopy studies

(a) RC combination studies

As already pointed out, complex impedance plots are useful for determining an appropriate equivalent circuit for a system and for estimating the values of the circuit parameters. The Complex impedance plots for R and C combinations are shown in fig 3.17 (a) , (b),(c) and (d). Fig 3 17 (c) shows the R and C in series and Fig 3.17 (d) shows the R and C in parallel. RC series combination describes almost a straight line parallel to y axis .ie. Zsinθ. And if we plot the graph between real and imaginary parts of the admittance then it describes a circle . This can be explained as follows.

For R and C in series, the complex impedance is given by

$$Z(\omega) = R + j(-1/\omega C)$$

Admittance $Y(\omega) = 1/Z(\omega) = 1/(R + 1/j\omega C)$

$$= R/(R^2 + 1/\omega^2C^2) + j/\omega C (R^2 + 1/\omega^2C^2)$$

e. $Y_R = R/R^2 + 1/\omega^2C^2$ ..... (1)

$$Y_I = 1/\omega C (R^2 + 1/\omega^2C^2) \quad \text{..... (2)}$$

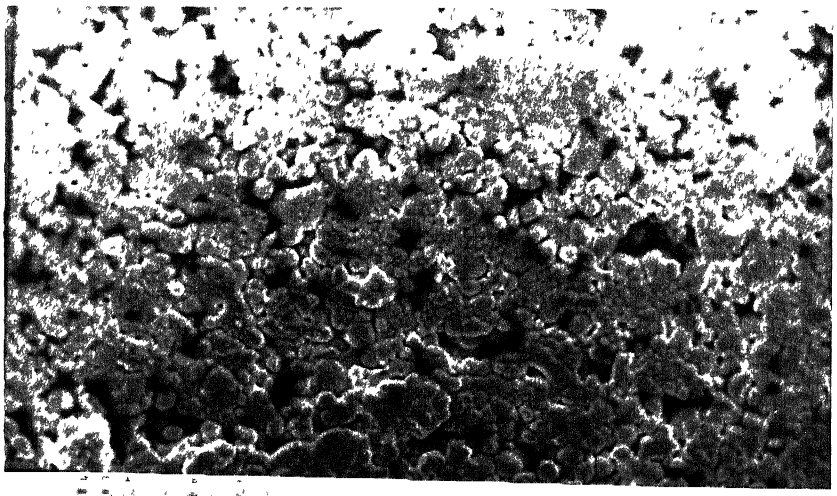

Fig 3.12 (a) SEM micrograph of BSO pure pressed pellet

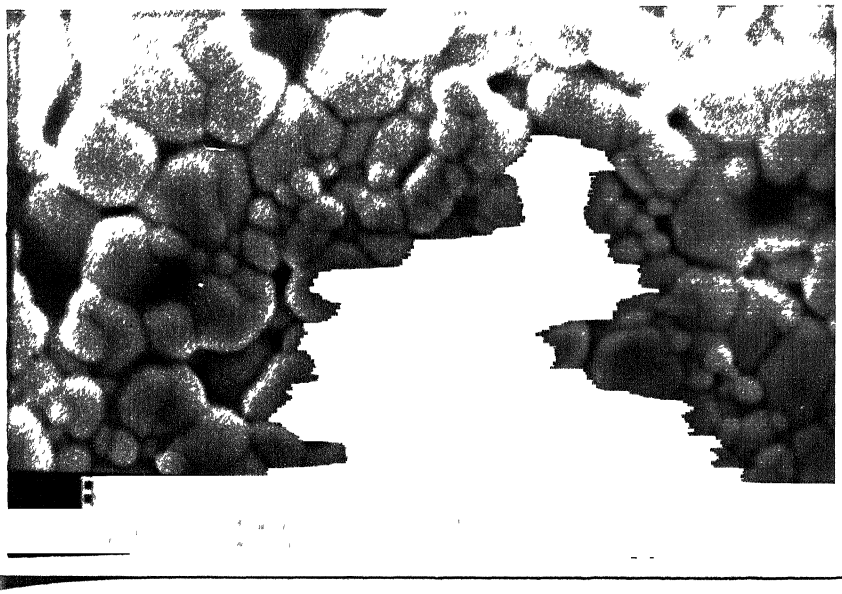

Fig 3.12 (b) SEM micrograph of BSO pressed pellet

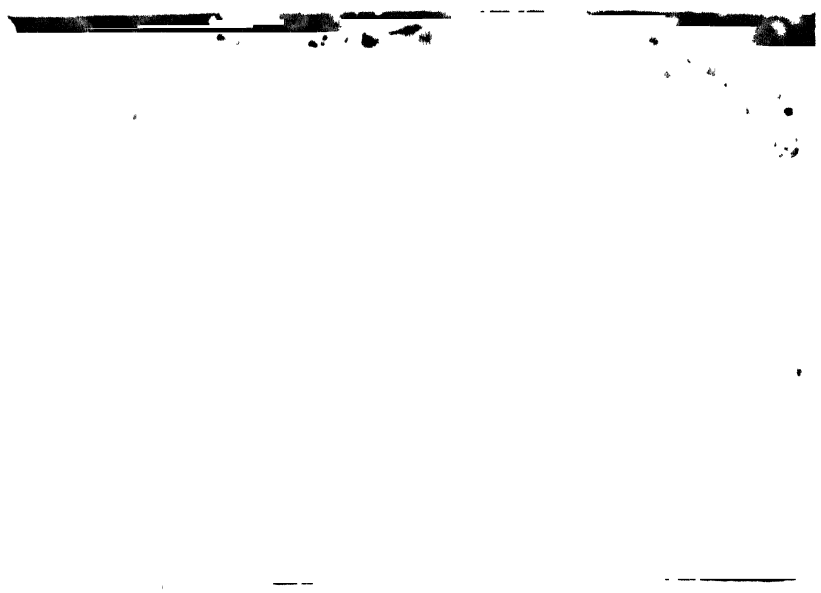

Fig 3.13 SEM micrograph of BSO.Al pressed pellet

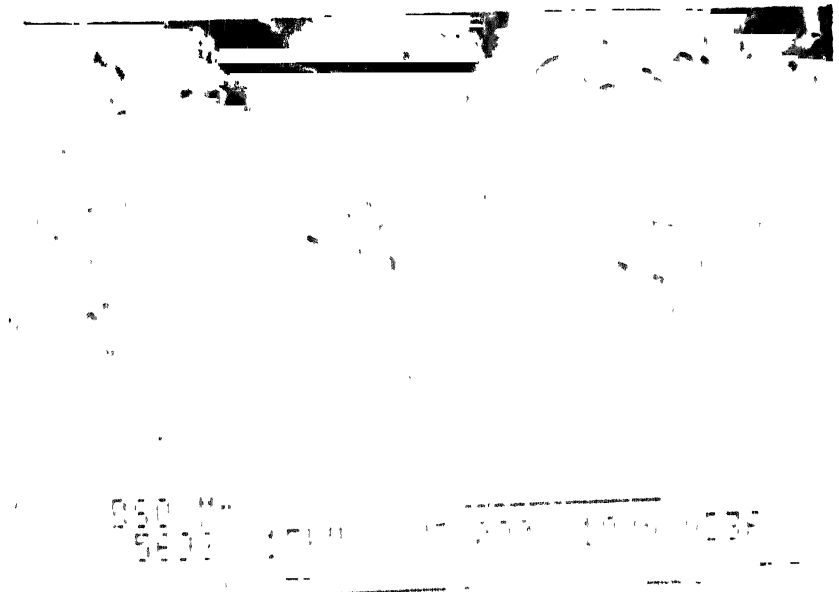

Fig 3.14 SEM micrograph of BSO Mg pressed pellet

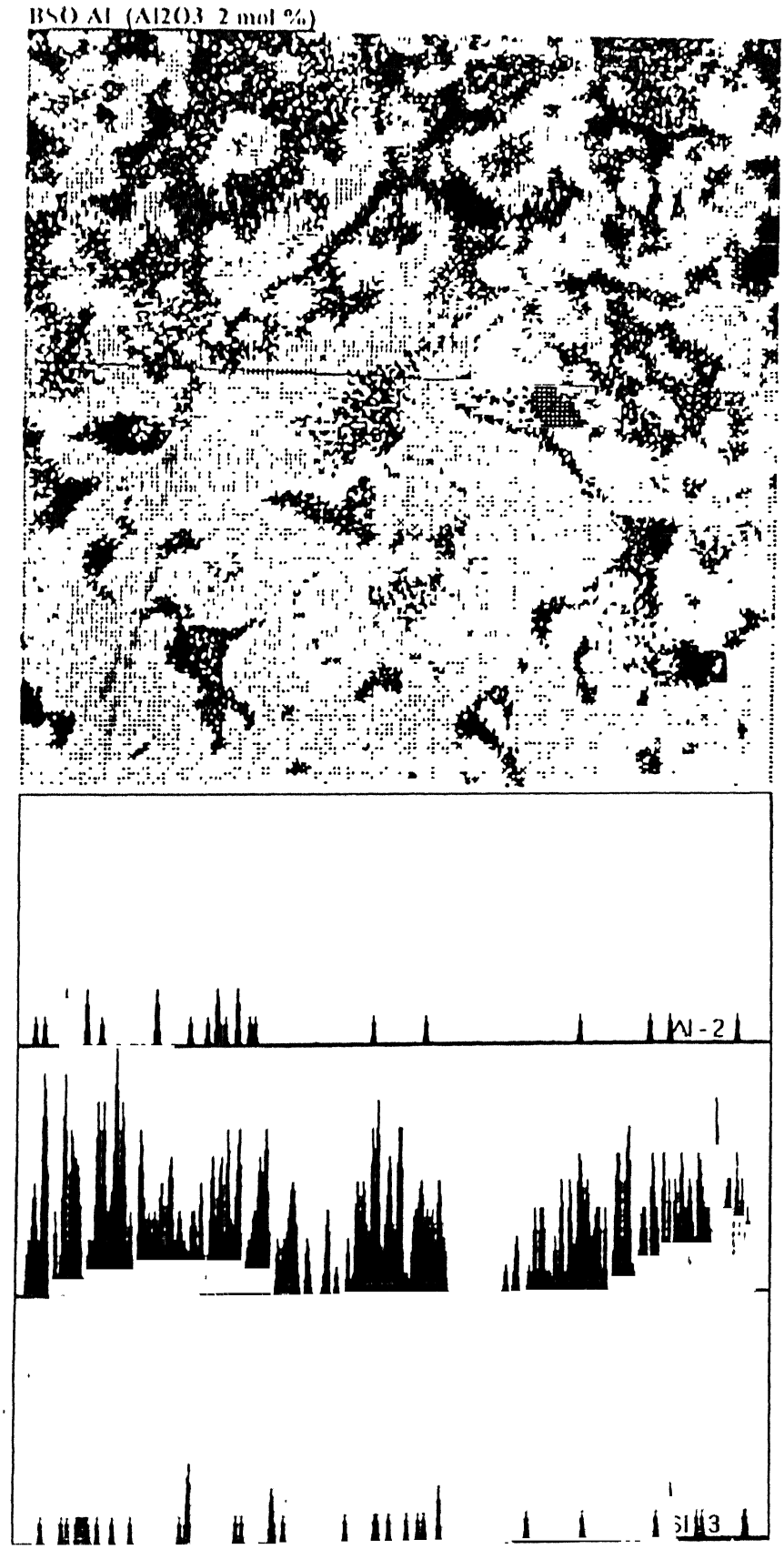

Fig 3.15 Elemental analysis profile of BSO.Al polycrystal

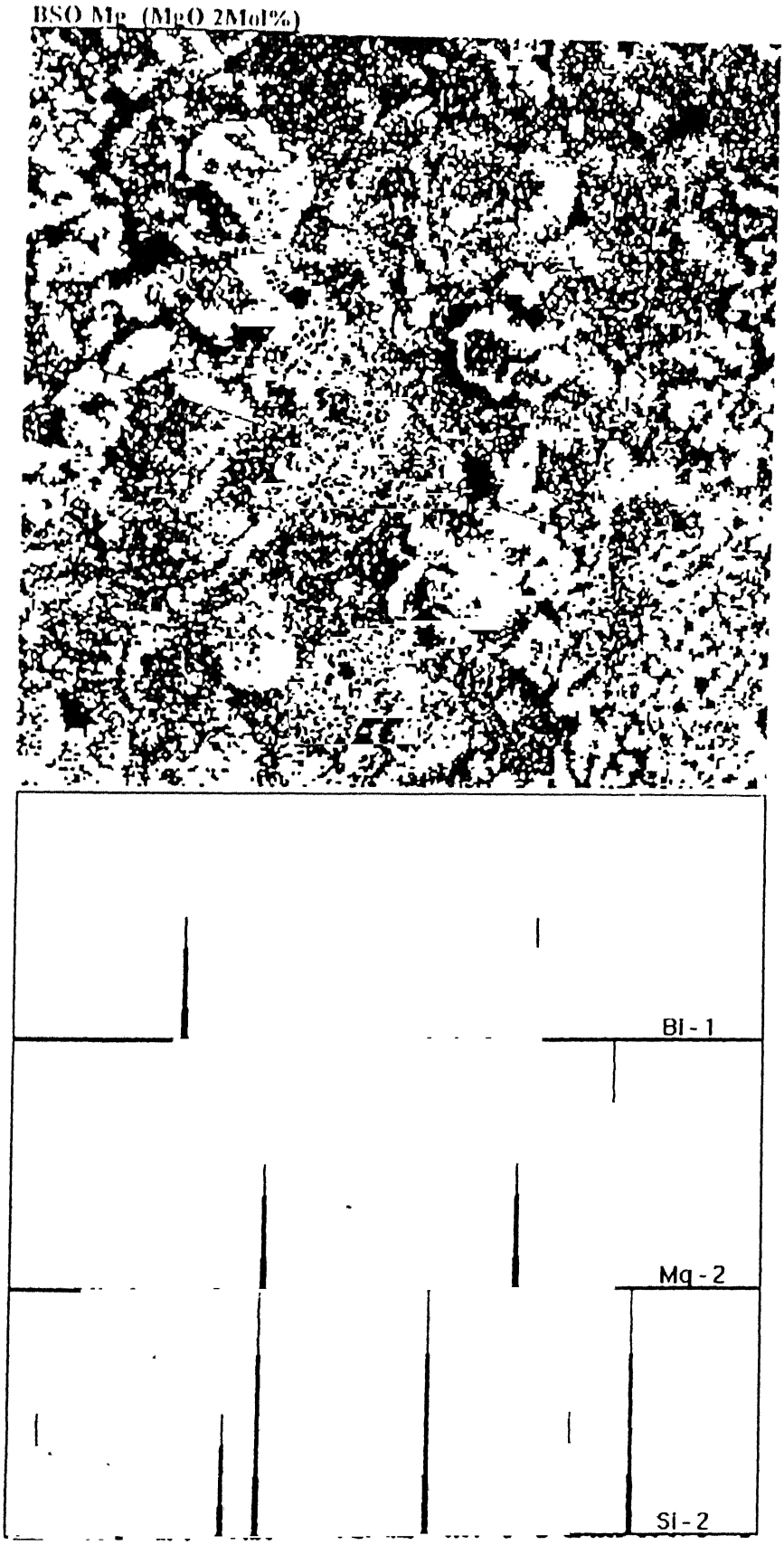

Fig. 3.16 Elemental analysis profile of BSO: Mg polycrystal

The locus of the points (Y_R , Y_I) defined by equations (1) and (2) can be shown to be a circle of radius R/2 having a centre at (R/2 , 0) . From equations (1) and (2) if we eliminate ω by squaring the equations (1) and (2) and then adding up,

we will end up with $Y_R^2 + Y_I^2 = Y_R / R$

or

$(Y_R - 1/2R)^2 + Y_I^2 = (1/2R)^2$ ..... (3)

This has the form of $(x-a)^2 + y^2 = a^2$ which is the equation of a cirlce of radius 'a' having it's centre at (a,0) . So here in eqn (3) radius is 1/2R and centre at (1/2R,0) where R is the resistance of the circuit. Thus, the inverse of the circle yields the resistance R of the sample/circuit element, as shown in fig 3.17 (c). The R and C parallel combination was already discussed in chapter 2. For this, the response Z_R Vs Z_I is semicircle

To get a feel for it, the complex impedance response for a set of R and C values have been studied It also helps one to calibrate the instrument One particular case (R = 4.4 k , C = 3nf) is shown in fig 3.18. Fig 3.18 (a) shows the R and C in series and Fig. 3.18 (b) shows the R and C in parallel .

(b) Conductivity studies

Extending the RC combination to the sample, the sample kept between the two electrodes is modelled as a parallel combination of R and C. Six samples (3 single crystals and 3 polycrystals) have been taken for conductivity studies. They are

1. BSO pure single crystal
2 BSO pure polycrystal
3. BSO:Al single crystal
4. BSO:Al polycrystal
5. BSO:Mg single crystal
6. BSO:Mg polycrystal

Using HP 4192A impedance analyzer, the samples were subjected to complex impedance analysis. By varying the frequency from 500 Hz to 10 MHz, and by changing the temperature from room temperature to 700° C, the impedance (Z) and phase angle (θ) were measured. All the samples from room temperature to 400° C, didn't show any semicircular response but after 400° C, they started showing the semicircle. So it has been divided into

) low temperature behaviour and

(ii) high temperature behaviour Some of the complex impedance plots of the samples are shown in figures from 3.19 to 3.22 .

(i) Low temperature bahaviour

Fig 3.19 (a) shows the complex impedance response($Z\cos\theta$ Vs $Z\sin\theta$)for BSO pure polycrystal at room temperature and 300° C The response is a straight line and not a semicircle. The phase angle in these cases remains almost constant with the frequency Also the phase angle is around 87 degrees This makes the real part very low (almost zero since $\cos 87 \cong 0$) and the imaginary part is increasing . This can be described by the so called "constant phase element" (CPE) which was discussed in chapter 1 and is given by

$$Y = Y_0 (j\omega)^n$$

$$Y = Y_0 \omega^n e^{jn\pi/2} = Y_0 \omega^n [\cos(n\pi/2) + j\sin(n\pi/2)] \text{ --------- (a)}$$

where n is a constant. If n =0, the CPE represents a pure resistor with $R = 1/ Y_0$ and if n =1, the CPE represents a pure capacitor with $C = Y_0$ and if n = -1, it is a pure inductor with $L = 1/Y_0$.

The impedance $Z = | Z | e^{j\theta} = |Z| (\cos\theta + j \sin\theta)$ ---------- (b)

Comparing equation (a) with (b) we can get the value of n for our sample .

The value of $\theta = 87° = n\pi / 2$

$$n = (2 / \pi) (87 \times \pi /180) \approx 0.97$$

This is almost equal to one and the CPE with n = 1 represents a pure capacitor . And for the apacitor the complex impedance response is a straight line along the Y - axis. i.e. along the naginary axis, $Z\sin\theta$. Fig . 3.19 (b) shows the nearly semicircular response. The transition om the straight line behaviour to semicircular behaviour starts materialising at this mperature (400° C) .

ii) High temperature behaviour

The complex impedance response for the samples from 400° C onwards is a semicircle d this data is presented in figures 3.19 (b), 3.20, 3.21 and 3.22. So the sample can be nsidered as a parallel combination of R and C and to retrieve the individual values of R and

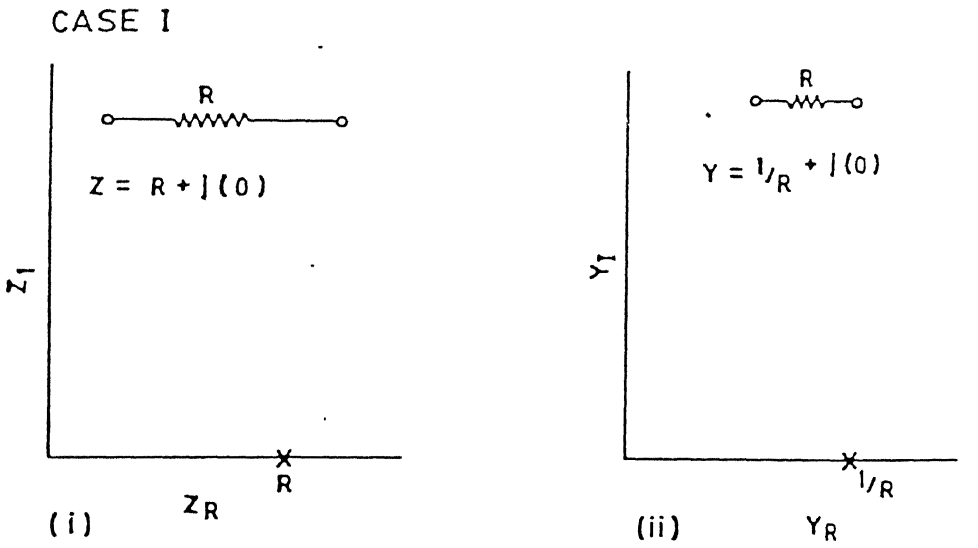

Fig 3.17 (a) Complex impedance and admittance plots for Resistor (R)

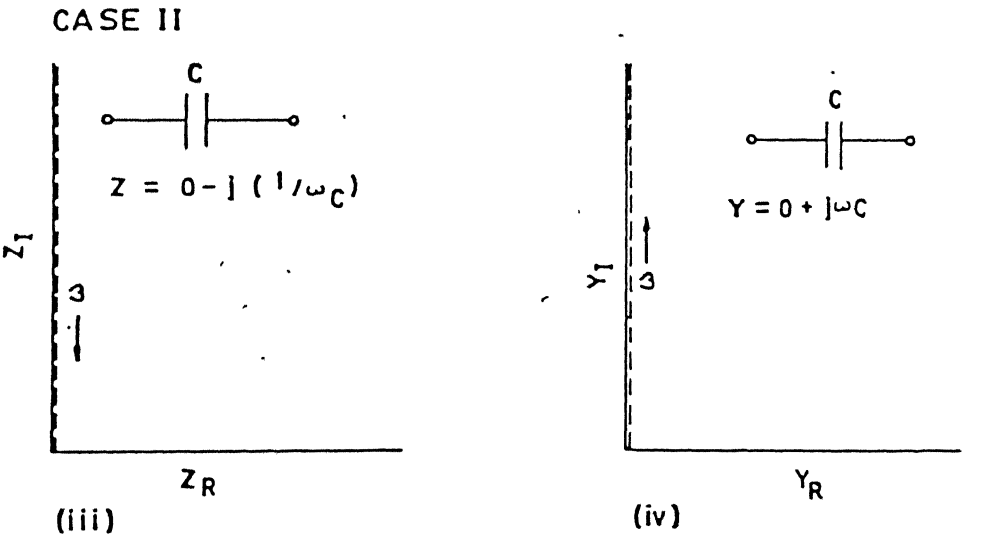

Fig 3.17 (b) Complex impedance and admittance plots for Capacitor (C)

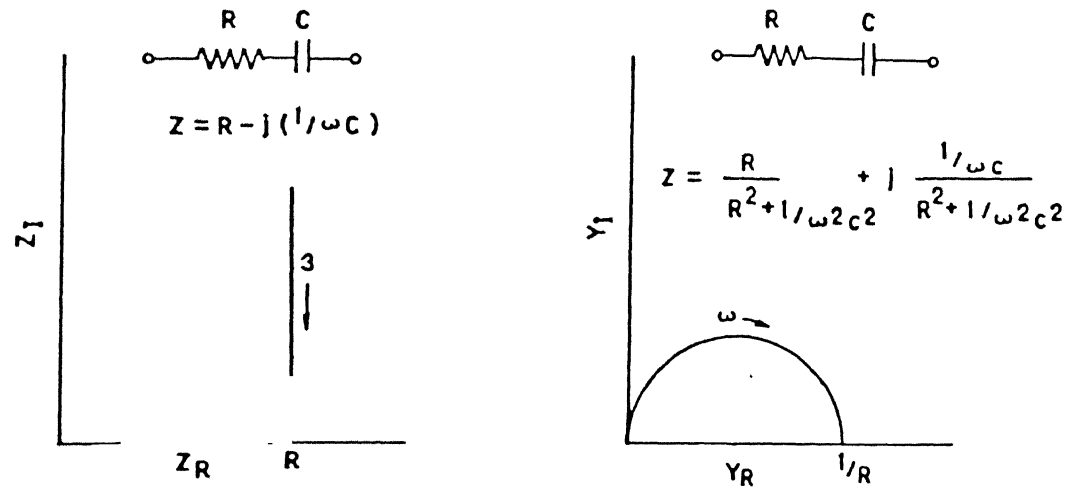

Fig 3.17 (c) Complex impedance and admittance plots for R and C in series

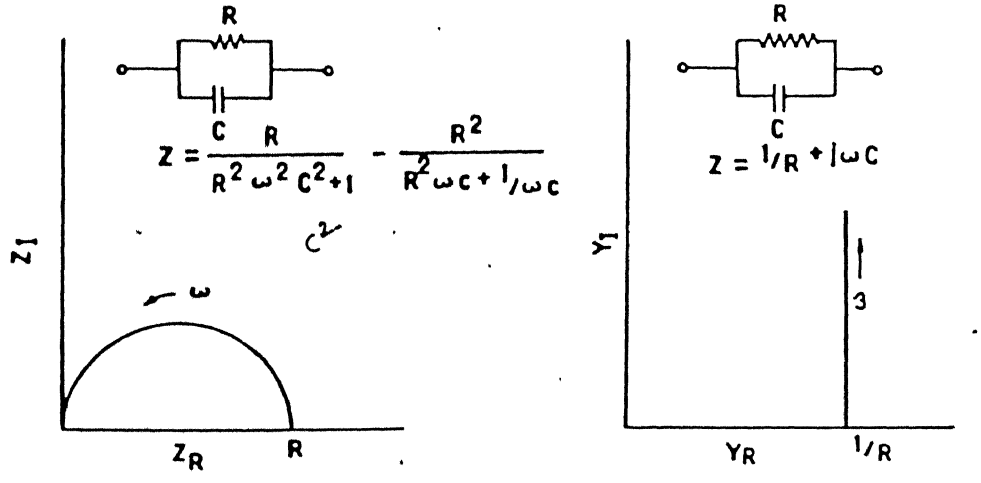

Fig 3.17 (d) Complex impedance and admittance plots for R and C in parallel

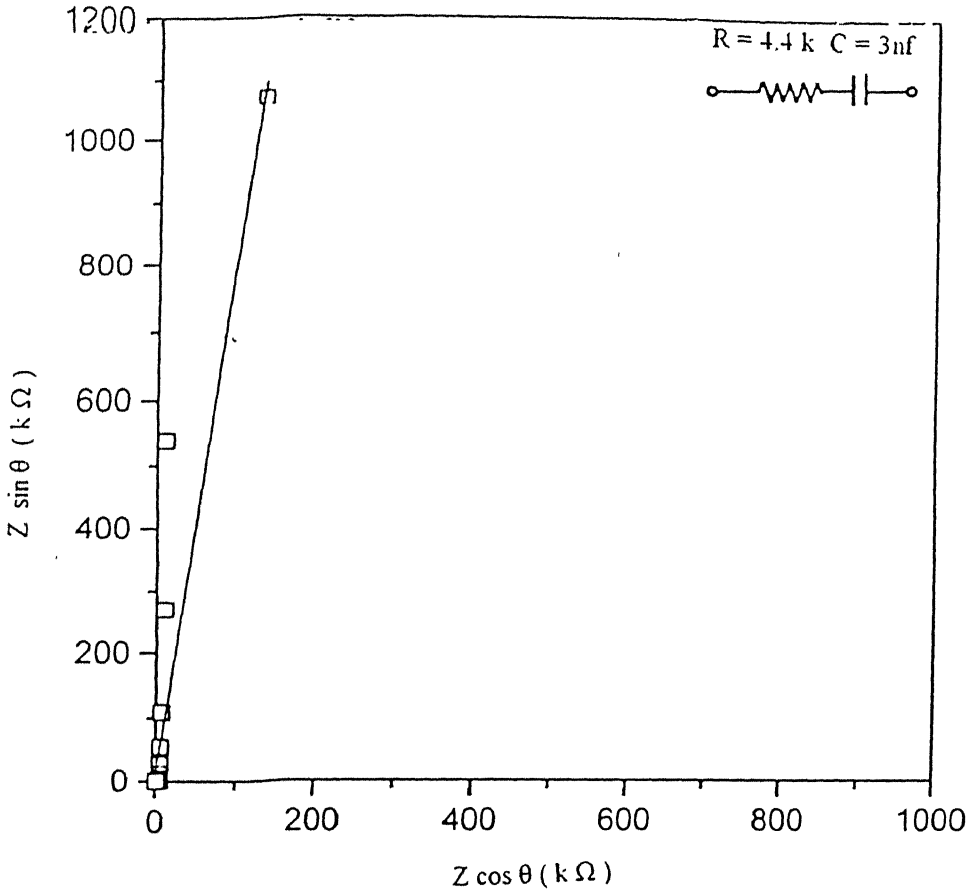

Fig 3.18 (a) Complex impedance plot for R = 4 4 k, C = 3 nf in series

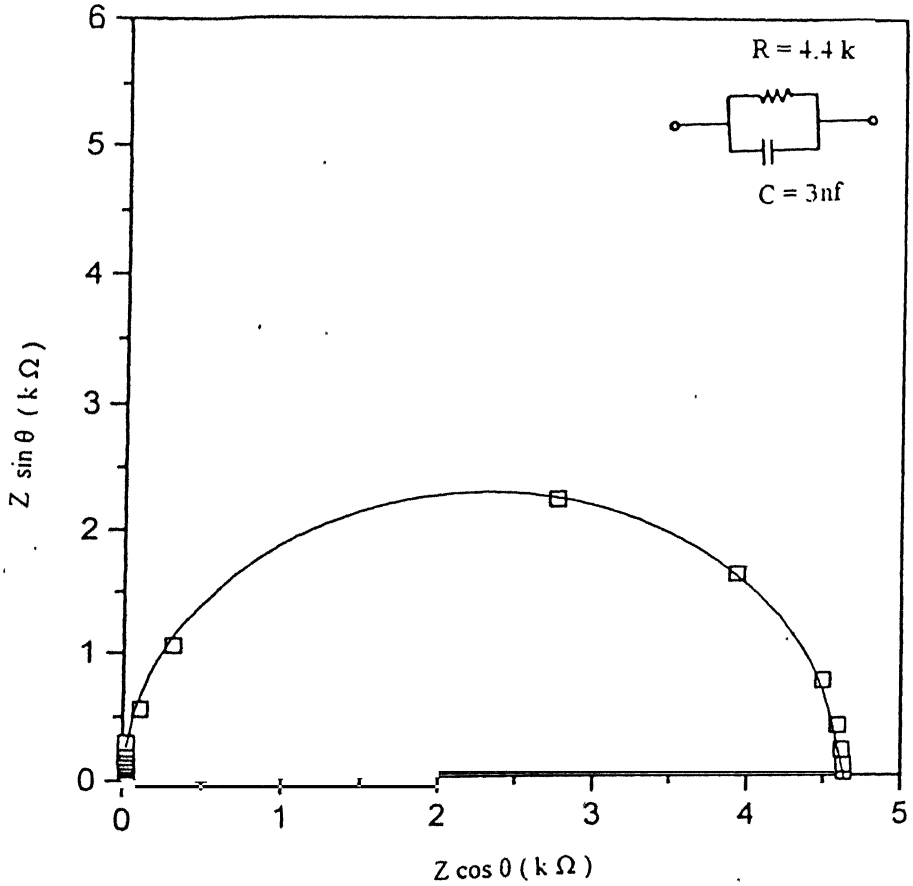

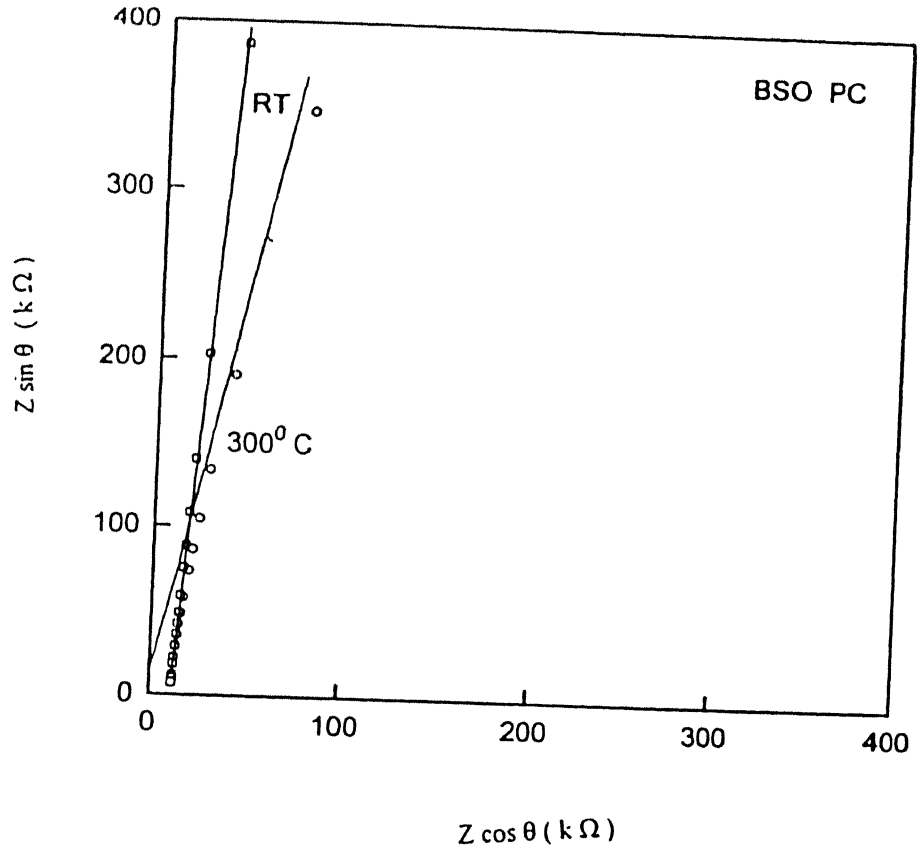

Fig 3.19 (a) Complex impedance plots for BSO polycrystal at room temperature and 300° C .

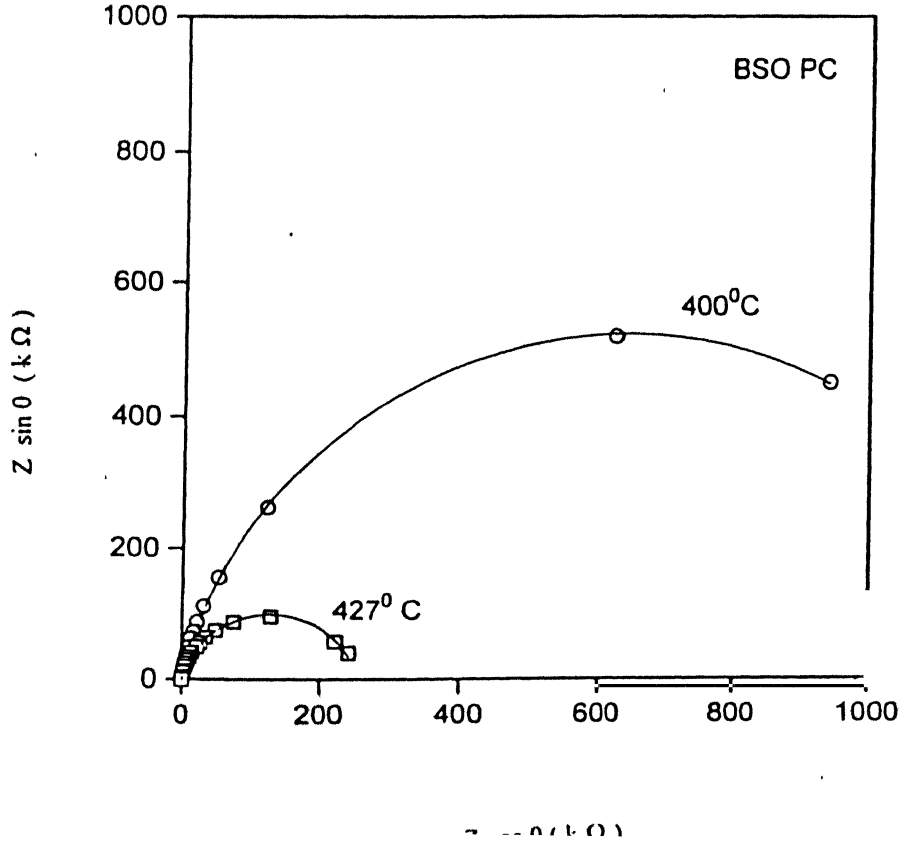

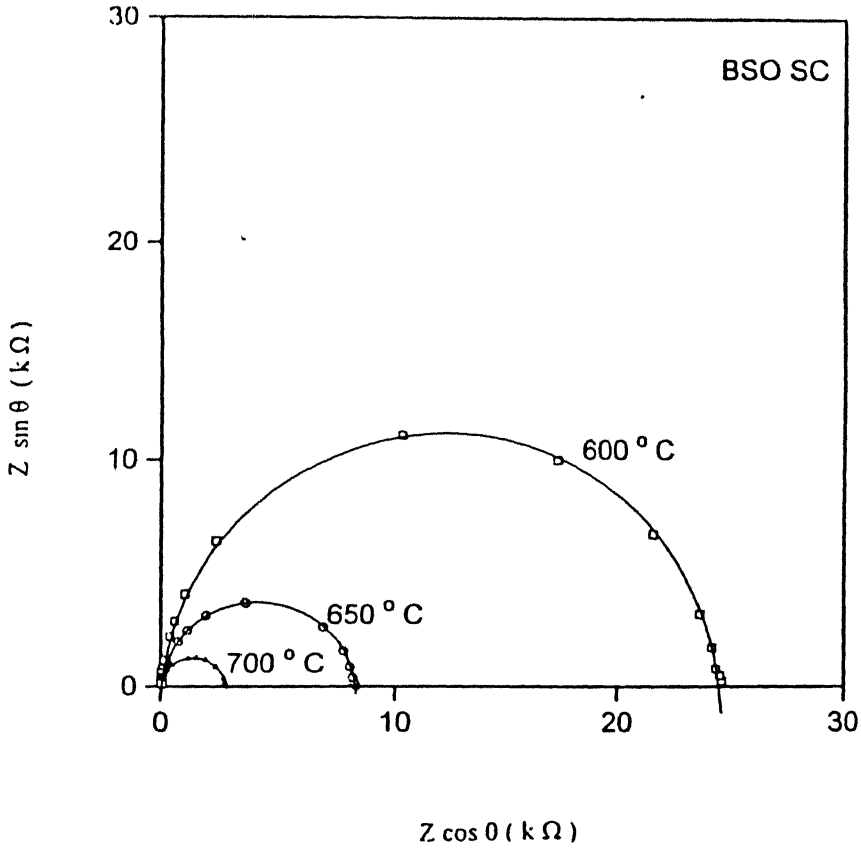

Fig 3.20 Complex impedance plots for BSO single crystal at three different temperatures 600° C , 650° C and 700° C.

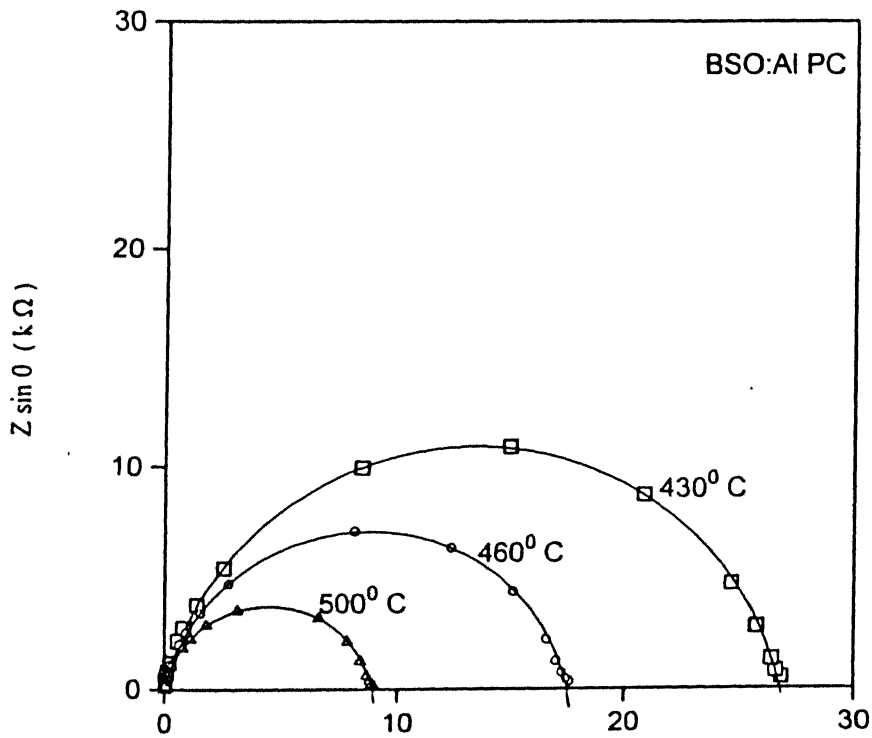

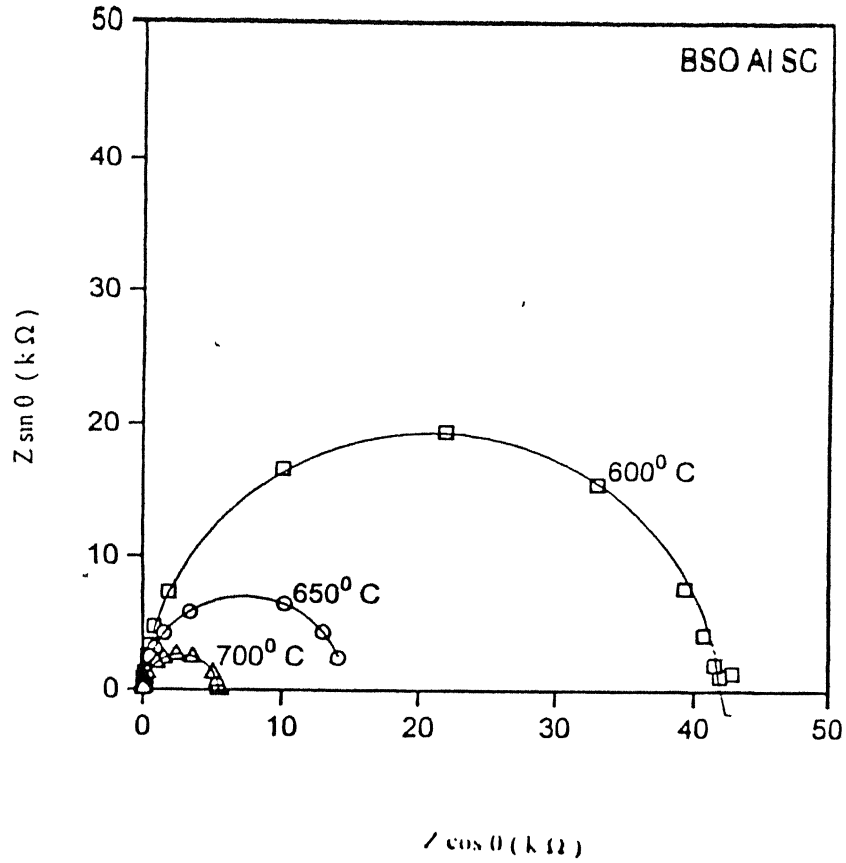

Fig 3.21 (b) Complex impedance plots for BSO Al single crystal at three different temperatures 600° C , 650° C and 700° C .

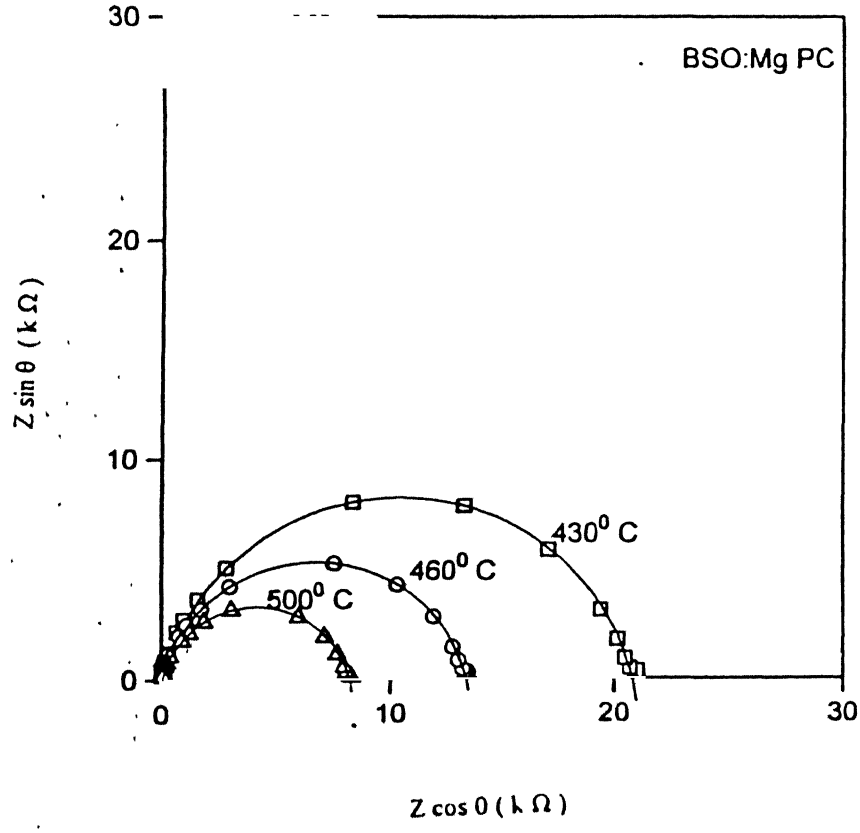

Fig 3.22 · Complex impedance plots for BSO.Mg polycrystal at three different temperatures 430° C , 460° C and 500° C .

C the complex impedance analysis is used as a tool. The diameter of the semicircle is the dc resistance. From this the dc conductivity can be calculated for each temperature. Also if we observe carefully, the diameter of the semicircle decreases with increase in temperature i.e decrease of resistance R with increase in temperature (T) This clearly reflects the fact that the samples under study are either **insulators or semiconductors** at room temperature.

DC Conductivity

The dc conductivity is frequency independent conductivity All the samples which show semicircles at various temperatures contribute to this conductivity. The temperature range is 400° C - 700° C .

DC conductivity , $\sigma_{dc} = l / AR$

where l = thickness of the sample

A = Area of cross section

R = Resistance of the sample

Since the pellets are circular in shape, Area $A = \pi r^2$

Thus one can measure the dc conductivity at a particular temperature. The log value of dc conductivity is plotted against 1000/ T. The dc conductivity plots for all the 6 samples are shown in figures 3.23 (a) and (b). Fig 3.23 (b) shows the linear fit for all the samples. If we carefully see the fig 3.23(a) , we can observe two regions in the dc conductivity curve for each sample. The bottom portion is called the extrinsic region which is appearing because of impurities. The top portion is called intrinsic region for which the conductivity is described by the famous Arrhenius equation

$$\sigma = \sigma_0 \exp (-E / kT)$$

Where σ_0 is the pre exponential factor

k is the Boltzmann constant

and E is the activation energy for conduction.

The slope of the fit gives E/1000k We know the value of k. So we can calculate the activation energy E . The extrapolation of the curve along the y axis gives y intercept which is log σ_0 (To be subtracted from the y value which is considered as origin for the y axis). From this the pre exponential factor σ_0 can be calculated. The log σ_0 and the activation

energy for all the six samples are tabulated in table 3 5 The temperature range for all the samples is 400° C - 700° C

Table 3.5

Sample	log σ_0 (ohm^{-1} cm^{-1})	E (eV)
BSO (pc)	4.6	0.78
BSO (sc)	2.4	0.54
BSO:Al (pc)	3.8	0.48
BSO:Al (sc)	2.8	0.52
BSO:Mg (pc)	3.8	0.36
BSO:Mg (sc)	3.05	0.58

Here a comparison of the values shows that the addition of impurities may reduce the activation energy responsible for conduction thereby reducing the band gap also. Band gap $E_g \cong 2$ E . This needs further investigation. But the addition of impurities does not significantly contribute to the conductivity .

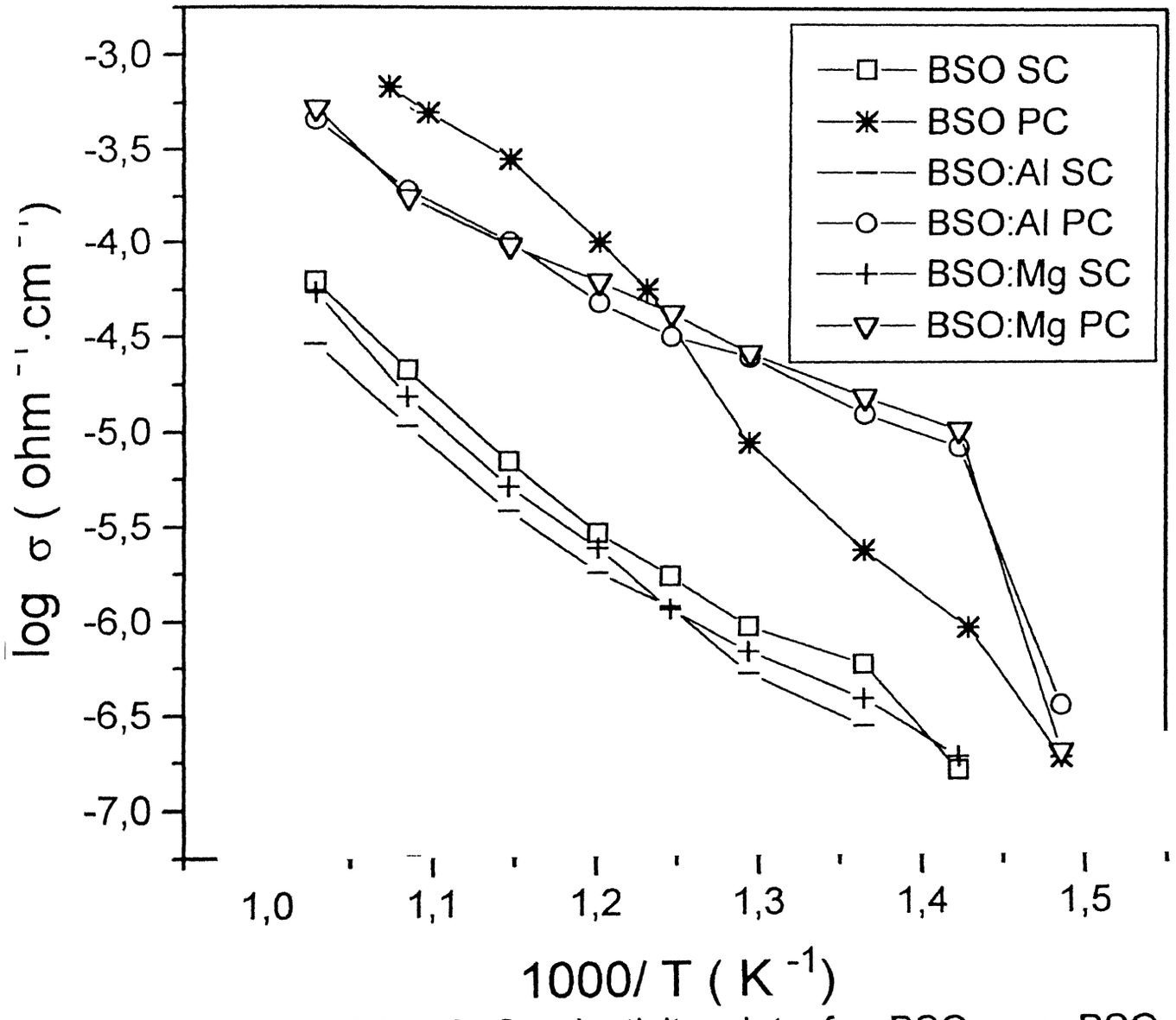

Fig 3.23 (a) DC Conductivity plots for BSO pure, BSO:Al and BSO:Mg single crystals and polycrystals

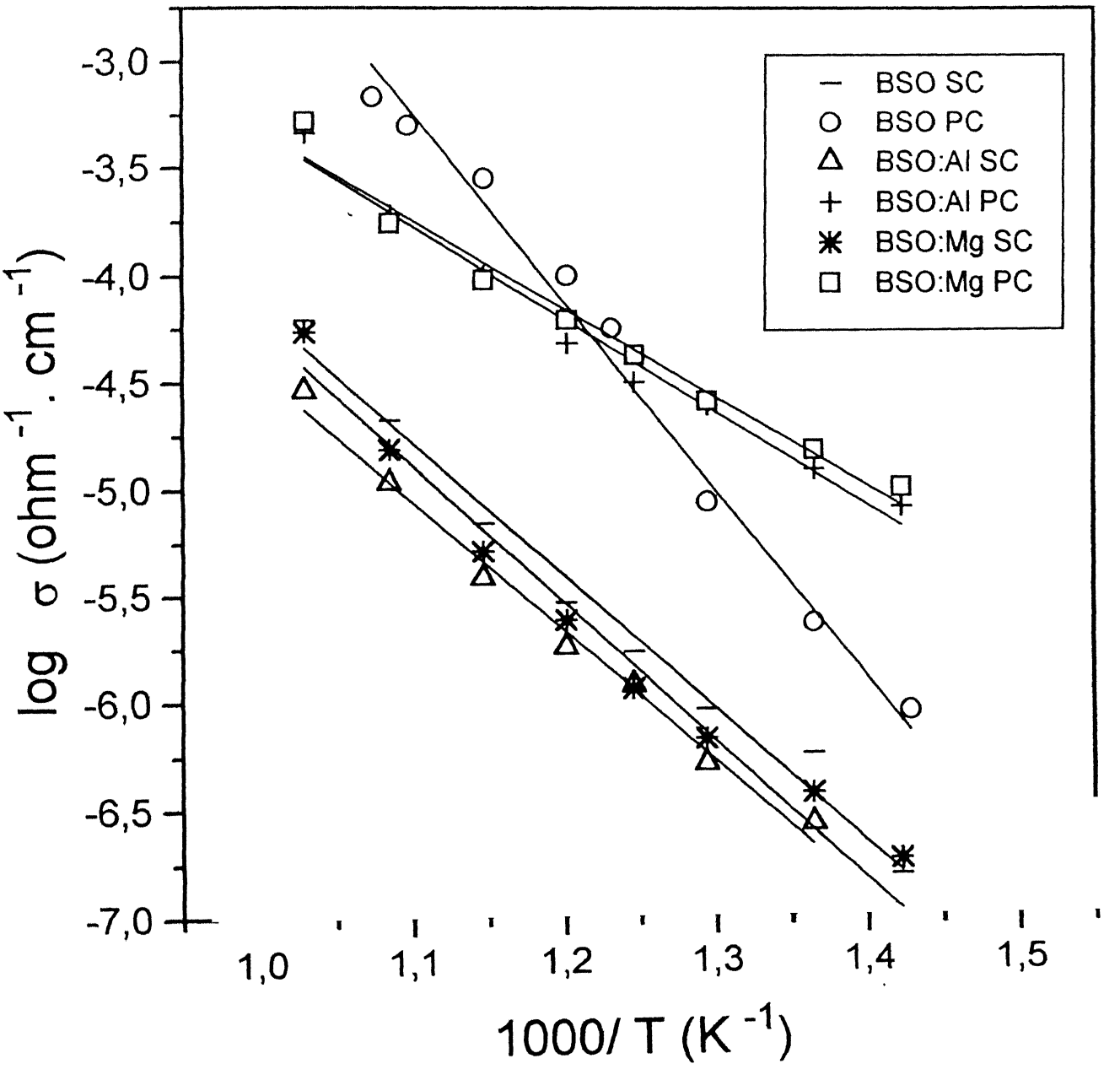

Fig 3.23 (b) DC Conductivity fit for BSO Pure, BSO:Al and BSO:Mg Single Crystals and Polycrystals

AC Conductivity

The AC conductivity $\sigma_{ac} = Y' (l / A) = Y \cos\theta \ (l / A)$

where

$Y\cos\theta$ = Real part of the admittance

l = thickness of the sample

A = Area of cross section of the sample

Also $Y = 1 / Z$, where Z = impedance

We can write $\sigma_{ac} = \cos\theta (l / AZ)$ ---------- (X)

The ac conductivity is frequency dependent So the phase angle θ comes into picture .

In fact , the conductivity itelf is a complex quantity.

we can write $\sigma = \sigma_{dc} + j \sigma_{ac}$

where, σ_{dc} is the frequency independent conductivity

σ_{ac} is the frequency dependent conductivity

In ac conductivity, the Z and θ values are taken for 3 different frequencies 5 KHz, 100KHz and 1 MHz. The temperature range is from room temperature to 700° C. The ac conductivity is then calculated using equation (X). Log σ Vs 1000/ T is then plotted for all the six samples. They are shown in figures from fig .3 24 to fig. 3.26.

(C) Dielectric studies

Using Complex impedance spectroscopy as a tool, the dielectric properties of BSO pure and doped single crystals and the corresponding polycrystals were studied. Like conductivity, the dielectric constant also is a complex quantity.

This can be written as follows:

$\epsilon_r^* = \epsilon' - j\epsilon'' = Y^* / j\omega C_0$

Where ϵ' = real part of the complex dielectric constant

ϵ'' = imaginary part of the complex dielectric constant

$\epsilon' = Y''/ \omega C_0 = C_p / C_0$

and $\epsilon'' = Y' / \omega C_0 = 1 / \omega C_0 R_p$

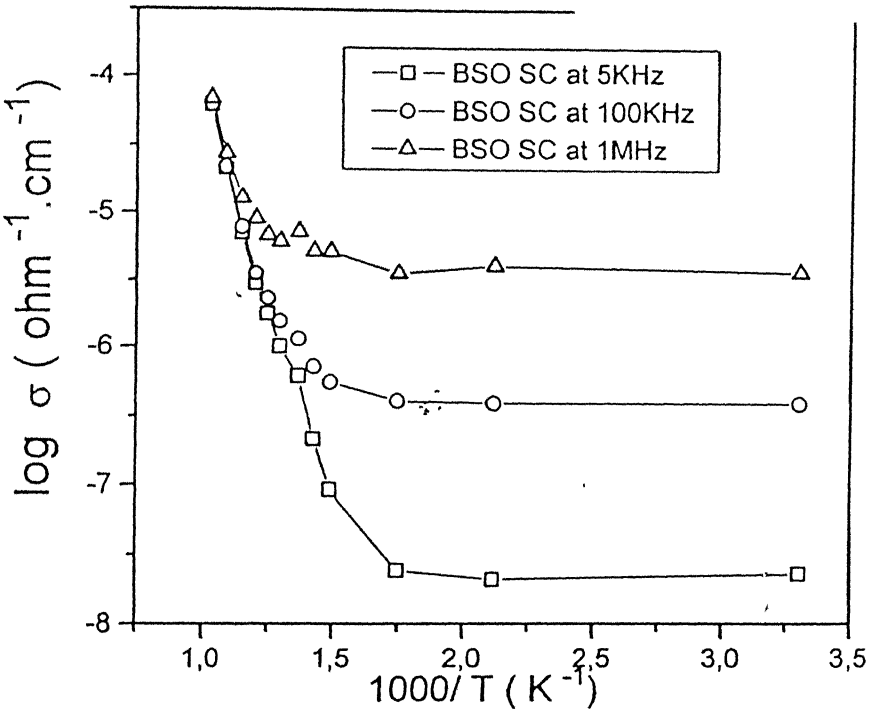

Fig 3.24 (a) Variation of ac conductivity as a function of inversion of temperature for BSO pure single crystal

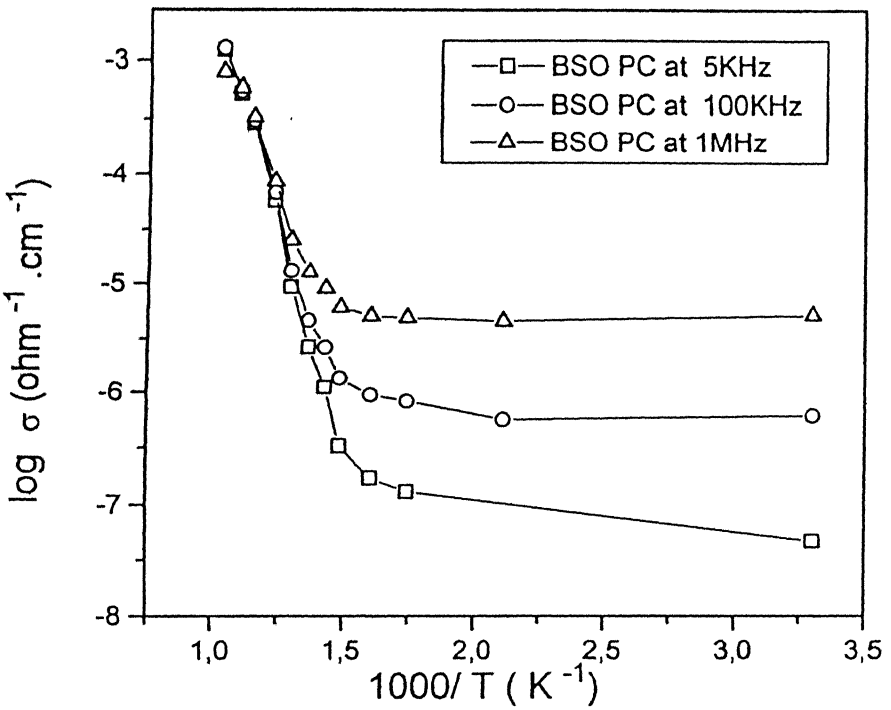

Fig 3.24 (b) Variation of ac conductivity as a function of inversion of temperature for BSO pure polycrystal

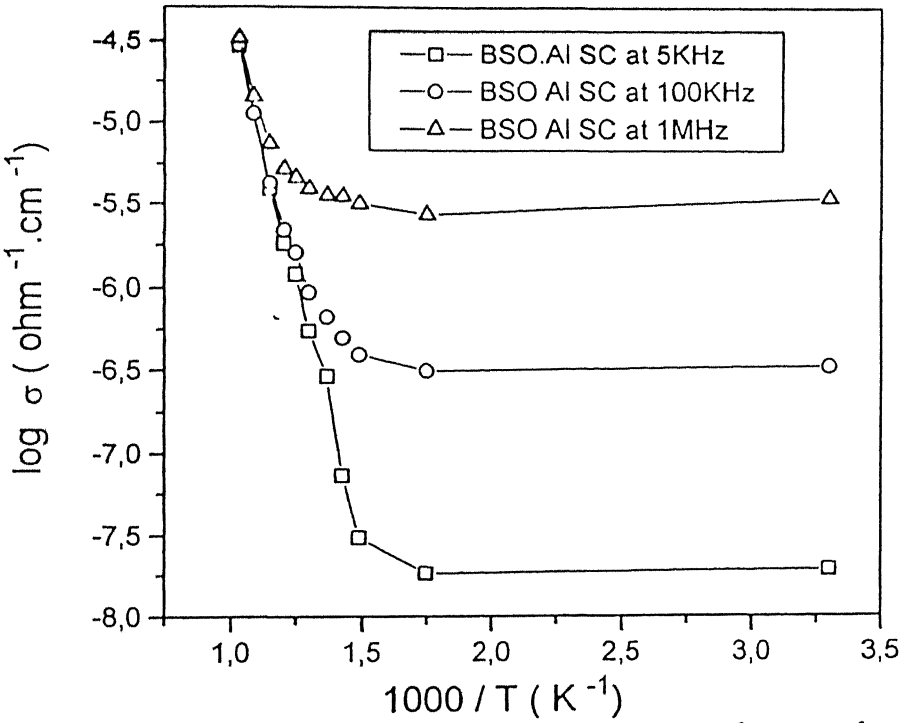

Fig 3.25 (a) Variation of ac conductivity as a function of inversion of temperature for BSO:Al single crystal

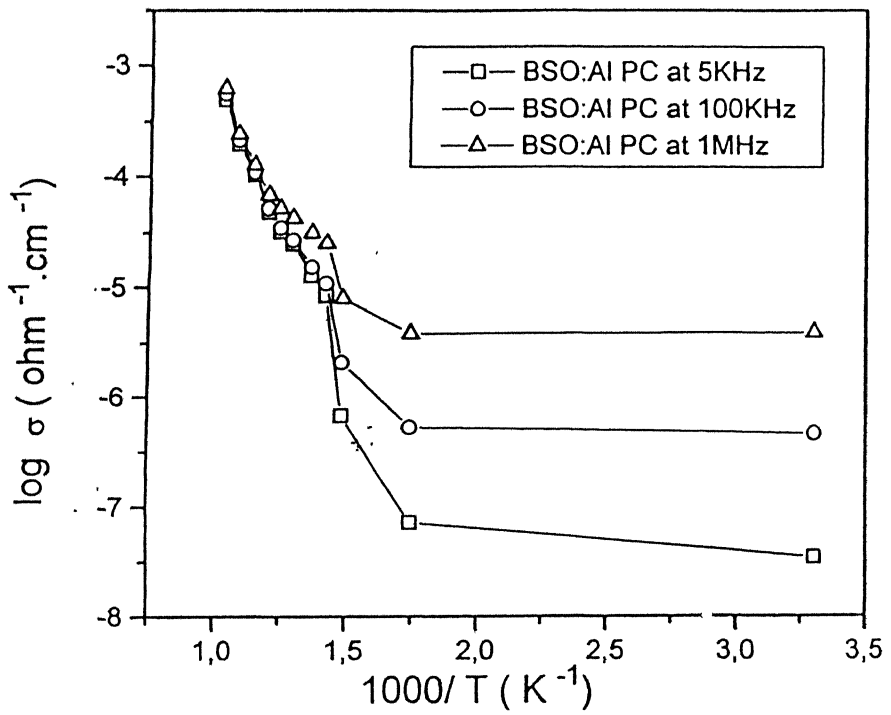

Fig 3.25 (b) Variation of ac conductivity as a function of inversion of temperature for BSO.Al polycrystal

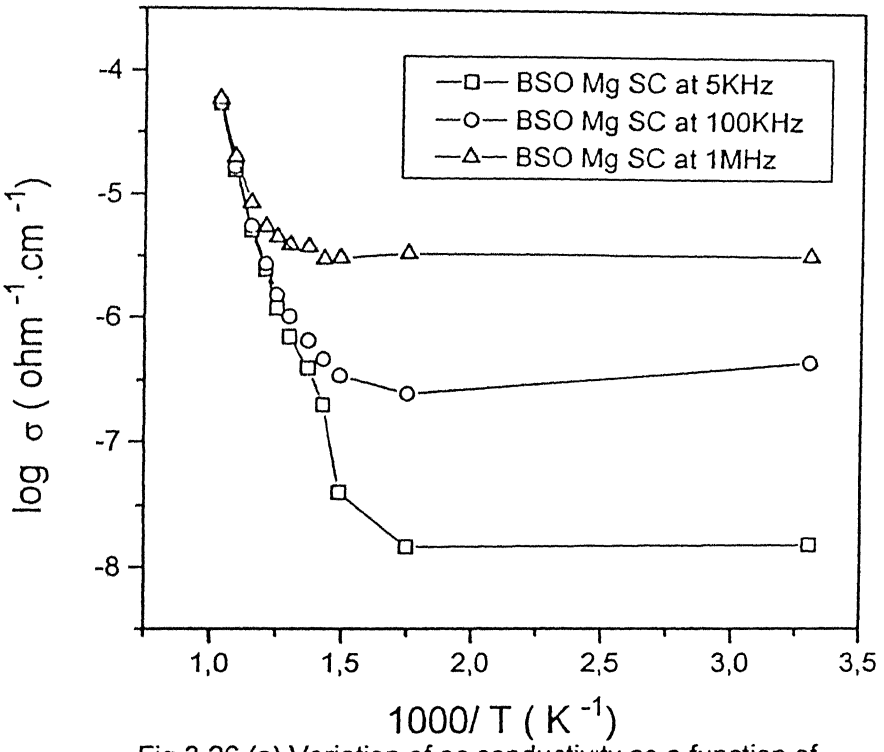

Fig 3.26 (a) Variation of ac conductivity as a function of inversion of temperature for BSO:Mg single crystal

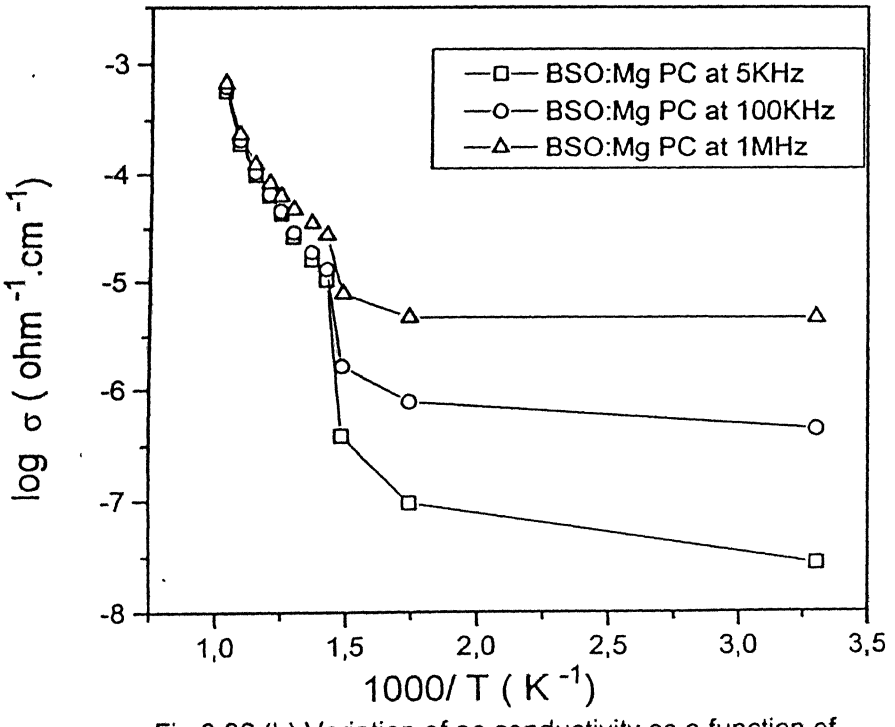

Fig 3.26 (b) Variation of ac conductivity as a function of inversion of temperature for BSO.Mg polycrystal

The dielectric loss or dissipation factor (D) or loss tangent is defined as,

$$D = \tan\delta = \epsilon''/\epsilon' = 1/\omega C_p R_p$$

The variation of the dielectric constant (ϵ') with frequency for BSO pure and doped single crystals and the corresponding polycrystals at room temperature is shown in fig 3 27 Also the variation of ϵ'' with frequency at room temperature is plotted for all the six samples This is shown in fig 3.28. The ϵ'' variation reflects the dielectric loss (D) . The dielectric constant ϵ' , decreases uniformly as frequency increases upto 5 MHz . Then the dielectric contant increases with the increase in frequency This is due to fluctuations at high frequencies and the HP 4192 A impedance analyzer may not be sensitive at these frequencies[52] . The dielectric constant of a material is composed of four polarization contributions: electronic, ionic, dipolar and space charge[53] . The nature of variation of ϵ' with frequency indicates which contributions are present. The space charge polarization depends on the purity and the perfection of the crystals and it's effect is noticeable in the low frequency region. Higher values of ϵ' and ϵ'' observed at low frequencies is due to the presence of space charge polarization[54] . The dipolar polarization may extend upto 10^{10} Hz in some materials . The ionic and electronic polarizations always exist at these frequencies . The dielectric constant and the loss of polycrystals is higher than that of the corresponding single crystals. The polycrystals may be thought of as a mixture of microcrystallites and air/vacuum filled voids[52] . Thus the total capacitance of the sample is the parallel equivalent of two individual capacitances, one air filled and the other filled by the material under examination,

i.e, $\epsilon'\epsilon_0 A/d = \epsilon_s\epsilon_0 A_s/d + \epsilon_a \epsilon_0 (A - A_s)/d$

where ϵ_s and ϵ_a are dielectric constants of sample and air, and A_s and A are effective and actual areas of the sample respectively This results in the increase of the dielectric constant and increase of loss in polycrystals. It has also been observed that the doping decreases the dielectric constant significantly. This needs a thorough knowledge of defect mechanism in BSO which is not available right now.

In fig 3.27, the ϵ' is practically constant . So ϵ'' is a measure of dielectric loss. The dielectric loss is due to the conversion of the movement of charges into vibrations of the lattice i.e.

phonons This can occur from a multiplicity of causes, particularly, as with ceramics, when the microscopic structure is complex . The loss is practically constant with frequency.

Fig 3.29 to fig 3 31 shows the variation of log ϵ' with 1000/ T at fixed frequencies 5KHz,100KHz and 1 MHz. It has been observed that the dielectric constant remains practically constant upto a temperature of 300^0 C As the temperature raises further, ϵ' starts increasing slowly upto 525^0 C and beyond this temperature it increases rather rapidly. The behaviour below 525^0 C, where ϵ' is either constant or changes slowly with temperature is a characteristic of ionic solids The region where the dielectric constant increases rapidly as temperature increases is attributable to the space charge polarization of the thermally generated charge carriers which are due to the defects in the dielectric material.

Fig 3.32 to fig 3.34 shows the variation of log ϵ'' with 1000/ T at three different frequencies. Here also the imaginary part of the dielectric constant is practically constant upto 300^0 C and increases slowly upto 525^0 C. After 525^0 C, it increases rapidly. This is in good agreement with electrical conductivity proportionally related to dielectric loss

$\sigma = Y' l / A = \omega \epsilon_0 \epsilon'' = \omega \epsilon_0 \epsilon' D$

Thus for a fixed frequency, the electrical conductivity σ is proportional to ϵ'' which in turn is proportional to D especially at lower temperatures where ϵ' is practically constant.

3.8 Conclusions and future directions

1. Three single crystals of BSO pure and doped and the corresponding polycrystals were synthesized and thoroughly examined by complex impedance analysis .

2. Powder XRD was done on all the polycrystalline samples to confirm the formation of the compound.

3. Using the single crystal XRD studies the lattice parameters of BSO pure,BSO:Al and BSO:Mg are determined.

4. Density measurements give an idea about the closeness of the material to single crystal and in the case of pure BSO the sintered density is above 90 %.

5 The addition of impurities like Al and Mg tend to decrease the activation energy responsible for conduction as well as reducing the band gap

6 BSO has reasonably a high value of dielectric constant which decreases with increase in frequency. The addition of dopants significantly reduces the dielectric constant

7. At low frequencies space charge polarization is responsible for high values of ϵ' and ϵ''.

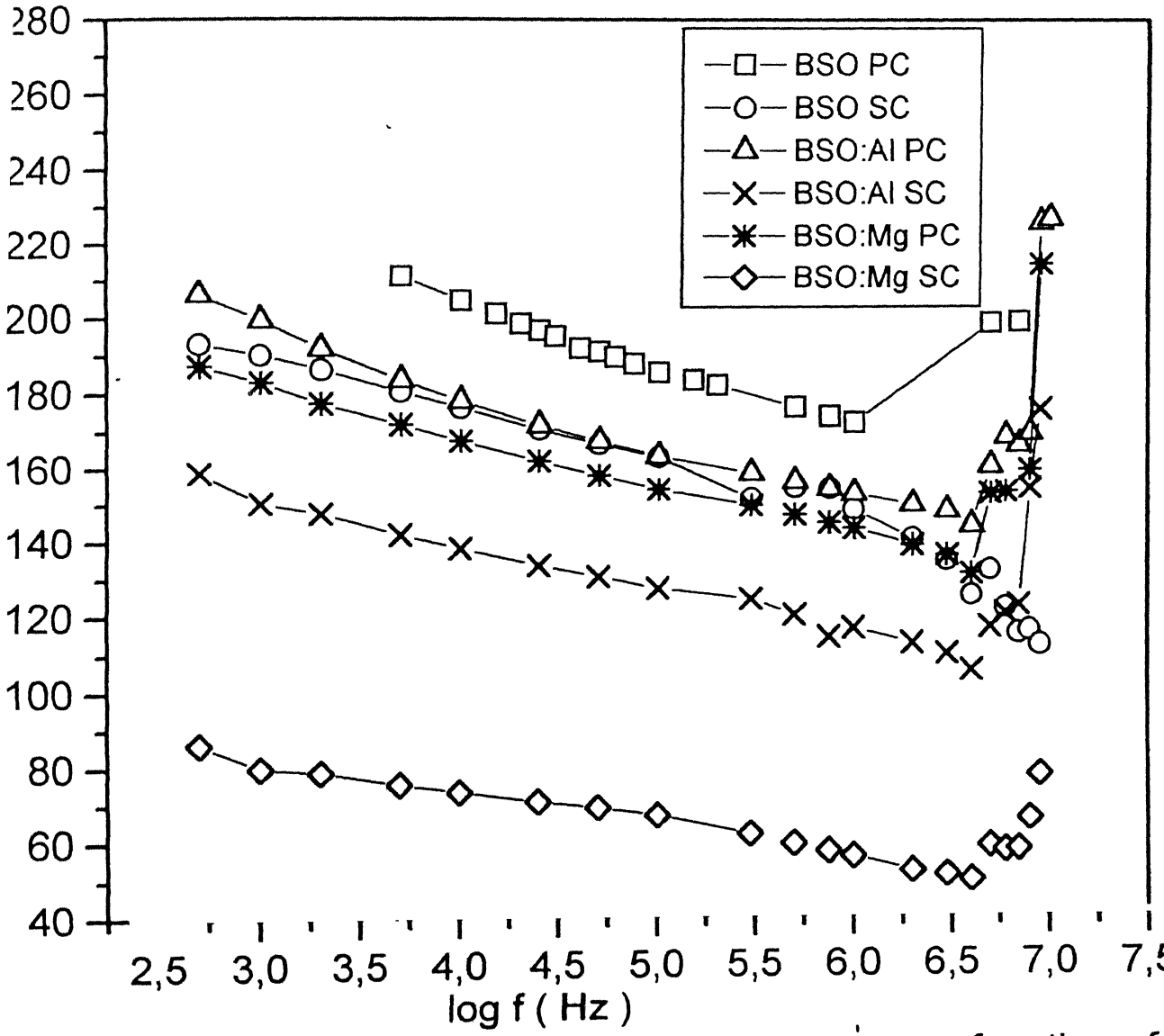

Fig 3.27 Variation of dielectric constant ε' as a function of log frequency for BSO, BSO:Al and BSO:Mg single crystals and polycrystals at room temperature

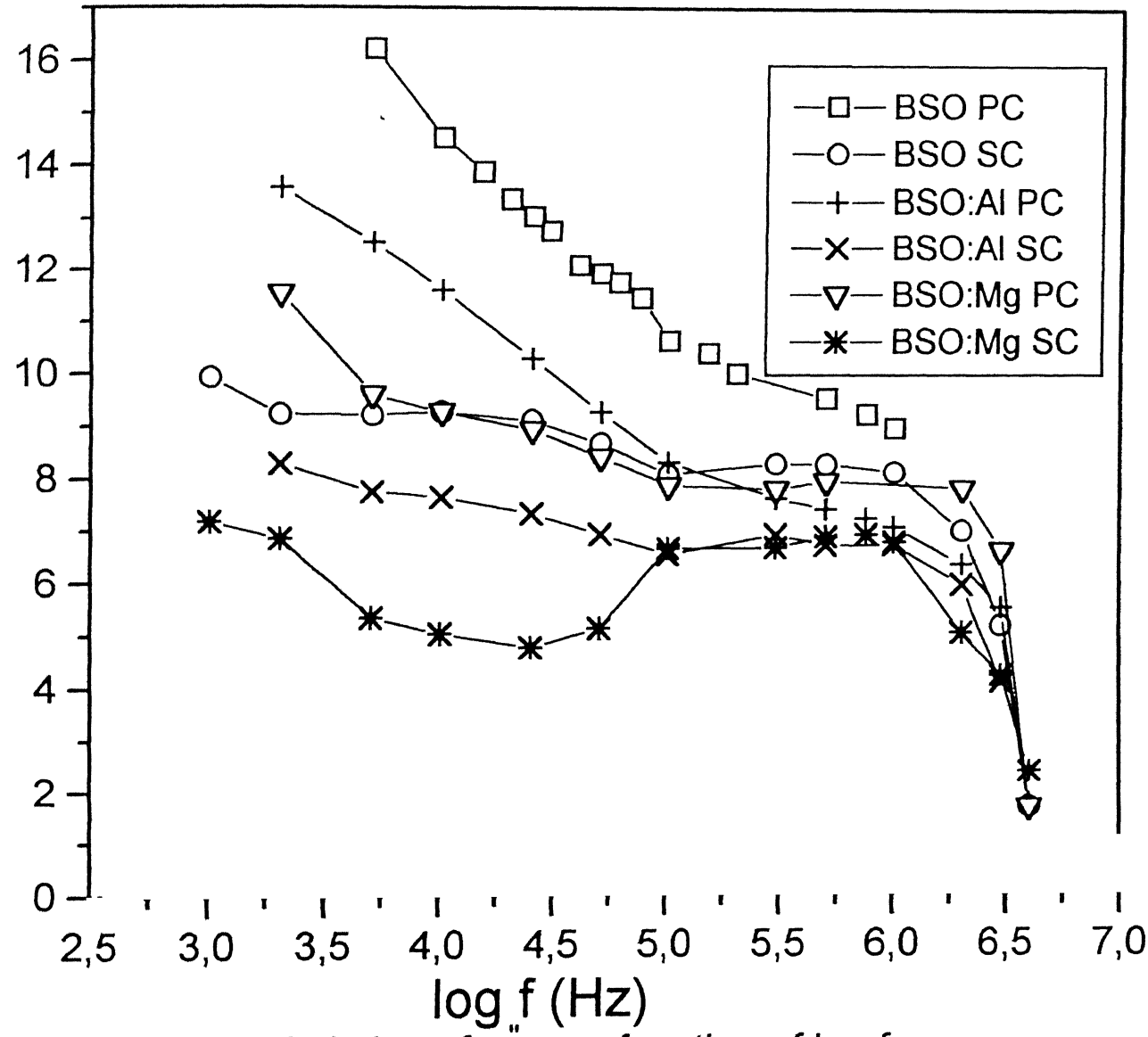

Fig 3.28 Variation of ε'' as a function of log frequency for BSO,BSO:Al and BSO:Mg single crystals and polycrystals at room temperature

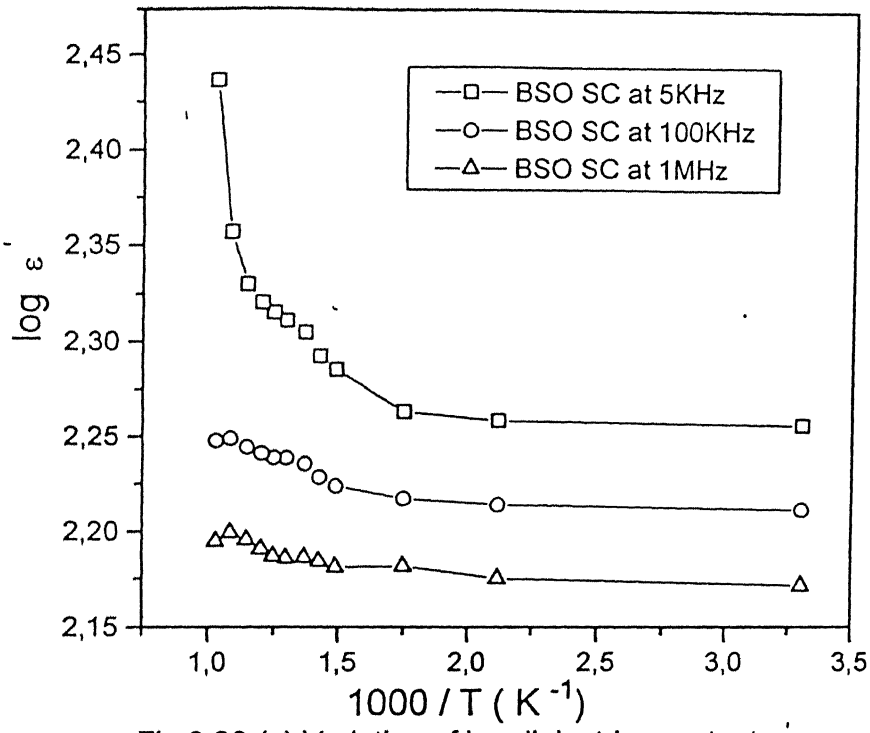

Fig 3.29 (a) Variation of log dielectric constant ε' as a function of temperature for BSO single crystal

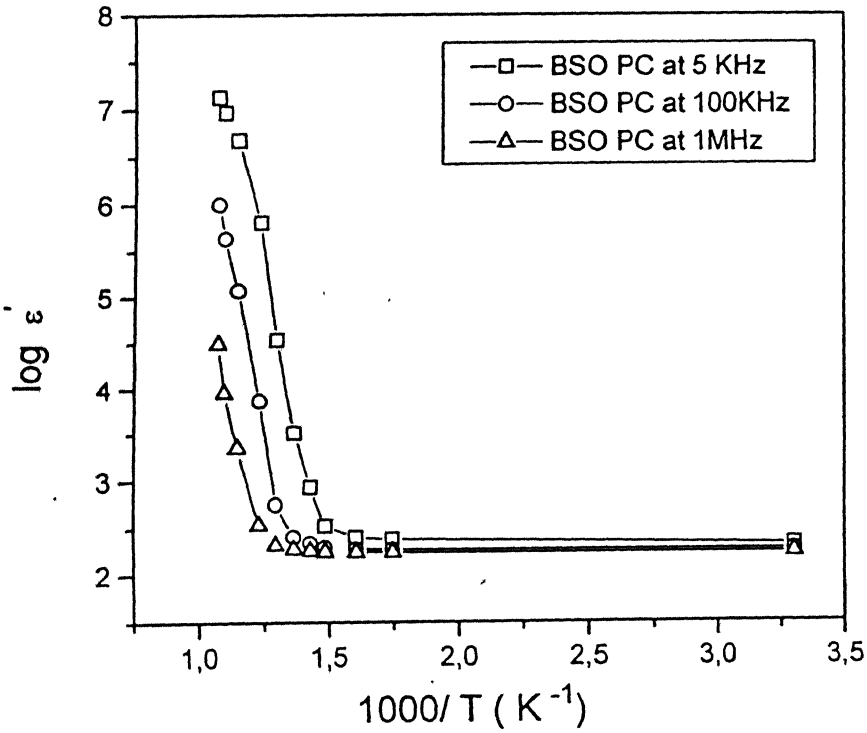

Fig 3.29 (b) Variation of log dielectric constant ε' as a function of temperature for BSO polycrystal

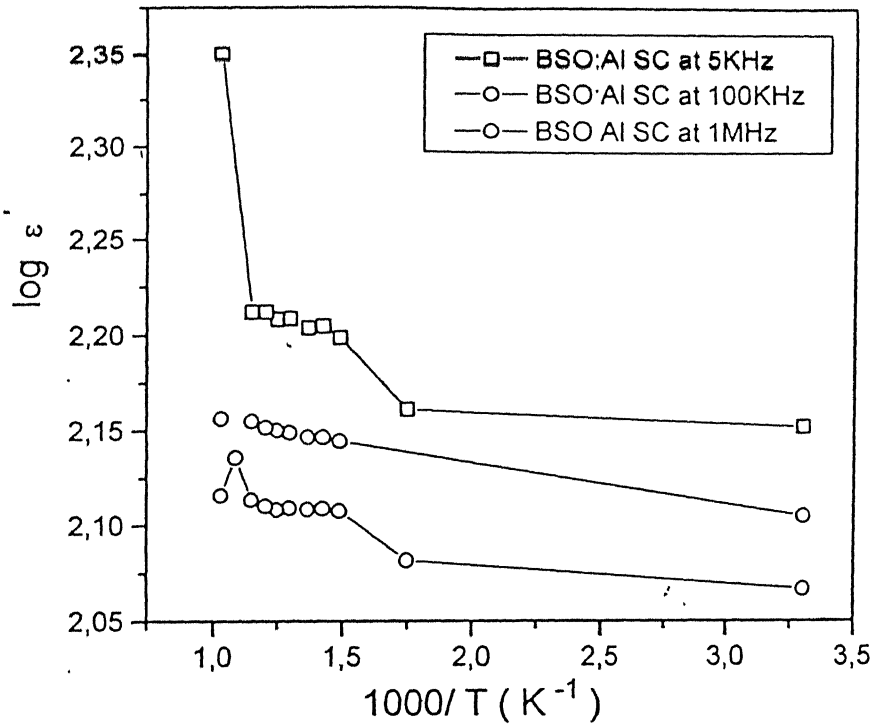

Fig 3.30 (a) Variation of log dielectric constant ε' as a function of temperature for BSO:Al single crystal

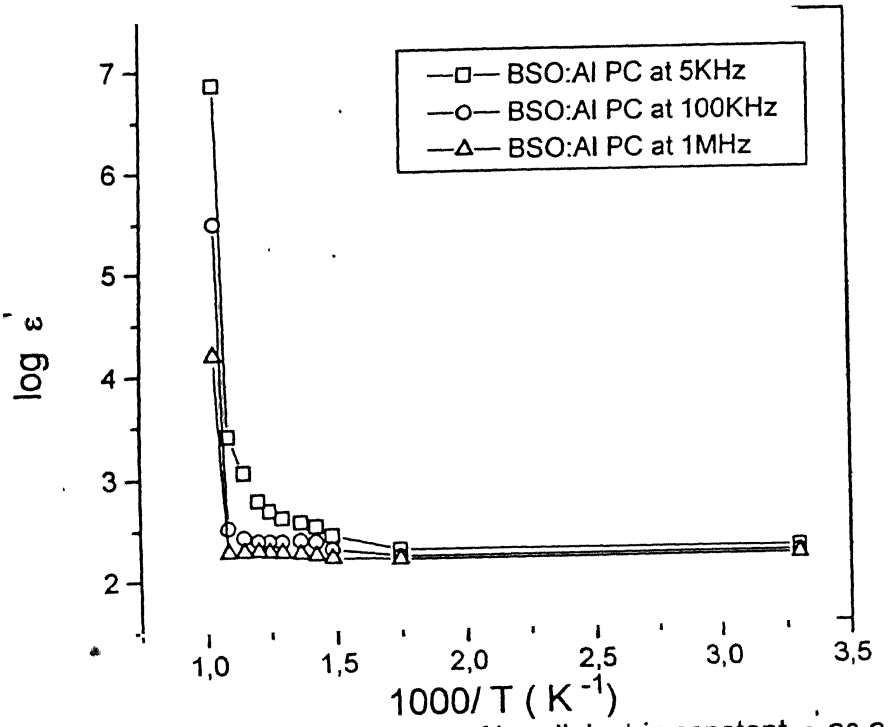

Fig 3.30 (b) Variation of log dielectric constant ε' as a function of temperature for BSO:Al polycrystal

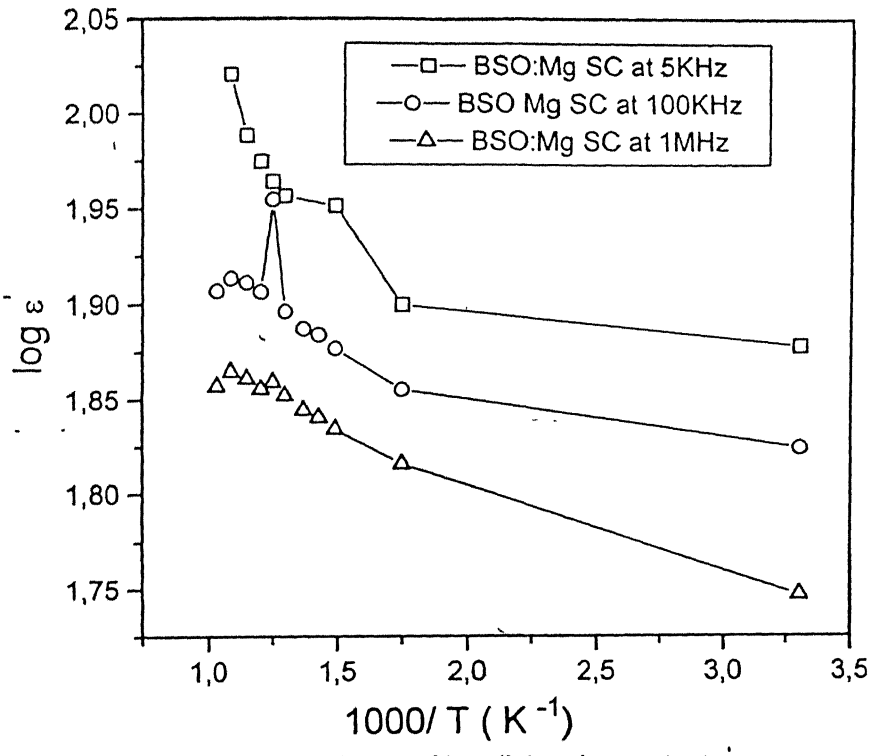

Fig 3.31 (a) Variation of log dielectric constant ε' as a function of temperature for BSO:Mg single crystal

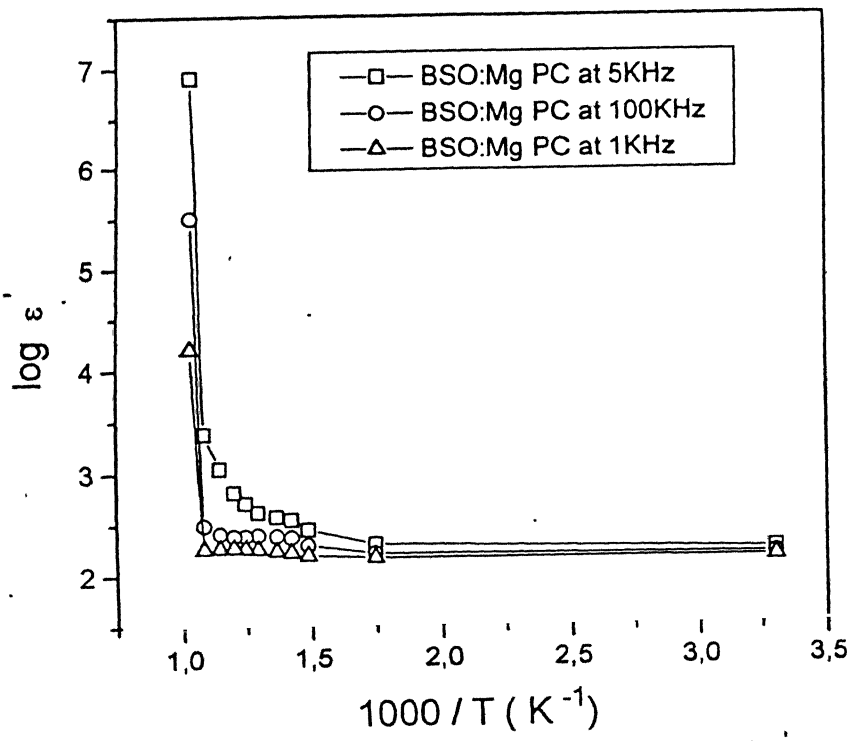

Fig 3.31 (b) Variation of log dielectric constant ε' as a function of temperature for BSO:Mg polycrystal

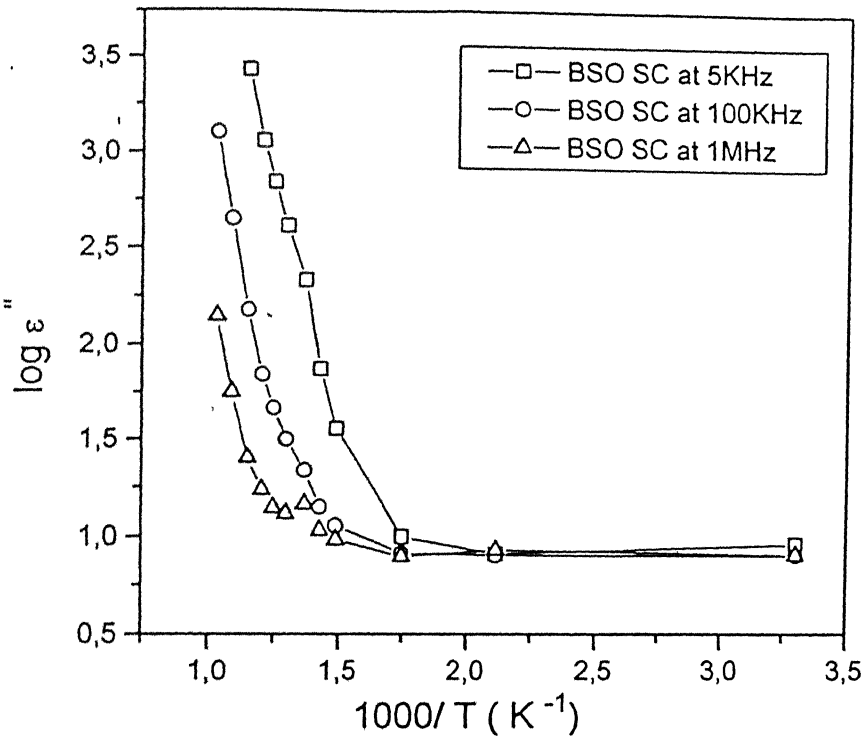

Fig 3.32(a) Variation of log ε" as a function of inversion of temperature for BSO single crystal

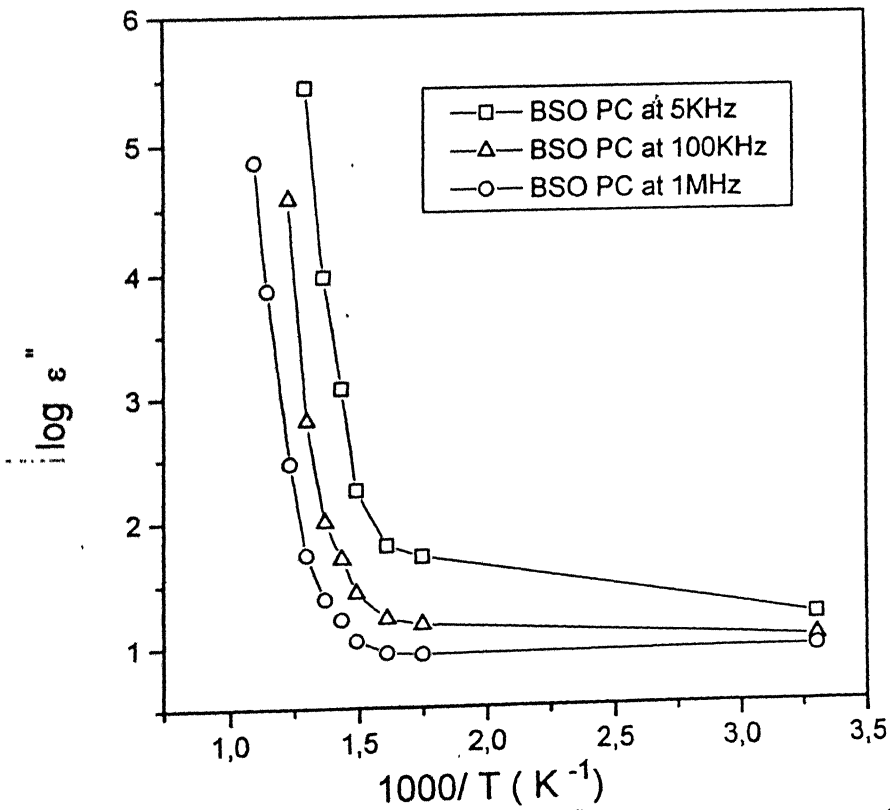

Fig 3.32 (b) Variation of log ε" as a function of inversion of temperature for BSO polycrystal

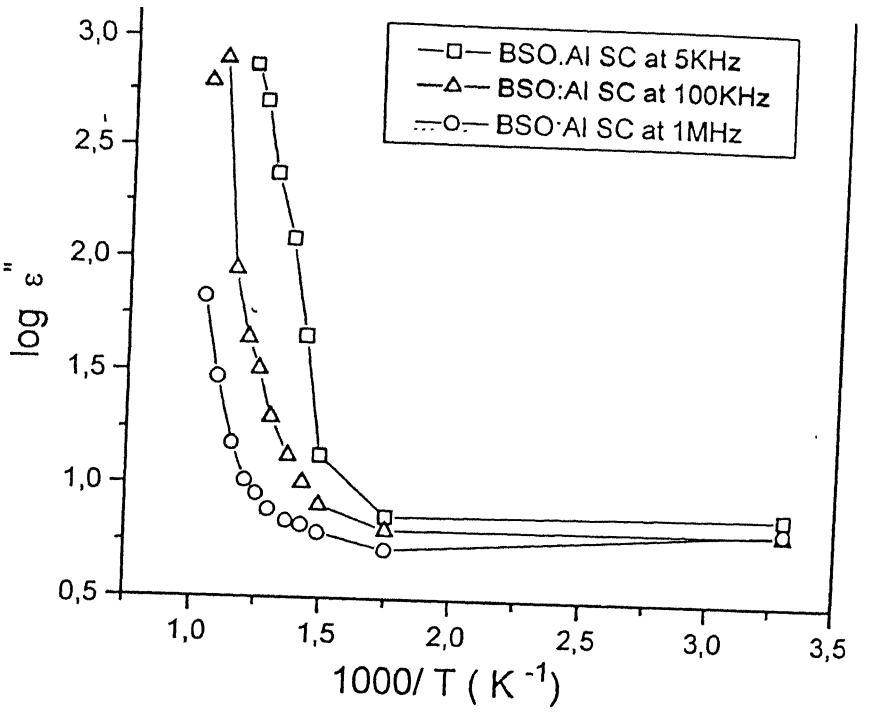

Fig 3.33 (a) Variation of log ε'' as a function of inversion of temperature for BSO:Al single crystal

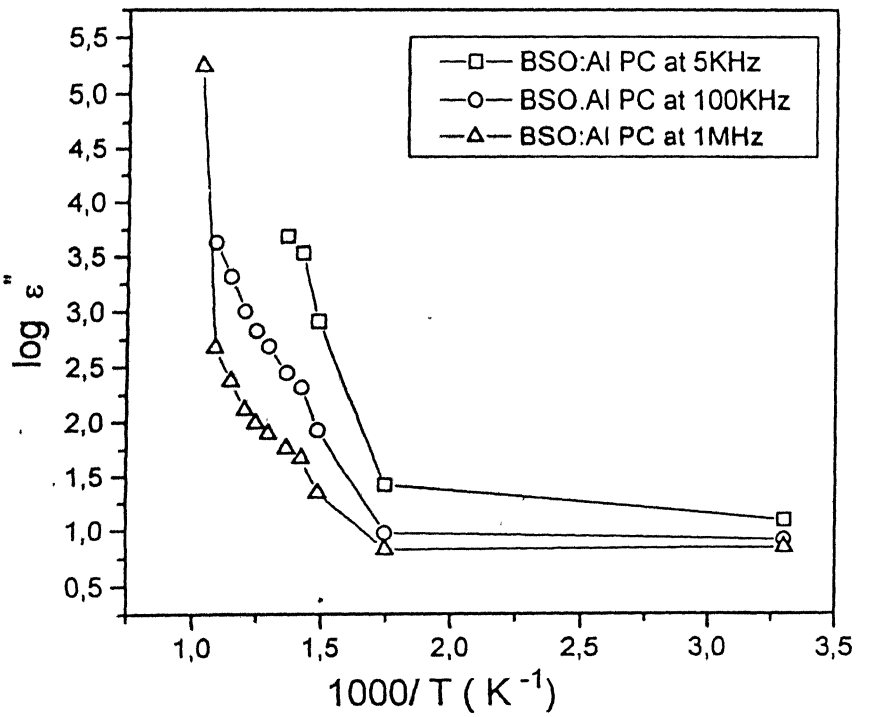

Fig 3.33 (b) Variation of log ε'' as a function of inversion of temperature for BSO:Al polycrystal

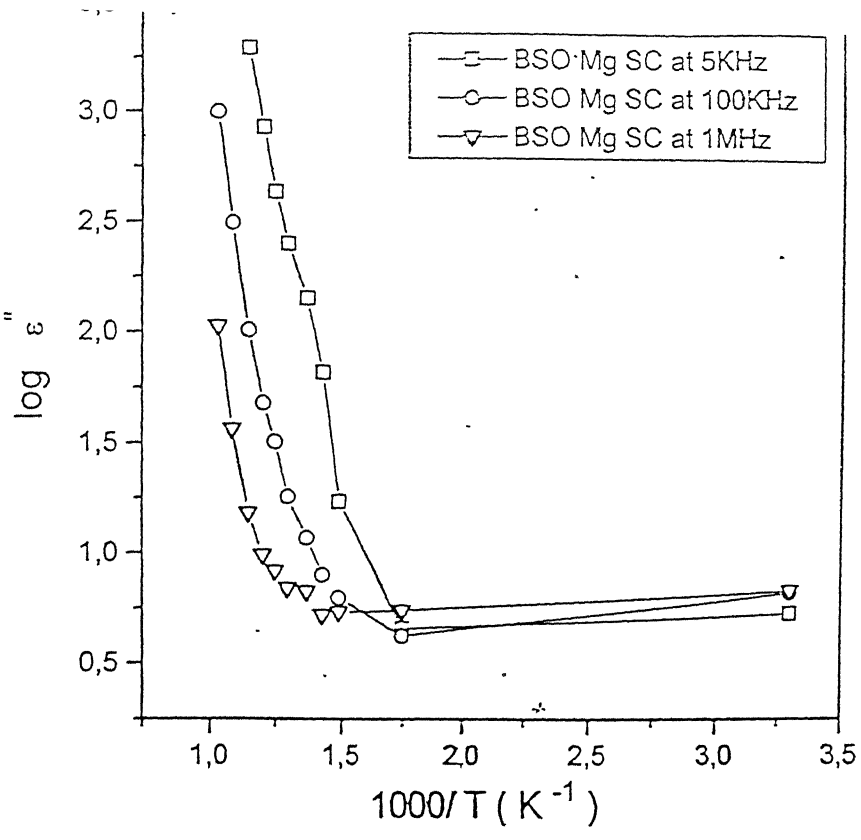

Fig 3.34 (a) Variation of log ε'' as a function of inversion of temperature for BSO:Mg single crystal

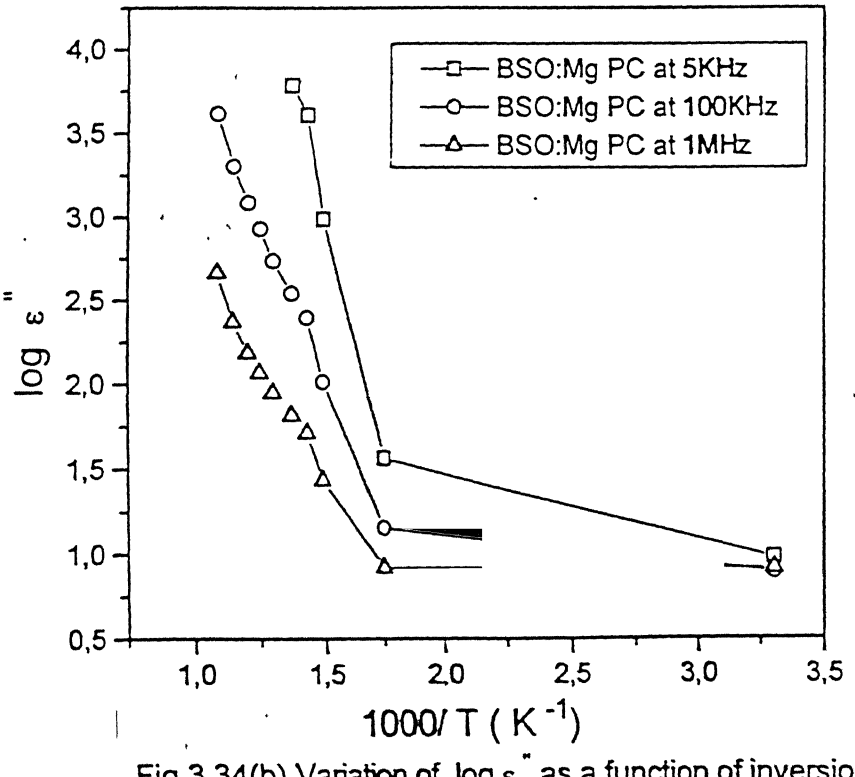

Fig 3.34(b) Variation of log ε'' as a function of inversion

8 As mentioned earlier , BSO is a complicated system We studied here the γ - BSO The other phase δ - BSO can be studied

9 The defect mechanism in BSO is not clearly established One can make a detailed study on it.

10 The single crystal structures of BSO:Al and BSO Mg are not solved so far. If the structures are solved ,then it will throw light on where exactly the dopant goes and occupies it's position This will give an idea whether the doping may really alter the electrical and dielectric properties of the system or not.

REFERENCES

1. L G Sillen , Arkiv kemi min Geol **12 A** , 1 (1937) .

2 A A. Ballman , J. Cryst. Growth **1** , 37 (1967)

3 A I Safonov, S A. Baryshev, T I Nikiforova , G N Anotonov and S.A Fedulov , Kristallografiya **13** , 914 (1968) [Sov.phys. crystallogr. **13** , 797 (1969)].

4 S.C Abrahams, P.B. Jamieson and J.L Bernstein, J Chem Phys **47** , 4034 (1967)

5. J.L. Bernstein , J. Cryst. Growth **1**, 45 (1967).

6 S C.Abrahams , J.L. Bernstein and C.Svensson , J Chem. Phys. **71(2)** , 15 July , 1979.

7. G.A. Babonas, E.A. Zhogova etal . Sov. Phys. Solid state 24 (6) , June 1982.

8. A. Sokolov etal. Electronics letters , **Vol.26** , No.16 . 2nd Aug 1990.

9. K. Magade and G. Brost , " Investigation of the internal field in Photorefractive materials and measurement of the effective electro optic coefficient ", J. Opt Society , **12** , 921 (1995) .

10 G. Roosen , " Photorefractive effect in BSO or BGO single crystals", 22 , 1253 (1987)

11. M.V . Shilova , " Kinetics of photoconductivity in single crystals of BSO", **22**, 1535 (1985) .

12. J.S. Mccullough etal. J.Appl.Phys . **78** (3) , 1st Aug.1995 .

13. K. Ukhtarev etal . Ferroelectrics , **22** , 949 (1979).

14. S.L. Hou , R.B. Lauer and R.E. Aldrich , J. Appl. Physics, **44** , 2658 (1973) .

15. Y. Nagao and Y. Mimura , Mater.Res . Bulletin , **24** , 239 (1989).

16. B.C. Grabmaier and R. Oberschmid , Phys.Status. Solidi **A 96**, 199 (1986).

17. T.S. Yeh etal. Appl. Phys. Lett. **65(10)** , 5 Sep 1994 .

18. D. Nesheva etal. J. Phys. Chem. Solids , **Vol . 56** , No.2 , 241-250 (1995).

19. E.V. Mokrushina etal. Optics Communications , **123** (1996) 592-596.

20. M.T. Harris , J.J. Larkin and J.J. Martin , Appl.Phys.Lett. **60**, 27 (1992).

21. R. Obserschmidt , Phys. Status Solidi **A89** , 263 (1985).

22. T Takamori and J. Just , J. Appl. Phys. **69** , 3958 (1991).

23. R. B. Lauer , J. Appl Phys. **42** , 2147 (1971).

24. W. Wardzinski etal. Physica B **11** , 47 (1988).

25. Senlin Fu and Hiroyuki ozoe , J. Phys. D. Appl, Phys. **29** (1996) 2032-2043.

26. National Bureau of standards of USA 1985 monograph **22** ; 1987 Powder diffraction file 37- 485 (Swarthmore : International centre for diffraction data (ICDD)).

27. Fus and H. Ozoe Metastable δ - Bi_{12} Si O_{20} and its effect on the quality of grown single crystals of γ - Bi_{12} SiO_{20} , J. Mater. Res. at press (1996).

28 . M. Tebaldi and N. Bolognini , Eur. J . Phys. **17** 236-243 (1996) .

29. A. L. Khromov etal. Optics Communications , **Vol** 77 , No:- s 2, 3 pages 139-143 , 1990.

30. Z. Karim etal. Appl. Phys. Lett. **70** , 21 (26 May , 1997).

31. Yasuyuki Nagao and Yoshinori Mimura , IEEE journal of quantum electronics , **Vol .** QE - **23** , No.12 , December 1987.

32. J. R. Macdonald and J. A. Garber , J. Electro Chemical Society , **124** , 1022 (1997) .

33. D. R. Franceschetti etal. Solid state ionics , **5** , 617 (1981).

34. B. A. Boukamp and G. A. Wiegers , Solid state ionics , **9/10** , 1193 (1983).

35. J. E. Bauerle , J. Phys. Chem . Solids , **30** , 2657 (1969) .

36. A.K. Jonscher Nature , **267** , 673 (1977).

37. Radzilowski R. H. etal. J. Appl. Phys. **40** , 4716 (1969).

38. J.R. Macdonald etal. Modern Physics , **28** , 393 (1956).

39. R. Matsui Solid state ionics , **18/19** , 888-891 (1986).

40. Macdonald and Garber , J. Electro Chem. Sci. and Tech. **24** , 1022 -1029 (1977).

41. B.A. Boukamp Solid state ionics **18/19** , 136-140 (1986).

42. J. R. Macdonald in " Impedance spectroscopy - Emphasizing solid materials and systems " , Willy , Newyork , 1987.

43. D. Ravaine and Souquet Comptes Rendus Acad. Sci. , 277 C (Paris 1973).

44. Superiohic solids , S. Chandra North-Holland publishing company,1981.

45. K.S. Cole and R. H. Cole , J. Chem . Phys. **9** , 341 (1941).

46. Raistrick , Solid state ionics , **18/19** , 40-49 (1986).

47. Senlin Fu and Hiroyuki Ozoe , Journal of American Ceramic Society , **80** [10] , 2501-2509 (1997).

48. E. M. Levin and R.S. Roth , " Polymorphism of Bismuth Sequioxide" . 2 nd effect of oxide additions on the polymorphism of Bi_2O_3 ", J. Res. Natl. Bur. Stand. , Sec A. **68A** [2], 197-206 (1964).

49. T. Takamori and T. J. Watson , " The system Bi_2O_3 - SiO_2 " , J. Am. Ceram. Soc., 73 [1], 158-160 (1990).

50. Y. Suematsu , "Optical devices and fibers " , Japan Annual Review in Electronics Computers and Telecommunications ", 11 , p -154 (1984).

51. "Powder diffraction file", Published by JCPDS, USA, 37 - 485 (1996).

52. "Complex impedance analysis and dielectric properties of BSO", by Prasant Kumar Senapathy thesis.

53. B. K. Roul , R. N . P. Choudhary and K. V. Rao , "Dielectric properties of $KNbO_3$ single crystals ", Proc. 3 rd. Nat. Seminar on Ferroelectrics and dielectrics , p 281 (Oct 17-19, 1984) .

54. Prameela devi and Lalitha sirdeshmukh , "Dielectric properties of $Bi_{12}GeO_{20}$ (BGO) ", Proc. 3rd . Nat. Seminar on Ferroelectrics and dielectrics , p 213 (Oct 17 -19 , 1984).